إقرار

أنا الموقع أدناه مقدم الرسالة التي تحمل العنوان:

An E-band Diplexer for Gigabit Wireless Communications Systems

أقر بأن ما اشتملت عليه هذه الرسالة إنما هي نتاج جهدي الخاص، باستثناء ما تمت الإشارة إليه حيثما ورد، وإن هذه الرسالة ككل، أو أي جزء منها لم يقدم من قبل لنيل درجة أو لقب علمي أو بحثي لدى أية مؤسسة تعليمية أو بحثية أخرى.

DECLARATION

The work provided in this thesis, unless otherwise referenced, is the researcher's own work, and has not been submitted elsewhere for any other degree or qualification

Student's name: **Mahmoud M. AbuHussain** **محمود موسى أبو حسين** :اسم الطالب

Signature: :التوقيع

Date: 15/5/2013 **2013/5/15 م** :التاريخ

بسم الله الرحمن الرحيم

The Islamic University – Gaza
Deanery of Graduate Studies
Faculty of Engineering
Electrical Engineering Department
Telecommunications Systems

الجامعة الإسلامية – غزة
عمادة الدراسات العليا
كلية الهندسة
قسم الهندسة الكهربائية
هندسة أنظمة الاتصالات

M.Sc. Thesis

An E-band Diplexer For Gigabit Wireless Communications Systems

By

Eng. Mahmoud M. AbuHussain

Supervisor

Dr. Talal F. Skaik

A Thesis Submitted In Partial fulfillment of the requirement for the degree of Master of Science in Electrical/telecommunication Engineering

1434 – م 2013

بسم الله الرحمن الرحيم

الجامعة الإسلامية – غزة
The Islamic University - Gaza

عمادة الدراسات العليا
هاتف داخلي: 1150

الرقم Ref ج س غ/35/
التاريخ Date 2013/05/15م

نتيجة الحكم على أطروحة ماجستير

بناءً على موافقة عمادة الدراسات العليا بالجامعة الإسلامية بغزة على تشكيل لجنة الحكم على أطروحة الباحث/ **محمود موسى عبدالقادر أبوحسين** لنيل درجة الماجستير في **كلية *الهندسة*** قسم/ **الهندسة الكهربائية- أنظمة الاتصالات** وموضوعها:

An E-band Diplexer for Gigabit Wireless Communications Systems

وبعد المناقشة العلنية التي تمت اليوم الأربعاء 05 رجب 1434هـ، الموافق 2013/05/15م الساعة الثانية عشرة ظهراً بمبنى القدس، اجتمعت لجنة الحكم على الأطروحة والمكونة من:

د. طلال فايز سكيك	مشرفاً ورئيساً	.....
د. فادي إبراهيم النحال	مناقشاً داخلياً	.....
د. مصطفي حسن أبو نصر	مناقشاً خارجيًا	.....

وبعد المداولة أوصت اللجنة بمنح الباحث درجة الماجستير في **كلية *الهندسة*/** قسم **الهندسة الكهربائية- أنظمة الاتصالات.**

واللجنة إذ تمنحه هذه الدرجة فإنها توصيه بتقوى الله ولزوم طاعته وأن يسخر علمه في خدمة دينه ووطنه.

والله ولي التوفيق،،،

عميد الدراسات العليا

أ.د. فؤاد علي العاجز

ص.ب. 108 الرمال، غزة، فلسطين هاتف Tel: +970 (8) 286 0700 فاكس fax: +970 (8) 286 0800 P.O. Box 108, Rimal, Gaza, Palestine
www.iugaza.edu.ps public@iugaza.edu.ps

Abstract

In this thesis, microwave diplexers are designed by different methods using rectangular waveguide cavities with chebyshev response. The diplexers can be used as front-end components in *E-band* [CH1:71-76 GHz and CH2:81-86 GHz] transceivers that are used in point-to-point mobile backhaul applications to offer gigabit wireless connectivity over a distance of a mile or more. Two diplexers have been designed, a T-junction diplexer and a manifold diplexer.

The T-junction diplexer has been designed by using two waveguide-cavity band-pass filters and then, the two filters are connected by a common H- plane T-Junction to divide power between filters equally. The manifold diplexer has been designed by connecting the channel filters by the manifold (transmission line sections and T-junctions). Each channel filter has been designed of five waveguide cavities coupled together using inductive apertures.

An EM simulation software CST has been utilized to design the diplexers by employing both parameter sweep and optimization techniques to achieve the required response. The simulation results show that the responses of both diplexers meet the requirements of the E-band diplexers in terms of return loss and isolation.

ملخص الرسالة

في هذه الاطروحة ، صمم جهاز المبدل التناوبي (Diplexer) والذي يفصل بين قناتين اثنتين، الاولى تحمل التردد الهابط (downlink) بعرض نطاق 71–76 جيجا هرتز، والأخرى تحمل التردد الصاعد (uplink) بعرض نطاق 81–86 جيجا هرتز باستخدام عشرة مرنانات (Resonators) موجيه باستجابة تشيبيشيف (Chebychev) ، والذي سوف يطبق ويدخل ضمن نظام الاتصالات اللاسلكية ذات الموجات القصيرة (millimeter waves) لنقل البيانات الكبيرة المرسلة والمستقبلة بنفس الوقت من نقطة الى نقطة أخرى على نفس خط الأفق أو أن لا يكون عائق بينهما (line –of –sight) التي يصل عرض نطاقها 5 جيجا بايت خلال شبكة الاتصالات اللاسلكية .

بداية تم تصميم كل مرشح موجه للموجات القصيرة (waveguide filter) على حدا، والمكون من خمسة مرنانات موجية مستطيلة الشكل بينها رنين مزدوج ناتج عن الاقتران المباشر (Direct Coupling) . أستخدم برنامج (CST MWS 2012) لتطبيقات الموجات الكهرومغناطيسية كوسيلة محاكاة حاسوبية في التصاميم السابقة.

أخذ بعين الاعتبار العزل (Isolation) الكامل بين الوصلتين حتى لا تدخل الطاقة العالية من الوصلة الصاعدة وتحرق الوصلة الهابطة ، وتم الحصول على التردد الرنيني (resonant frequency) للمرشحين من خلال البرنامج المذكور سابقا وطرق التحسين الموجودة خلاله (optimization) بالاضافة لاستخدام طريقة (parameter sweep) .

بعد تصميم المرشحين والحصول على النتائج المرجوه لكل مرشح، جاءت الخطوة الاخيرة بربطهما للحصول على المبدل التناوبي المراد تصميمه، أستخدمت طريقتين مختلفتين للربط بينهما ، حيث كانت الطريقة الاولى باستخدام تقاطع الوصلة الخارجية (T–junction) والطريقة الثانية باستخدام الوصلة التشعبية (Manifold) ، وتمت المقارنة بين النتائج لكل تصميم وتبين أن افضل النتائج بالنسبة للفقد الراجع S_{11} والعزل S_{23} التي تم الحصول عليها كانت من خلال الطريقة الاولى.

To my Father and Mother ….

To my Family…

ACKNOWLEDGEMENTS

First of all, I am grateful to the Almighty God for establishing me to complete this thesis. There are a number of people without whom this thesis might not have been written, and to whom I am greatly indebted.

To my parents, Mousa and Mazouza, I thank you for your encouragement and inspiration to me throughout my life, thank you both for giving me strength to reach for the stars and chase my dreams. A very special thank for their providing and for nurturing me through the months of writing this thesis.

I am deeply indebted to my supervisor Dr. Talal F. Skaik whose stimulating, motivation, and valuable ideas helped me to complete this work, and who expertly guided me through my graduate education and who shared the excitement of a year of discovery. I also thank the Islamic University of Gaza for its helping and supporting.

Special thanks to my grateful wife, Nour, for her moral support and always standing by me in my hard times during this work. Also I never forget my son ,Omar, and my daughter ,Tala , they supported me a lot in this work and blessed me with a life of joy in the hours when I was tired . I also indebted to my family, brothers and sisters, whose value to me only grow with age and deserve my wholehearted thanks as well.

To all my friends, thank you for your understanding and encouragement in my many, many moments of crisis. I also place on record, my sense of gratitude to one and all who, directly or indirectly, have lent their helping hand in this thesis.

Mahmoud

Table of Contents

List of Tables

List of Figures

List of Abbreviations

EM	Electromagnetic
ITU	International Telecommunication Union
WARC	World Radio communication Conference
FCC	Federal Communications Commission
PTP	Point-to-Point
CEPT	European Conference for Postal and Telecommunications
ETSI	European Telecommunications Standards Institute
EU	European
LOS	line-of-sight
GigE	Gigabit -Ethernet
BPSK	Binary Phase Shift Keying
FSK	Frequency Shift Keying
EIRP	Equivalent Isotropic Radiated Power
LPD	Low Probability of Detect
LPI	Low Probability of Intercept
Wi-Fi	Wireless Fidelity
4G	Fourth-Generation
LTE	Long Term Evolution
WiMAX	Worldwide Interoperability for Microwave Access
UMB	Ultra Mobile Broadband
QoS	Quality of Service
QAM	Quadrature Amplitude Modulation
FSO	Free space optic
HSPA	high speed packet access
DSL	Digital Subscriber Line
BS	Base Stations
MAN	Metropolitan Area Networks
RF	Radio Frequency
BPF	Band Pass Filter
DL	Downlink
UL	Uplink
CST	Computer Simulation Technology
FBW	Fractional Bandwidth
Q	Quality Factor
TE	Transvers Electric
TM	Transvers Magnetic

Chapter 1
Introduction

The term *microwaves* may be used to describe electromagnetic (EM) waves with frequencies ranging from 300 MHz to 300 GHz, which correspond to wavelengths (in free space) from 1 m to 1 mm. The EM waves with frequencies above 30 GHz and up to 300 GHz are also called *millimeter* waves because their wavelengths are in the millimeter range (1–10 mm) as shown in figure 1.1.

The millimeter wave spectrum at 30-300 GHz is of increasing interest to service providers and systems designers because of the wide bandwidths available for carrying communications at this frequency range. Such wide bandwidths are valuable in supporting applications such as high speed data transmission and video distribution [1].

Today, as the demand for bandwidth increases daily, operators who rely on Wireless backhaul are turning to new frequency spectrums to lower their wireless backhaul costs. Wireless systems operating in the newly-allocated E-Band spectrum (71-76 GHz for downlink, 81-86 GHz for uplink) have clear technological and economic advantages. The E-Band spectrum is expected to become the "Next Generation Wireless Backhaul Spectrum" playing an important role in easing the backhaul pain of mobile operators [1].

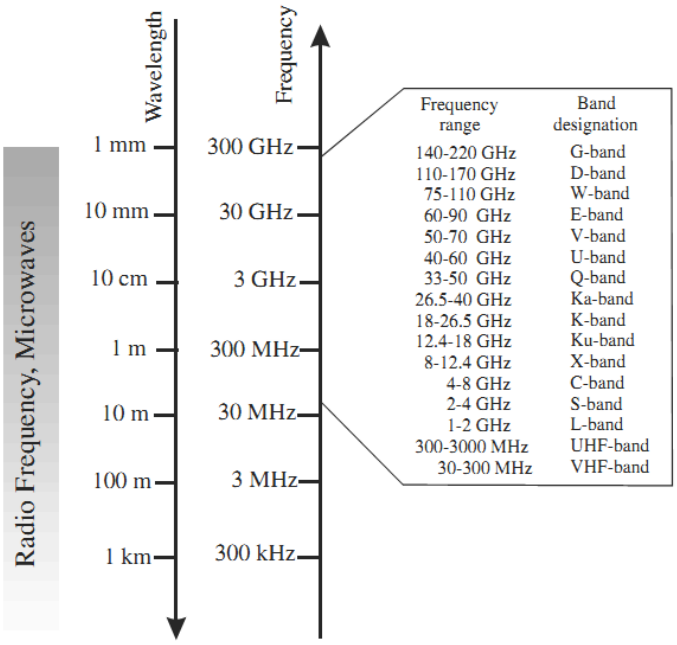

Figure 1.1: RF/microwave spectrums

The millimeter wave spectrum above 70 GHz is especially suitable for high data rate fixed links with cost effective, fiber like wireless performance. Because of the unique propagation characteristics in these bands it is possible to employ highly directional "pencil beams," allowing multiple services and

applications to be implemented without interference concerns, ensuring highly efficient reuse of the spectrum [2].

1.1 E- band Technology Overview

The 71-76 and 81-86 GHz bands (widely known as "E-band") are permitted worldwide for ultra-high capacity point-to-point communications. E-band wireless systems are available that offer full duplex Gigabit connectivity at data rates of 1 Gb/s and higher in cost effective radio architectures, with carrier class availability at distances of a mile and beyond [3].

The significance of the E-band frequencies cannot be overstated. The 10 GHz of spectrum available represents by far the most ever allocated by the Federal Communications Commission (FCC) at any one time, representing 50-times the bandwidth of the entire cellular spectrum. With 5 GHz of bandwidth available per channel, gigabit and greater data rates can easily be accommodated with reasonably simple radio architectures. With propagation characteristics comparable to those at the widely used microwave bands, and well characterized weather characteristics allowing rain fade to be understood, link distances of several miles can confidently be realized [3].

1.2 A Brief History of the E-band System

The 71-76 GHz and 81-86 GHz E-band allocations for fixed services were established by the International Telecommunication Union (ITU) almost 30 years ago at 1979 , World Administrative Radio communication Conference (WARC-79). However not much commercial interest was shown in the bands until the late 90's, when the FCC's Office of Engineering and Technology published a study on the use of the millimeter wave bands[4].

At the conference 2000 WARC-00, ITU delegates discussed enabling high density fixed services at high frequencies. At this time, several events were converging that caused interest in E-band wireless system. Firstly, device technology had advanced to the point where components operating in the millimeter wave frequencies could be commercially fabricated. Secondly, crowding in the widely used microwave bands (6 to 38 GHz) meant designers had to start considering alterative frequency bands. Finally, with a vision for multi-megabit and even gigabit per second speeds required by newer generation communication and multimedia services, new paradigms for wireless transmission were needed [3].

Following petition by the wireless industry, the FCC released a Notice of Proposed Rulemaking in 2002 [5] that resulted in the opening of the bands under existing Part 101 fixed service point-to-point rules in 2003 [6]. A novel "light licensing" scheme was introduced in 2005 and the first commercial E-band radios were installed soon after [7].

The wireless regulators in Europe quickly followed the United States (US) lead. In 2005, the European Conference for Postal and Telecommunications Administrations (CEPT) released a European-wide band plan similar to the US [8]. In 2006, the European Telecommunications Standards Institute (ETSI) released technical rules for equipment operating in the 71-76 and 81-86 GHz bands. These were consistent with European (EU) rules to allow E-band wireless equipment to be commercially used in Europe [9].

Many parts of the world have now followed the US and EU lead, and opened up the E-band frequencies for high capacity line-of-sight (LOS) wireless systems, enabling gigabit speed transmission in the millimeter wave bands [3].

1.3 The E-band Frequency Allocation

The E-band frequency allocation consists of the un channelized bands 13 GHz of spectrum at 71 to 76 GHz, 81 to 86 GHz, and 92 to 95 GHz was available for, as shown in figure 1.2. The allocation 71 to 76 GHz and 81 to 86 GHz is significant for two main reasons. Firstly, the combined 10 GHz of spectrum is significantly larger than any other frequency allocation. Together this is over 50-times larger than the entire spectrum allocated in the USA for all generations, technologies and flavors of cellular services, and much larger than all the widely used microwave communication bands. The availability of such a large spot of spectrum enables a whole new generation of wireless transmission to be realized [4] [5].

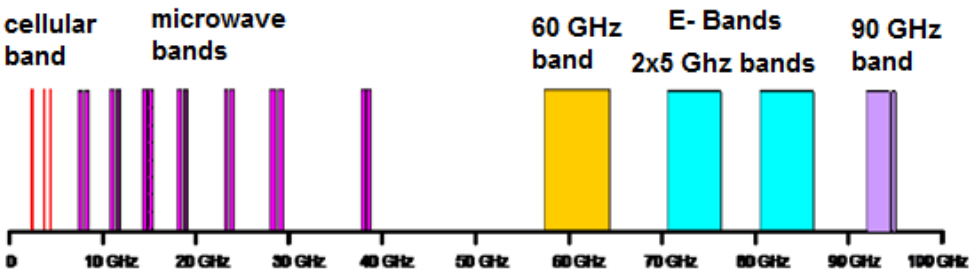

(a)

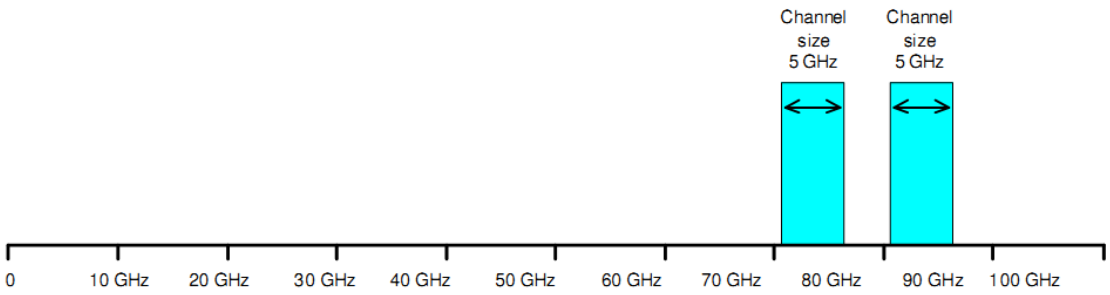

(b)

Figure 1.2: (a) Significant USA frequency allocations, (b) ITU allocation of e-band frequencies

Secondly, the E-band allocation, sub divided into two paired 5 GHz per channel, is not further partitioned, as is the case in the lower frequency microwave bands. In the USA, the FCC dived each common carrier microwave band into channels of no more than 50 MHz . This channel size ultimately limits the amount of data that can be squeezed into the channel. With 5 GHz channels at E-band allocation, 100-times the size of even the largest microwave band, significantly more data can be carried by each signal. The E-band spectrum allocation is enough to transmit a gigabit of data (1 Gb/s or GigE – Gigabit Ethernet) with simple modulation schemes such as binary phase shift keying (BPSK). Since there is not the need to compress the data into small frequency channels, systems can be realized with relatively simple architectures. Radio equipment can take advantage of low order modulation modems, non-linear power amplifiers, low cost diplexers, direct conversion receivers, and many more relatively non-complex wireless building blocks, reducing system cost and complexity, whilst increasing reliability and overall radio performance [3].

1.4 Wireless Propagation at E-band

At E-band frequencies the Wireless propagation is well understood. Characteristics are only slightly different to those at the widely used lower frequency microwave bands, enabling transmission distances of many miles to be realized. The atmospheric attenuation of radio waves varies significantly with frequency. Its variability has been well characterized and is shown in figure 1.3 [3].

At the microwave frequency bands of up to 38 GHz, the attenuation due to the atmosphere at sea level is low at 0.3 dB /km or less. A small peak is seen at 23 GHz, followed by a large peak at 60 GHz, corresponding to absorption by water vapor and oxygen molecules respectively. This effect at 60 GHz in particular, where absorption increases to 15 dB/km, significantly limits radio transmission distance at this frequency. Above 100 GHz, numerous other molecular absorption effects occur, limiting the performance of radio transmissions [3].

A clear atmospheric window can be seen in the spectrum from around 70 GHz to 100 GHz. In this area, low atmospheric attenuation around 0.5 dB/km occurs, close to that of the popular microwave frequencies, and very favorable for radio transmission. For this reason, E-band wireless systems can transmit high data rate signal over many miles under clear conditions with efficient effectiveness [3].

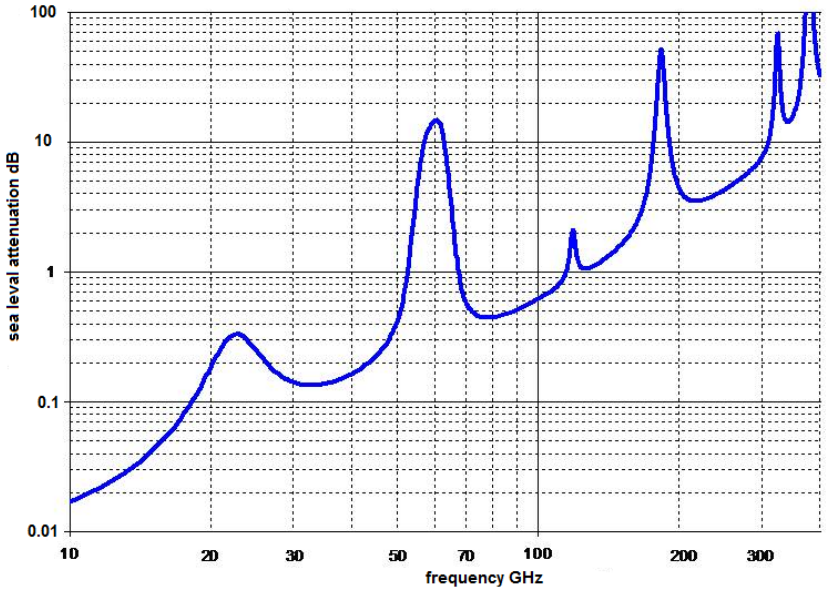

Figure 1.3: Atmospheric and molecular absorption.

1.5 E-band Technical Attributes

There are a number of additional physical and regulatory enabled technical characteristics that add to the attractiveness of E-band slice as useful spectrum for wireless communications technology [3].

Firstly, the gain of an antenna increases with frequency. Thus it is possible to realize large gains from relatively small antennas at E-band frequencies. Figure 1.4 shows the variation in gain for a 1 ft. (30 cm) parabolic antenna. At the popular 18 GHz common carrier band, such an antenna has about 32.5 dBi of gain. At E-band technology, an equivalent size antenna has 44 to 45 dBi of gain. This equates to an extra 12 dB for E-band or so of system gain per link a significant number when one considers that just an additional 6 dB of system gain allows a link to be doubled in length [3].

Secondly, the FCC permits E-band radios to operate with up to 3W of output power. This is significantly higher than available at other millimeter wave bands. Also the bandwidth of 5 GHz wide E-band channels enable the radio to pass high data rate signals with only low level modulation schemes (for example, BPSK modulation can easily allow 2 Gb/s data rates in the 5GHz channels). At high output power and high antenna gain allows E-band radios to operate with very high equivalent isotropic radiated power (EIRP) and hence overcome the higher rain fading at higher frequencies, enabling system performances that are equivalent to the widely used microwave point-to-point (PTP) radios system [3].

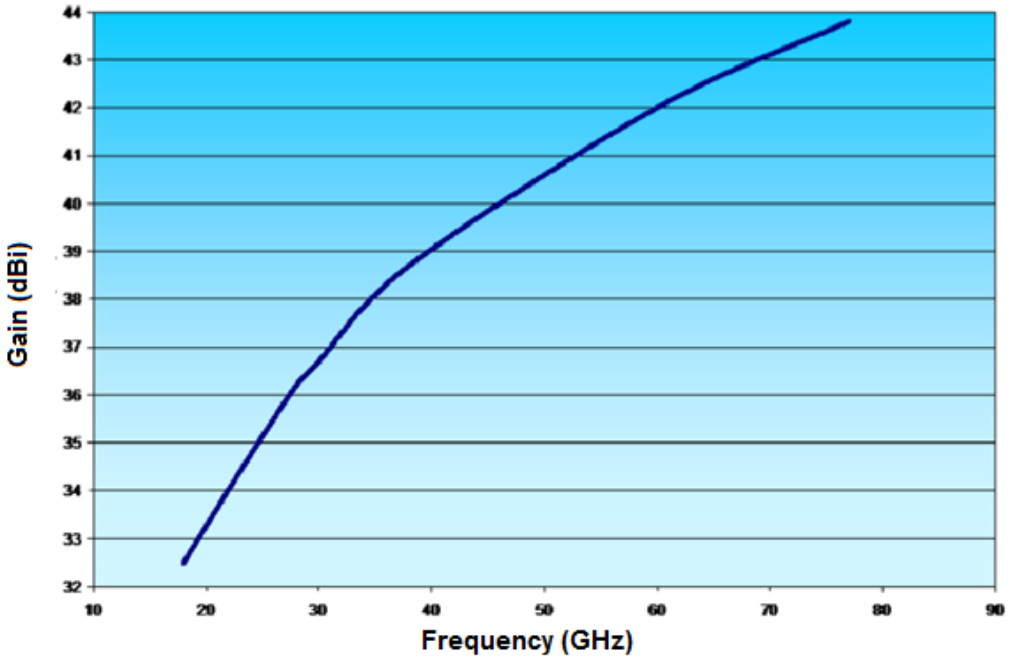

Figure 1.4: The effect of frequency on antenna gain for a 1ft (30 cm) parabolic antenna.

1.6 E-band benefits over other wireless spectrum

E-Band wireless technology allows Gb/s data rates to be transmitted with very high weather availability over distances of a mile or more. Characterized as Low Probability of Detect/Low Probability of Intercept (LPD/LPI), it is a perfect technology to satisfy hostile territory battlefield situations where there's a need for high security, high speed, point-to-point, non-wire-line communications. A novel licensing structure coupled with an ability to quickly deploy links permits rapid response to homeland defense and other time critical security applications [11].

There are many technologies competing to provide wireless broadband connectivity and bridge the last mile gap. This section explores how E–band wireless systems compete effectively against these alternatives, and brings significant advantages to wireless system providers and network designers [12].

1.6.1 High capacity wireless landscape

Figure 1.5 illustrates the major higher capacity wireless technologies available in present, and how they fit together to make up the current broadband wireless landscape [3].

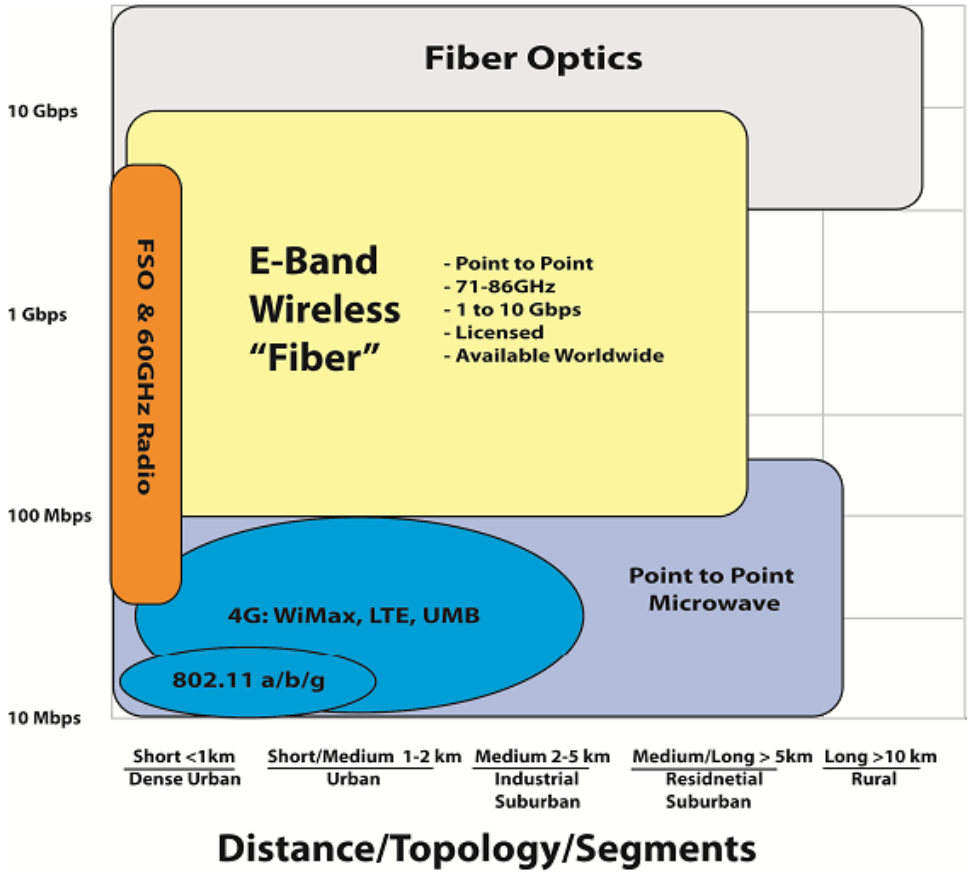

Figure 1.5: high speed wireless and wired technology landscape.

1.6.1.1 Wi-Fi – 802.11 a/b/g

The wireless fidelity (Wi-Fi) is a short distance, multi-access technology. Its popularity stems from being able to take a single data connection (usually a residential or equivalent broadband internet connection) and enable several users within a "hot spot" area to share that data connection. Equipment is currently widely available that can offer data rates of up to 54 Mbps and coverage distances of up several tens of yards, enabling users with suitable connection equipment fast and easy wireless access to whatever services are being offered. Extended versions of the Wi-Fi family are constantly evolving, improving performance and speeds. The latest 802.11n version offers improved data rates through the introduction of multiple antennas and wider channel transmissions, which supports up to 600 Mbps [12].

Like most technologies, Wi-Fi has a number of limitations. Practically, data rates are dependent on the distance from the access point, the number of users sharing the capacity, and the usually constrained size of the access point's broadband connection. In commercial hot spot environments, users would typically realize only 1 Mbps or so connectivity. By necessity, Wi-Fi is also an

unlicensed, broadcast, point-to-multipoint technology, allowing users to easily connect and disconnect from the service. This means interference, data contention and data collisions are difficult to avoid, resulting in network outages, connectivity issues and security concerns [3].

For these reasons, Wi-Fi is not a useful technology for wide area high data rate connectivity. It is a very useful wireless technology for easy access, short range coverage within a limited range properties that have made the technology very popular [3].

1.6.1.2 4G – WiMAX, LTE and UMB

in [11], Fourth-Generation (4G) wireless systems – the technologies of worldwide Interoperability for Microwave Access (WiMAX), long term evolution (LTE) and Ultra Mobile Broadband (UMB) – promise a substantial increase in data rates over existing second (2G) and third generation (3G) cellular systems.

WiMAX is the closest of these technologies to realization. It is often described as a "big brother" version of Wi-Fi. The WiMAX standard has addressed many of the quality of service (QoS) and security issues inherent with Wi-Fi and when properly implemented, provides a much higher user experience. In addition, WiMAX is usually implemented using licensed technology in frequencies close to the cellular bands, further improving the QoS . Theoretical data rates of many tens of Mbps are possible, and real systems are offering user data rates of 2 to 4 Mbps and up over cell sizes of a few miles. Future extensions to the WiMAX family (for example 802.16m, or mobile WiMAX release 2.0) will further extend user data speeds and experiences. WiMAX does offer the benefit of mobility, making the analogy to advanced cellular systems more accurate than to Wi-Fi networks [3].

LTE and UMB technologies are the next generation of the existing 3G cellular technologies. Theoretically, data rates to 100 Mbps and beyond are possible. Complete standards are likely to be realized in the next few years, and early experimental systems demonstrating improved data throughput are already being seen today. For these reasons, 4G technologies are ideally placed to be useful for wide area, mobile connectivity, with data rates higher than existing cellular standards. As 4G technologies are all access technologies, upgrade of the backhaul networks are required to support the 4G increases in data rates. That makes these technologies very complementary to the high data rate point-to-point technologies introduced later in this section [3].

1.6.1.3 Point-to-Point Microwave link

Fixed wireless radios at microwave frequencies from 6 to 38 GHz are widely used for point-to-point (PTP) data transmission. PTP microwave is used to interconnect cell site and fiber points of presence, its widely available with data rates from a few Mbps up to several hundred Mbps. PTP microwave radios have to compress the data into the narrow channels that are required in the microwave frequency bands. These can be up to 50 or 56 MHz, but are typically 28 or 30 MHz and below. Thus PTP microwave radios employ sophisticated signal processing circuitry and high order 128 or 256 Quadrature Amplitude Modulation (QAM) to squeeze data into the narrow available channels [3].

Microwave radios have an important role to play for high quality line of sight connectivity. Systems can be engineered to reliably transmit for several miles and the use of licensed technology means the systems will be robust and reliable. However limited regulated channel sizes in the microwave bands means that even the most complex and sophisticated widely available systems are limited to 311 Mbps or so data rates [3].

1.6.1.4 60 GHz wireless technology

60 GHz has been used as a wireless transmission frequency for many years, due to the property that oxygen in the atmosphere strongly absorbs radio waves at this frequency, Small beam sizes coupled with oxygen absorption makes these links highly immune to interference from other 60GHz radios [13]. Users, particularly in the military, have exploited this characteristic by developing short range systems that will transmit a few hundred yards before the signal rapidly deteriorates and so cannot be eavesdropped. The availability of large amounts of bandwidth at these frequencies has resulted in recent commercial interest for high data rate short range commercial applications [2] [3].

Differing worldwide spectrum allocations of the 60 GHz bands means regional differences in available equipment. In the USA, large amounts of bandwidth are available, enabling cost effective systems that can transmit data rates to 1 Gb/s to be realized. However the natural oxygen attenuating properties and low regulated power limits means such system can only reliability transmit a few hundred yards. With “best effort” connectivity, system can be engineered to transmit up to half a mile. Since the band is designated as license exempt in the US, systems are potentially at risk from interference, either from other links or from future services which might use the open bands. In Europe, the bands are managed very differently, with narrow channels limiting the data throughput of systems [3].

For these reasons, 60 GHz radios are very useful for providing high data rate interconnections . However systems are limited in distance to just a few hundred yards, and the unlicensed nature of the bands poses problems for sophisticated users who do not want to risk downtime due to interference outages [3].

1.6.1.5 Free space optics

Free space optic (FSO) systems use modulated lasers to transmit very high data rates in the invisible optical spectrum close to the visible bands at a distance nearly 2km. Systems are available that can transmit data rates of 1 Gb/s and beyond [3].

FSO suffers from the disadvantage that as a highly focused optical technology, any deterioration or blockage of the laser like signal path will affect the link quality. Atmospheric effects such a fog, dust, sand, air turbulence and sunlight shimmer limit practical link distances to just a few hundred yards in many parts of the world. In addition, practical effects such as flying objects breaking the beams, or tiny building or tower movements unlocking the precisely pointed equipment, means that sophisticated tracking mounts and multiple transmitters and receivers are required. This results in high complexity equipment, adding to system cost, and introducing reliability and maintenance concerns. Finally the use of lasers raises eye safety concerns, and also reliability questions due to the naturally high failure rate of optical devices [3].

Like 60 GHz radios, FSO systems are useful for high data rate transmission over distances of a few hundred meters. High performance systems can be very complex and expensive to maintain, with equipment reliability and failure rates much higher than standard radio systems [3].

1.6.1.6 E-band wireless system

The 71-76 and 81-86 GHz E-band channels were implemented in part to address the shortfalls of these other wireless technologies. The bands are globally available for fixed wireless point-to-point communications. The 10 GHz of bandwidth available the largest international telecommunication union (ITU) bandwidth allocation for such services provides such a large bandwidth that ultra-high data rate wireless capacities of 1 Gb/s and beyond can be realized with relatively simple, low cost radio architectures. The 71-86 GHz frequencies occur in an “atmospheric window”, whereby atmospheric attenuation is similar to the well-used lower frequency microwave bands of 23 and 38 GHz. With similar propagation characteristics to these popular bands, and well characterized weather attributes allowing rain fade to be understood and predicted, link distances of several miles can confidently be realized. To encourage uptake of services in these bands, the FCC, along with various other wireless regulatory agencies around the world, have implemented “light licensing” regimes for the bands, whereby the full benefits of interference protection are awarded to system providers, but with licenses that can be quick and cheaply obtained [3].

1.6.2 E-band wireless benefits

E-band system offer numerous benefits, these include [3]:

- **Highest data rates** of any wireless technology, with systems available that offer 1 Gb/s and above full duplex throughput.
- **Guaranteed data rates**, unlike Wi-Fi, WiMAX and other broad coverage technologies whose system performance depends heavily on the radio environment, number of users, distance from base station and even installation quality, E-band systems offer guaranteed data throughput performance, even under deteriorated transmission conditions.
- **Long distance transmissions** , E-band wireless offers the longest transmission distances of the higher capacity wireless systems. Under any environmental condition, a 1 Gb/s E-band system can transmit many times further than similar data rate 60 GHz or FSO systems.
- **Robust weather resilience**, all the higher frequency wireless systems – microwave, 60 GHz, FSO and E-band – are sensitive to rain fades. Unlike FSO, E-band is not subject to fog, dust, air turbulence or any other atmospheric impairment that can take down optical links for hours over regular cycles.
- **Guaranteed interference protection** ,Since E-band is a licensed technology, all links have to be registered with national wireless regulators and coordinated with other links in the area. This gives links full interference protection from other nearby wireless sources.
- **Low cost, rapid license availability**, in many countries, links are licensed under a "light license" process, whereby licenses can be obtained quickly and cheaply.
- **Cost effective, fiber-like wireless solution** , high capacity wireless systems are available at a fraction of the cost of buried fiber alternatives.

1.7 The Mobile Backhaul Challenge

The introduction of broadband cellular technologies such as high speed packet access (HSPA) , LTE and WiMAX which provide users with Digital Subscriber Line (DSL) like and higher data speeds at flat rate pricing models is changing consumer mobile phone usage habits making mobile web browsing and emailing routine. This changing user behavior generates huge amounts of data, leading to congestion in bandwidth demands as data traffic doubles and even triples. This data explosion places an ever increasing strain on operators' mobile backhaul networks [14].

The *mobile backhaul* network is commonly referred to as the transport links connect cell sites as Base Stations (BS), Node B, E-UTRAN Node B (e NodeB) with the core switching and management elements (as can be seen in figure 1.6). Traffic, both voice and data transported to and from the cell sites via the backhaul network required services with high reliability and availability [14].

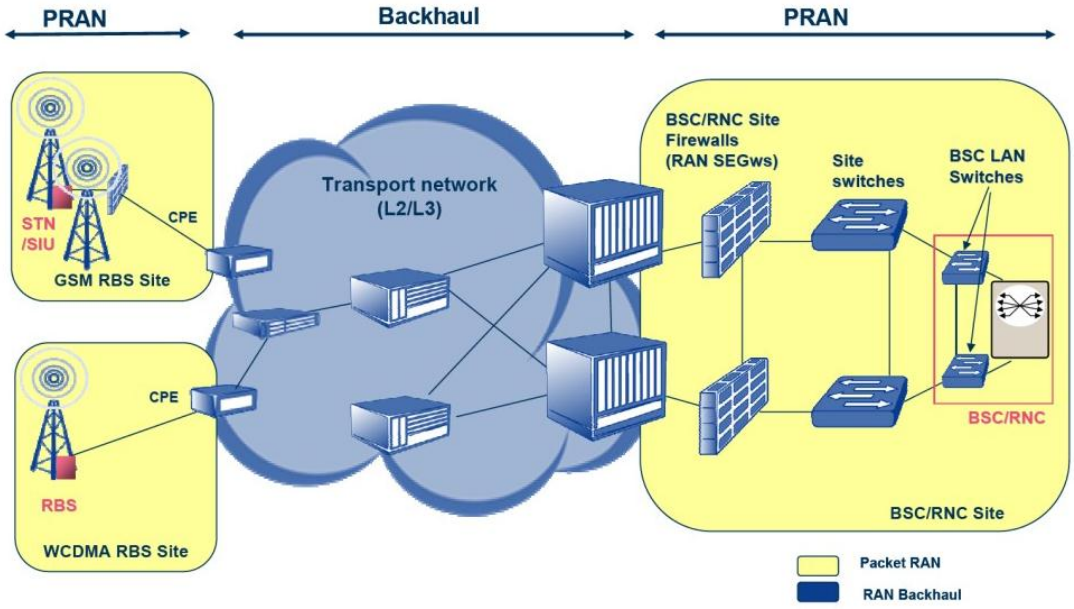

Figure 1.6: a snapshot of the mobile backhaul network [14]

1.8 High data rate wireless and fiber comparisons

in [3], E-band wireless system offer a compelling alternative to these different broadband technologies, often with many advantages over other systems. A summary of how the most important system parameters and network characteristics compare are detailed in the table 1.1.

Table1.1: Comparison of key system parameters for leading high data rate technologies [3].

	Wi-Fi	3 / 4 G	microwave	60 GHz	FSO	Fiber	E-band
Data Rates	Variable, typically 1 Mbps	Variable, typically 10 Mbps	2 to 311 Mbps	100 Mbps to 1 Gb/s	100 Mbps to 1 Gb/s	To 40 Gb/s	100 Mbps to 3 Gb/s today; to 10 Gb/s in the future
Typical link distances	20 yards	2 miles	5 miles	500 meters	200 meters	Unlimited	1-3 miles & higher
Spectrum availability and licensing	Freely unlicensed	Spectrum very scarce Owned	Usually available for area licensing	Varies, Available for unlicensed use in USA	Spectrum freely available as technology not regulated	n\a	Available , usually as a low cost “light license”
Guaranteed interference and regulatory protection	No	Usually	Yes	No	No	Yes	Yes
Relative cost of ownership	Low	High	Medium	Medium	Medium	High	Medium
Install and commissioning time	Hours	Months /Years	Weeks /Months	Hours/Days	Hours/Days	Months/ Years	Hours/Days

1.9 E-Band Applications

E-band technology is well-suited for a variety of applications: Mobile backhaul [15]

- WiMAX/LTE/4G backhaul
- Ethernet connectivity
- Remote Storage Access
- Redundant Access/Network Diversity
- Local Area Network Extension
- Wide Area Networks
- Metropolitan Area Networks (MAN)

1.10 Overview of Diplexers and applications

The 71-76 GHz and 81-86 GHz E-band frequencies are globally available for ultra-high capacity point-to-point communications, providing Gigabit Ethernet data rates of 1 Gb/s and beyond. Cost effective radio architectures have been realized that enable carrier class availability at distances of a mile and further [16]. E-Band diplexer is a fundamental part of E-Band radio link which is commonly used for LTE backhauling [17] as illustrated in figure 1.7.

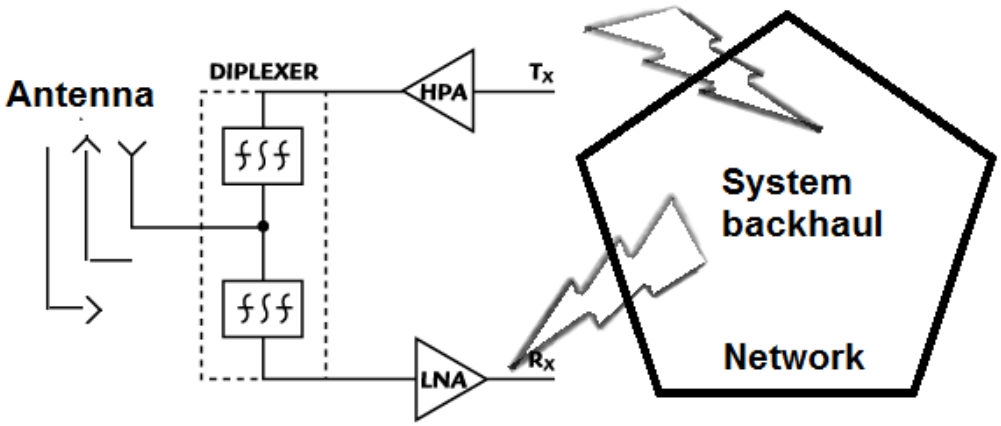

Figure 1.7: diplexer in network

Electrically a diplexer is a device using sharply tuned resonate circuits to isolate a transmitter from a receiver signals. This allows both of them to operate on the same antenna at the receiver same time without the transmitter Radio Frequency (RF) frying the receiver. Note that there must be a separation of transmit and receive frequency [18].

A diplexer is a device for either splitting a frequency range band into two sub-bands or combining two sub-bands into one broader frequency range. This device is widely used on board PTP wireless communication link because it permits the use of the same antenna for different frequency bands, and, therefore, an important

Reduction of mass and volume is achieved. The diplexer consists of power divider and two channel filters [19].

Diplexers were widely studied in the early 1960s by G. L. Matthaei [20] and Robert Wenzel [21] and in the last years the synthesis of microwave diplexers has been studied intensively. The general theory for the synthesis of diplexers is indeed published in the 1970s and the effort has been continued by many researchers, especially in recent years [22].

Microwave diplexers are typically employed to connect the receiver *RX* and transmitter *TX* filters of a transceiver to a single antenna through a suitable three port junction as shown in figure 1.8. The increasing development over the last years of mobile communication systems has stimulated the need for compact high selectivity diplexers to be used in both combiners for base stations and millimeter wave point-to-point radio links [23]. Diplexers may consist of high-pass and low-pass, band-pass and band-pass, band-pass and band-stop, and other combinations [24].

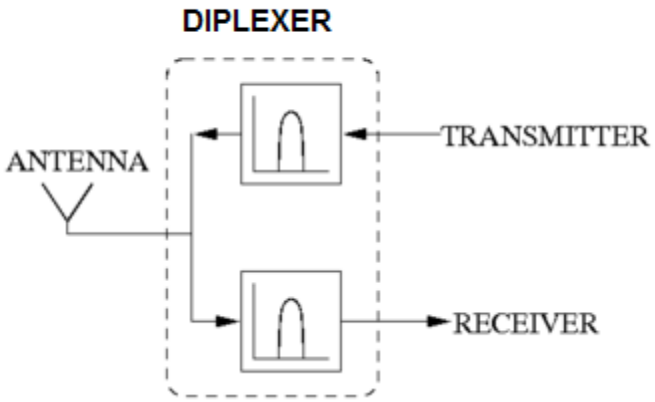

Figure 1.8: Diplexer scheme

The band-pass filter in the transmitter path (BPF-TX) stops the transmitter noise artificially increasing the receiver noise figure, while the bandpass filter in the receiver path (BPF-RX) stops the transmitter signal overloading the receiver [25].

1.11 Thesis Motivation

The main goal of this thesis is the analysis and designs a microwave diplexer for E-band system. This component will be used as a front-end in the microwave transceiver of a point-to-point in mobile backhaul application, which offers Gigabit wireless connectivity over a distance of a mile or more. It is specified to work at the frequency channel bands [DL CH1: 71-76 GHz and UL CH2: 81-86 GHz]. The diplexer will be designed using two methods to combine the two bandpass filters: first method uses external waveguide H-plane T-junction, and the second method is by employing a manifold. The performance of all design techniques will be compared in terms of isolation and return loss.

1.12 Thesis Overview

The objective of this research is to analyze and design a waveguide diplexer that is specified to work at the frequency channels E- band [DL CH1: 71-76 GHz and UL CH2: 81-86 GHz]. The diplexer is designed of two bandpass filters and a combining network and the aim is to obtain small insertion loss and good isolation between the channel ports.

Chapter 1 presents background technology of E-band wireless system, overview of diplexer and its applications.

Chapter 2 explains the different types of filters. It presents the derivation of the coupling matrix of resonator filters, and transformation method of filters

Chapter 3 explains the types of diplexers configurations such as T-junction, manifold and star junction. Also explain the different structures.

Chapter 4 presents the design procedure of diplexers for E-band system and the relationship between the coupling coefficients and the physical structure of coupled resonators in order to find the physical dimensions of the diplexer. Then, it shows the whole structure of the diplexer and its response resulting from computer simulation technology (CST2012) based on finite integral technique (FIT). Finally I will make a comparison between two designs and another comparison of commercial diplexers with my thesis work.

Chapter 5 provides summary and conclusions drawn from this work and future work

References

[1] J. Hong and M. Lancaster, "Microstrip Filters for RF/Microwave Applications", *John Wiley & Sons, Inc. NY, 2001.*

[2] J. Wells ,"Light licensing benefits of the 71-76 & 81-86 GHz frequency bands" , *E-Band Communications Corp V051310, 2010, San Diego, CA 92131 USA*

[3] J. Wells, "The Benefits of E-band Systems over other wireless technologies", *E-Band Communications Corp V051310, 2010, San Diego, CA 92131 USA.*

[4] FCC, Office of Engineering and Technology, "Millimeter Wave Propagation: Spectrum Management Implications", *Bulletin 70, on July 1997, pp.1-26, Washington, DC 20554, USA.*

[5] FCC Notice of Proposed Rule Making 02-180, "Allocations and Service Rules for the 71-76 GHz, 81-86 GHz, and 92-95 GHz Bands," *June, 2002, pp3-5, Washington, D.C. 20554, USA.*

[6] FCC Report and Order 03-248, "Allocations and Service Rules for the 71-76 GHz, 81-86 GHz, and 92-95 GHz Bands," *November, 2003, Washington ,USA.*

[7] FCC Memorandum Opinion and Order *05-45,"* Allocations and Service Rules for the 71-76 GHz, 81-86 GHz, and 92-95 GHz Bands *", March, 2005, Washington ,USA.*

[8] ECC Recommendation (05)07, "Radio frequency channel arrangements for fixed service systems operating in the bands 71-76 GHz and 81-86 GHz", *European Conference of Postal and Telecommunications Administrations (CEPT), Dublin, October 2005.*

[9] ETSI TS 102 524 V1.1.1 (2006-07), "Fixed Radio Systems; Point-to-Point equipment; Radio equipment and antennas for use in Point-to-Point Millimeter Wave applications in the Fixed Services (MMWFS) frequency bands 71 GHz to 76 GHz and 81 GHz to 86 GHz,", *Sophia Antipolis Cedex ,pp.5-15, July 2006, France*

[10] ITU-R, "Attenuation by atmospheric gases," *Electronic Publication, P.676-6, 2005, Geneva.*

[11] J. Wells, "New multi-gigabit wireless systems satisfy high-security rapid response applications*", Military embedded systems ,journal 2006*

[12] B. Lee, and S. Choi, "Broadband Wireless Access and Local Networks Mobile WiMAX and Wi-Fi", *artech house, INC, pp353, 2008*

[13] 60GHz Wireless Technology Overview, [online], Available on: *http://www.mmwaves.com/products.cfm/product/20-194-0.htm*

[14] S. Peleg , "The Advantages of E-Band Wireless Systems in Mobile Backhaul Applications *", Siklu company, Jerusalem, March 2009*

[15] E-band backhaul [Online]. Available on:
http://www.sabertek.com/e-band-backhaul.html

[16] E-Band Wireless Propagation [Online]. available on:
http://www.e-band.com/index.php?id=86

[17] E-band waveguide diplexer, ABF Electronica, RF devices & Microwave subsystems , *srl Via Ciro Menotti, 60 – 20043, 2000 Arcore (Mi) – Italy*

[18] S. Das, "Mobile Handset Design", *edition 2010, by John Wiley & Sons Asia, # 02-01, pp.124-125.*

[19] J. Rebollar, J. Garai ,"Asymmetric H-plane T-junction for broadband diplexer applications", *IEEE, Antennas and Propagation Society International Symposium – (APSURSI) conference , 2000, Politecnica de Madrid, Spain*

[20] G. Matthaei, and E. Cristal, "Multiplexer channel-separating units using inter-digital and parallel-coupled filters", *IEEE Transaction microwave Theory Tech., 1965, 13, pp. 328–334*

[21] R. Wenzel, "Printed-circuit complementary filters for narrow bandwidth multiplexers", *IEEE Transaction microwave theory tech., 1968, 16,pp. 147–157*

[22] D. Zhang, Y. Zhao, W. Liu, W. Zhao, Q. Sun, " A Fast Synthesis Approach for Diplexer with E-plane T-junction Design ", *IEEE , Information Science and Engineering (ISISE), 2010International Symposium on 2010, pp.133 , Astronaut., Nanjing, china.*

[23] G. Macchiarella, "Novel Approach to the Synthesis of Microwave Diplexers", *IEEE transactions on microwave theory and techniques, vol. 54, no. 12, December 2006, pp. 4281*

[24] E. Christian and E. Egon, "Filter Design Tables and Graphs". *John Wiley & Sons, Inc., 1966.*

[25] J. Daniel Company, Diplexers – An Introductory Tutorial, [Online]. available on : http://www.rfsolutions.com/duplex.htm

Chapter 2

Overview of Microwave Filters

2.1 Introduction

The microwave filter is necessary and vital component in a huge variety of electronic systems, including mobile radio, satellite communications and radar. Such component is used to select or reject signal at different frequencies. Although the physical realization of microwave filters may vary, the circuit network theory is common to all. They are, by nature, distributed networks that usually consist of periodic structures to exhibit passband and stop band characteristics in various frequency bands. It is desirable that a design method would be able to determine the physical dimensions of a filters structure having the desired frequency characteristics. Research on microwave filters has spanned more than sixty years, and the number of contributions devoted to the design methods of microwave filters is enormous. Reviews on the topic of filters designs in a historical perspective can be found in [1, 2, and 3].

2.2 Overview of coupled resonator filters

Coupled resonator circuit prototypes are most commonly used in the design of microwave coupled resonator bandpass filters in the sense that they can be applied to any type of resonator despite its physical structure. They have been applied to the design of coaxial filters [4,5] as illustrated in figure 2.1, waveguide filters [6,7] as shown in Figure 2.2, dielectric resonator filters [8], ceramic combine filters [9] as illustrated in Figure 2.3, Microstrip filters [10-13] as illustrated in figure 2.4, superconducting filters [14] as shown in figure 2.5, and micro-machined filters [15] see figure 2.6. The design method is based on the coupling coefficients of the inter-coupled resonators and the external couplings of the input and output resonators. Therefore, a relationship between the coupling coefficients and the physical structures needs to be established. The formulations for extracting the couplings are given next section for different cases.

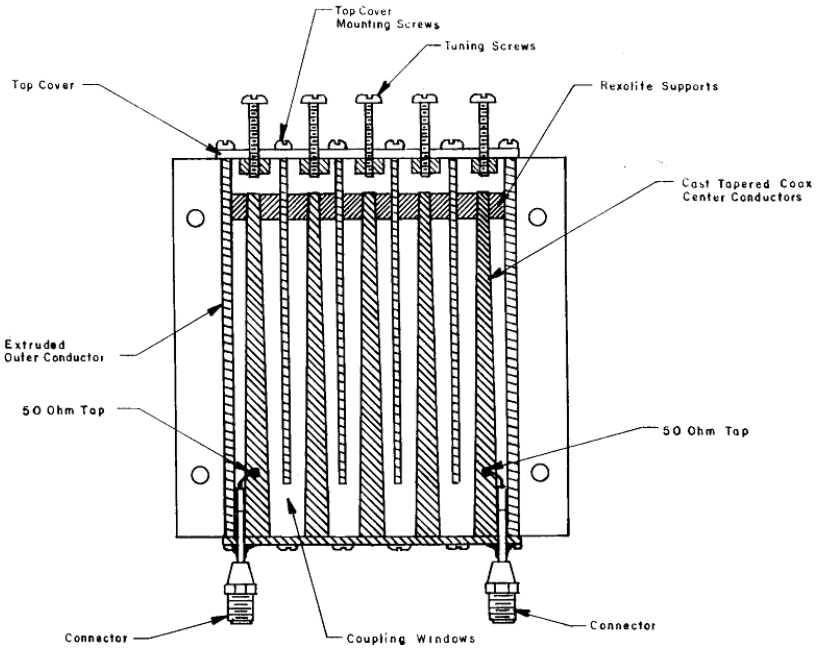

Figure 2.1: Tapered coaxial resonator filter.

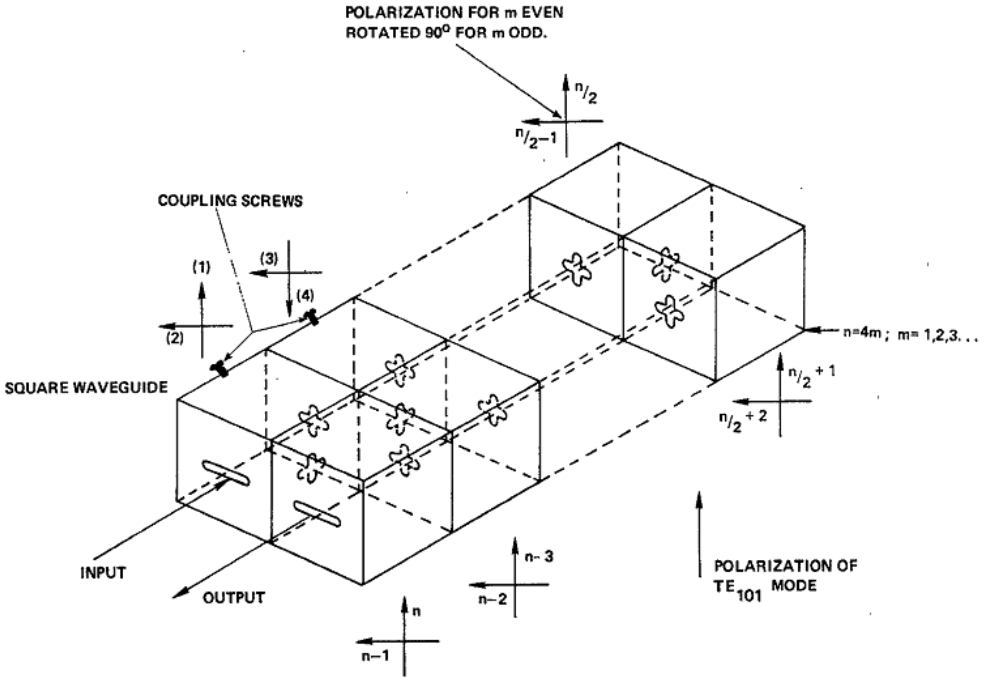

Figure 2.2: General coupled-cavity filter

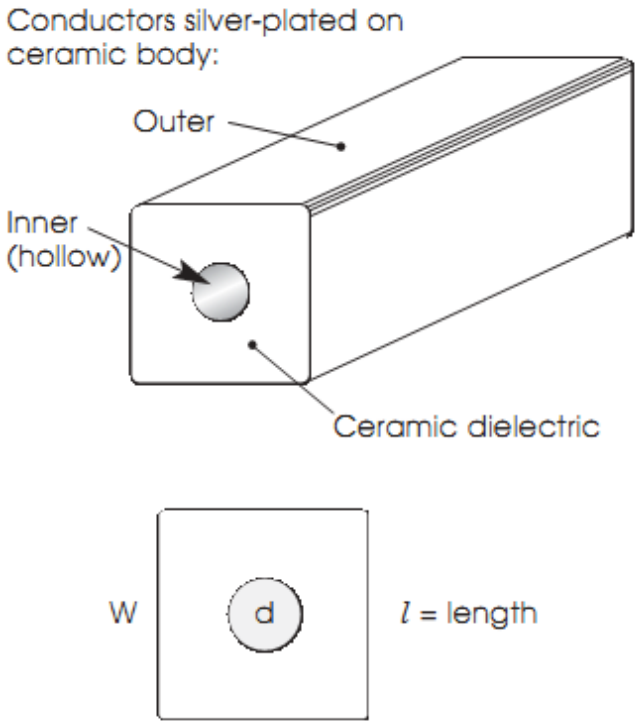

Figure 2.3: Construction of a ceramic coaxial resonator

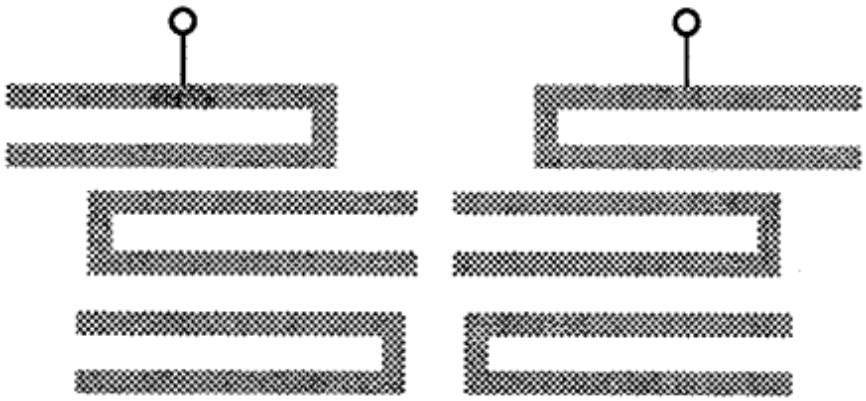

Figure 2.4: Typical cross-coupled Microstrip bandpass filters.

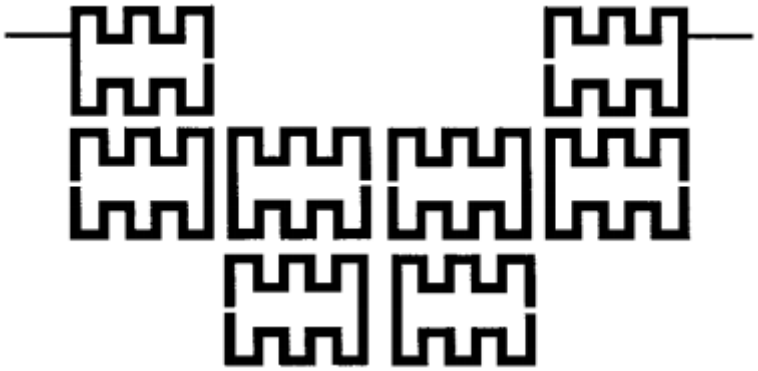

Figure 2.5: Superconducting Microstrip filters.

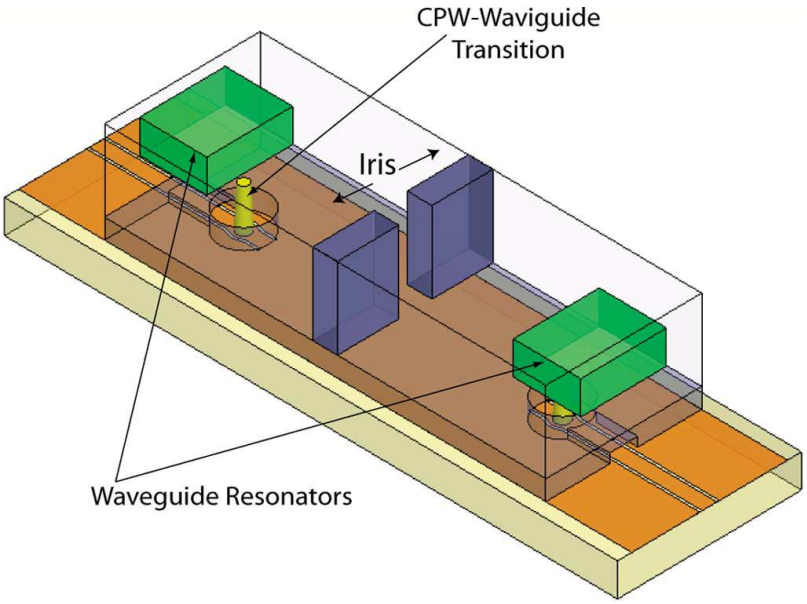

Figure 2.6: W-Band Micro-machined Cavity Filter [16]

2.3 Coupling matrix representation

Coupling between resonators can generally be electric or magnetic or mixed electric-magnetic as illustrated in figure 2.7, In the cases of magnetically coupling resonators, using Kirchhoff's voltage law, the loop equations are derived from the equivalent lumped element circuit model shown in figure 2.8 (a), and represented in impedance matrix form; whereas for electrically coupled resonator, using Kirchhoff's current law, node equations are derived from the equivalent lumped element circuit model in figure 2.8 (b) and represented in admittance matrix form. The derivations show that the normalized admittance matrix has identical form to the normalized impedance matrix [10].

2.3.1 Circuits with magnetically coupled resonators

Figure 2.8 (a) is an equivalent circuit of n-coupled resonators *L*, *C*, and *R* denote the inductance, capacitance and resistance, respectively [10].

Using Kirchhoff's voltage law, the loop equations are derived as follows,

$$\begin{aligned}
&\left(R_1 + jwL_1 + \frac{1}{jwC_1}\right)i_1 - jwL_{12}i_2 \cdots - jwL_{1n}i_n = e_s \\
&-jwL_{12}i_1 + \left(jwL_2 + \frac{1}{jwC_2}\right)i_2 \cdots - jwL_{2n}i_n = 0 \\
&\vdots \\
&-jwL_{n1}i_1 - jwL_{n2}i_n + \ldots + jwL_{(n-1)2}i_{(n-1)} + \left(R_n + jwL_n + \frac{1}{jwC_n}\right)i_n = 0
\end{aligned} \tag{2.1}$$

Where $L_{ij} = L_{ji}$ denotes the mutual inductance between resonators *i* and *j*, which can be represented in matrix form

$$\begin{bmatrix}
R_1 + jwL_1 + \frac{1}{jwC_1} & -jwL_{12} & \cdots & -jwL_{1n} \\
-jwL_{21} & jwL_2 + \frac{1}{jwC_2} & \cdots & -jwL_{2n} \\
 & \vdots & & \\
-jwL_{n1} & -jwL_{n2} & \cdots & R_n + jwL_n + \frac{1}{jwC_n}
\end{bmatrix}
\begin{bmatrix} i_1 \\ i_2 \\ \vdots \\ i_n \end{bmatrix} =
\begin{bmatrix} e_s \\ 0 \\ \vdots \\ 0 \end{bmatrix} \tag{2.2}$$

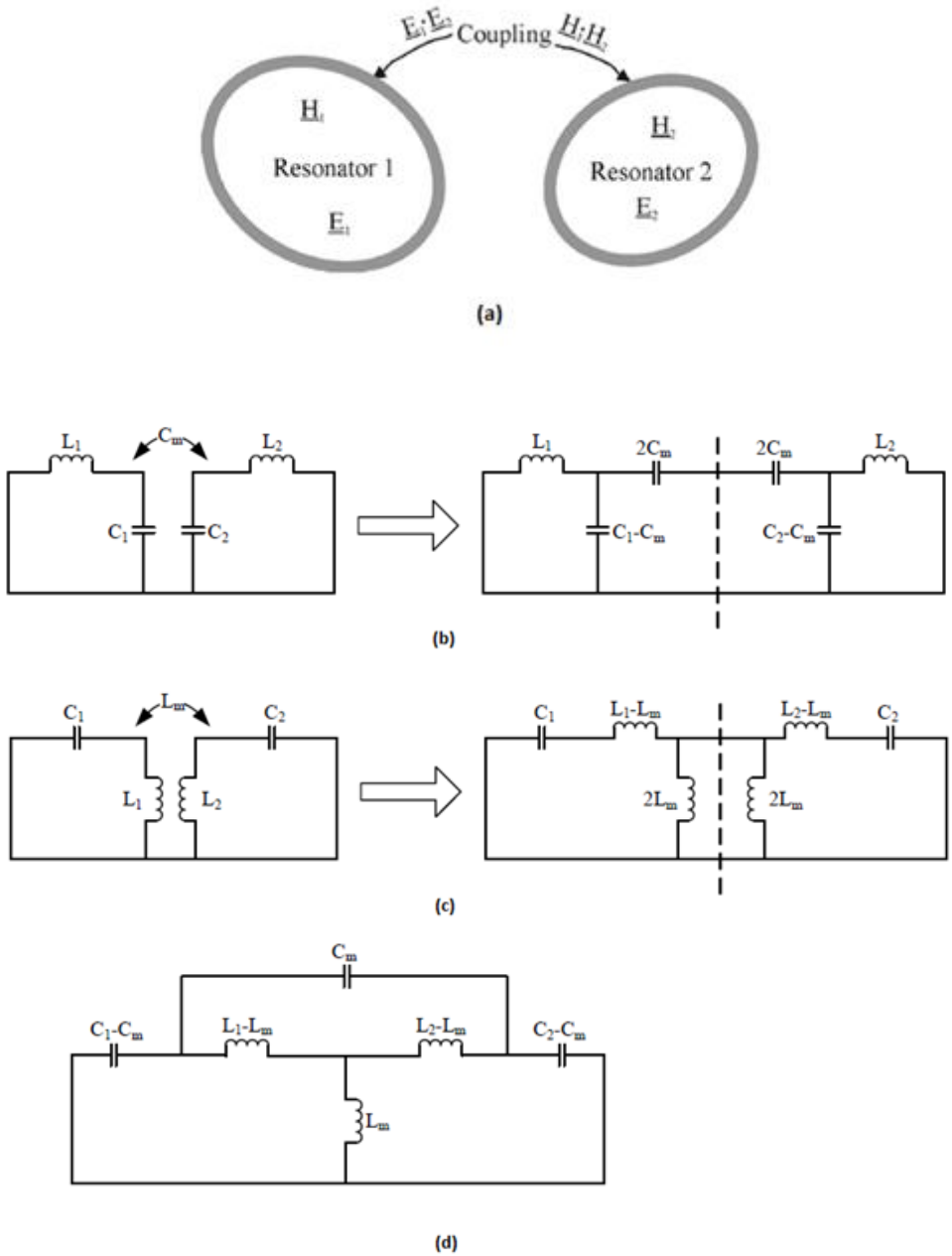

Figure 2.7: Inter-coupling between coupled resonators. (a) General coupled RF/microwave resonators where resonators 1 and 2 can be different in structure and have different resonant frequencies (b) Coupled resonator circuit with electric coupling. (c) Coupled resonator circuit with magnetic coupling. (d) Coupled resonator circuit with mixed electric and magnetic coupling.

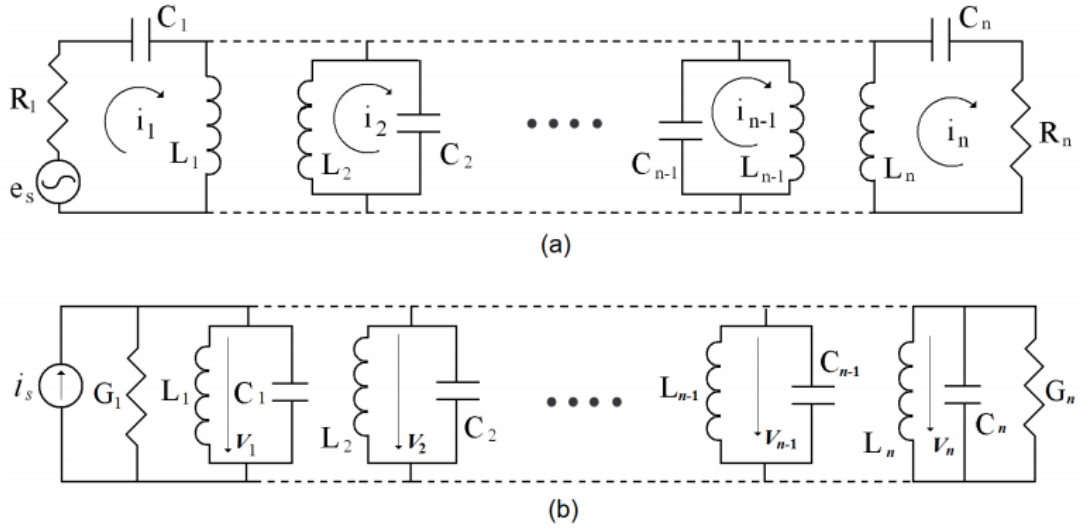

Figure 2.8: (a) Equivalent circuit of magnetically resonator filters, (b) Equivalent circuit of electrically resonator filters.

Equation 2.2 can be written in the form:

$$[Z].[i]=[e]$$

Where $[Z]$ $n\times n$ impedance matrix, for is simplicity, let us first consider a synchronously tuned filter; in this case, all the resonators have the same resonant frequency $\omega_0 = 1/\sqrt{LC}$, where $L=L_1=L_2=\cdots L_n$ and $C=C_1=C_2=\cdots C_n$; The impedance matrix $[Z]$ can be expressed by $[Z]=\omega_0 L.FBW.[\overline{Z}]$, where FBW= $\Delta\omega/\omega_0$ is the fractional bandwidth, and $[\overline{Z}]$ is the normalized impedance matrix, given by,

$$[\overline{Z}]=\begin{bmatrix} \frac{R_1}{\omega_0 L(FBW)}+P & -\frac{jwL_{12}}{\omega_0 L}\frac{1}{FBW} & \cdots & -\frac{jwL_{1n}}{\omega_0 L}\frac{1}{FBW} \\ -\frac{jwL_{21}}{\omega_0 L}\frac{1}{FBW} & P & \cdots & -\frac{jwL_{2n}}{\omega_0 L}\frac{1}{FBW} \\ & \vdots & & \\ -\frac{jwL_{n1}}{\omega_0 L}\frac{1}{FBW} & -\frac{jwL_{n2}}{\omega_0 L}\frac{1}{FBW} & \cdots & \frac{R_n}{\omega_0 L(FBW)}+P \end{bmatrix} \quad (2.3)$$

With $P=\frac{j}{FBW}\left(\frac{\omega}{\omega_0}-\frac{\omega_0}{\omega}\right)$ is the complex low pass frequency variable. It should be

Noticed that for series external circuit:

$$\frac{R_i}{\omega_0 L} = \frac{1}{Q_{ei}} \qquad \text{For i=}1,\ n \tag{2.4}$$

Q_{e1} and Q_{en} are the external quality factors of the input and output resonators, respectively. Defining the coupling coefficients as:

$$K_{ij}=L_{ij}/L \tag{2.5}$$

We can simplify equation (2.3)

$$\overline{[Z]} = \begin{bmatrix} \frac{1}{q_{e1}} + P & -jk_{12} & \cdots & -jk_{1n} \\ -jk_{21} & P & \cdots & -jk_{2n} \\ & \vdots & & \\ -jk_{n1} & -jk_{n2} & \cdots & \frac{1}{q_{en}} + P \end{bmatrix} \tag{2.6}$$

where q_{ei} is the scaled external quality factor ($q_{ei} = Q_{ei}.FBW$) and k_{ij} is the normalized coupling coefficient ($K_{ij} = k_{ij}.FBW$).A network representation of the circuit of figure 2.8 (a) is shown in figure 2.9, where V_1, V_2 and I_1, I_2 are the voltage and current variables at the filter ports and the wave variables are denoted by a_1, b_1, a_2, b_2. By inspecting the circuit of figure 2.8 (a) and the network of figure 2.9, it can be identified that $I_1 = i_1, I_2 = -i_n$ and $V_1 = e_s - i_i R_1$ [10]

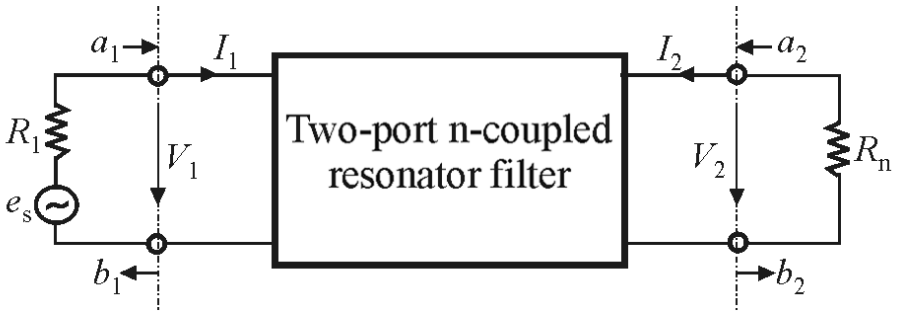

Figure 2.9: Equivalent circuits of n-coupled resonators

We have

$$a_1 = \frac{e_s}{2\sqrt{R_1}} \qquad b_1 = \frac{e_s - 2i_1R_1}{2\sqrt{R_1}}$$

$$a_2 = 0 \qquad b_2 = i_n\sqrt{R_n} \tag{2.7}$$

And, hence,

$$S_{11} = \frac{b_1}{a_1}\Big|_{a_2=0} = 1 - \frac{2R_1i_1}{e_s}$$

$$S_{21} = \frac{b_2}{a_1}\Big|_{a_2=0} = \frac{2\sqrt{R_1R_n}\,i_n}{e_s} \tag{2.8}$$

Solving equation (2.1) for i_1 and i_n, we obtained

$$i_1 = \frac{e_s}{\omega_0 L.FBW}[\overline{Z}]_{11}^{-1}$$

$$i_n = \frac{e_s}{\omega_0 L.FBW}[\overline{Z}]_{n1}^{-1} \tag{2.9}$$

and by substitution of equations (2.9) into equations (2.8), we have,

$$S_{11} = 1 - \frac{2R_1}{\omega_0 L.FBW}[\overline{Z}]_{11}^{-1}$$

$$S_{21} = \frac{2\sqrt{R_1R_n}}{\omega_0 L.FBW}[\overline{Z}]_{n1}^{-1} \tag{2.10}$$

In terms of external quality factors $q_{ei} = \omega_0 L.FBW / R_i$, the S-parameters become,

$$S_{11} = 1 - \frac{2}{q_{e1}} \overline{[Z]}_{11}^{-1}$$

$$S_{21} = \frac{2}{\sqrt{q_{e1} q_{en}}} \overline{[Z]}_{n1}^{-1} \tag{2.11}$$

In the case that the coupled-resonator circuit of figure 2.7 (a) is asynchronously tuned, and the resonant frequency of each resonator, which may be different, is given by $\omega_{0i} = 1/\sqrt{L_i C_i}$, the coupling coefficient of asynchronously tuned filter is defined as

$$K_{ij} = \frac{L_{ij}}{\sqrt{L_i L_j}} \text{ For } i \neq j \tag{2.12}$$

It can be shown that equation (2.6) becomes

$$\overline{[z]} = \begin{bmatrix} \frac{1}{q_{e1}} + P - jk_{11} & -jk_{12} & \cdots & -jk_{1n} \\ -jk_{21} & P - jk_{21} & \cdots & -jk_{2n} \\ & \vdots & & \\ -jk_{n1} & -jk_{n2} & \cdots & \frac{1}{q_{en}} + P - jk_{nn} \end{bmatrix} \tag{2.13}$$

2.3.2 Circuits with electrically coupled resonators

As can be seen, the coupling coefficients introduced in the above section are all based on mutual inductance and, hence, the associated couplings are magnetic couplings. The formulation of the coupling coefficients that result from a two-port n-coupled resonator filter with electric couplings will be explained in this section. Let us consider the *n*-coupled-resonator circuit shown in figure 2.8 b, where v_i denotes the node voltage, *G* represents the conductance, and i_s is the source current [10]. According to the current law, which is the other one of Kirchhoff's two circuit laws and states that the algebraic sum of the currents leaving a node in a network is zero, with a driving or external current of i_s the node equations for the circuit of figure 2.8 b are [10]

$$\begin{aligned}
&\left(G_1 + jwC_1 + \frac{1}{jwL_1}\right)v_1 - jwC_{12}v_2 \cdots - jwC_{1n}v_n = i_s \\
&- jwC_{12}i_1 + \left(jwC_2 + \frac{1}{jwL_2}\right)v_2 \cdots - jwC_{2n}v_n = 0 \\
&\vdots \\
&- jwC_{n1}v_1 - jwC_{n2}v_n + ... + jwC_{(n-1)2}v_{(n-1)} + \left(G_n + jwC_n + \frac{1}{jwL_n}\right)v_n = 0
\end{aligned} \tag{2.14}$$

where $C_{ij} = C_{ji}$ denotes the mutual capacitance between resonators a and b. The matrix form representation of these equations is as follows,

$$\begin{bmatrix}
G_1 + jwC_1 + \frac{1}{jwL_1} & - jwC_{12} & \cdots & - jwC_{1n} \\
- jwC_{21} & jwC_2 + \frac{1}{jwL_2} & \cdots & - jwC_{2n} \\
 & \vdots & & \\
- jwC_{n1} & - jwC_{n2} & \cdots & G_n + jwC_n + \frac{1}{jwL_n}
\end{bmatrix}
\begin{bmatrix} v_1 \\ v_2 \\ \vdots \\ v_n \end{bmatrix} =
\begin{bmatrix} i_s \\ 0 \\ \vdots \\ 0 \end{bmatrix} \tag{2.15}$$

$[Y].[v] = [i]$, where $[Y]$ is the admittance matrix.

Similarly, the admittance matrix in equation (2.15) may be expressed by

$$[Y] = \omega_0 C.FBW.[\overline{Y}] \tag{2.16}$$

Where $\omega_0 = 1/\sqrt{LC}$ is the mid band frequency of filter, FBW is the fractional bandwidth and $[\overline{Y}]$ is the normalized admittance matrix. In the case of synchronously tuned filter, $[\overline{Y}]$ is given by

$$[\overline{Y}] = \begin{bmatrix}
\frac{G_1}{\omega_0 C(FBW)} + P & -\frac{jwC_{12}}{\omega_0 C}\frac{1}{FBW} & \cdots & -\frac{jwC_{1n}}{\omega_0 C}\frac{1}{FBW} \\
-\frac{jwl_{21}}{\omega_0 L}\frac{1}{FBW} & P & \cdots & -\frac{jwC_{2n}}{\omega_0 C}\frac{1}{FBW} \\
 & \vdots & & \\
-\frac{jwC_{n1}}{\omega_0 C}\frac{1}{FBW} & -\frac{jwC_{n2}}{\omega_0 C}\frac{1}{FBW} & \cdots & \frac{G_n}{\omega_0 C(FBW)} + P
\end{bmatrix} \tag{2.17}$$

Where p is the complex low pass frequency variable, Notice that:

$$\frac{G_i}{\omega_0 C} = \frac{1}{Q_{ei}} \quad \text{For i=}1, n \tag{2.18}$$

Q_{e1} and Q_{en} are the external quality factors of the input and output resonators, respectively. Defining the coupling coefficients as:

$$K_{ij} = \frac{C_{ij}}{C} \tag{2.19}$$

And assume $\omega/\omega_0 \approx 1$ for the narrow-band approximation. A simpler expression of equation (2.17) is obtained:

$$\overline{[Y]} = \begin{bmatrix} \frac{1}{q_{e1}} + P & -jk_{12} & \cdots & -jk_{1n} \\ -jk_{21} & P & \cdots & -jk_{2n} \\ & \vdots & & \\ -jk_{n1} & -jk_{n2} & \cdots & \frac{1}{q_{en}} + P \end{bmatrix} \tag{2.20}$$

Where $q_{ei} = Q_{ei}.FBW$ the scaled external quality is factor, and $K_{ij} = k_{ij}.FBW$ is the normalized coupling coefficient.

Similarly, it can be shown that if the coupled-resonator circuit of figure 2.7 (b) is asynchronously tuned, equations. (2.20) and (2.21) become

$$\overline{[Y]} = \begin{bmatrix} \frac{1}{q_{e1}} + P - jk_{11} & -jk_{12} & \cdots & -jk_{1n} \\ -jk_{21} & P - jk_{21} & \cdots & -jk_{2n} \\ & \vdots & & \\ -jk_{n1} & -jk_{n2} & \cdots & \frac{1}{q_{en}} + P - jk_{nn} \end{bmatrix} \tag{2.21}$$

To derive the two-port *S*-parameters of coupled-resonator filter, the circuit of figure 2.8 b is represented by a two-port network of figure 2.10, where all the variables at the filter ports are the same as those in Figure 2.9. In this case, $V_1 = v_1$, $V_2 = -v_n$, and $I_1 = i_s - v_1 G_1$

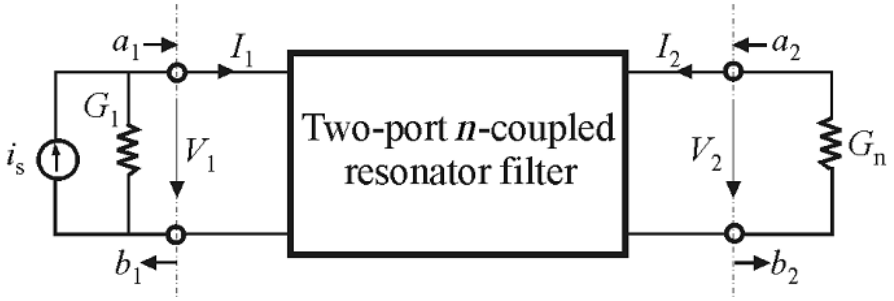

Figure 2.10: Equivalent circuit of n-coupled resonators

$$a_1 = \frac{i_s}{2\sqrt{G_1}} \qquad b_1 = \frac{i_s - 2i_1 G_1}{2\sqrt{G_1}}$$

$$a_2 = 0 \qquad b_2 = v_n\sqrt{G_n} \tag{2.22}$$

$$S_{11} = \frac{b_1}{a_1}\Big|_{a_2=0} = 1 - \frac{2G_1 v_1}{i_s}$$

$$S_{21} = \frac{b_2}{a_1}\Big|_{a_2=0} = \frac{2\sqrt{G_1 G_n}\,v_n}{i_s} \tag{2.24}$$

Finding the unknown node voltages v_1, and v_n, from equation (2.15)

$$v_1 = \frac{i_s}{\omega_0 C.FBW}\overline{[Y]}_{11}^{-1}$$

$$v_n = \frac{i_s}{\omega_0 C.FBW}\overline{[Y]}_{n1}^{-1} \tag{2.25}$$

and by substitution of equations (2.25) into equations (2.24), we have,

$$S_{11} = 1 - \frac{2G_1}{\omega_0 C.FBW}\overline{[Y]}_{11}^{-1}$$

$$S_{21} = \frac{2\sqrt{G_1 G_n}}{\omega_0 C.FBW}\overline{[Y]}_{n1}^{-1} \tag{2.26}$$

This can be simplified as

$$S_{11} = 1 - \frac{2}{q_{e1}} \overline{[Y]}_{11}^{-1}$$

$$S_{21} = \frac{2}{\sqrt{q_{e1} q_{en}}} \overline{[Y]}_{n1}^{-1} \tag{2.27}$$

2.3.3 General coupling matrix

In the foregoing formulations, the most notable is that the formulation of normalized impedance matrix $\overline{[Z]}$ is identical to that of normalized admittance matrix $\overline{[Y]}$. This is very important, because it implies that we could have a unified formulation for a *n*-coupled resonator filter regardless of whether the couplings are magnetic or electric or even the combination of both. Accordingly, equations (2.11) and (2.27) may be incorporated into a general one [10]:

$$S_{21} = \frac{2}{\sqrt{q_{e1} q_{en}}} [A]_{n1}^{-1}$$

$$S_{11} = \pm \left(1 - \frac{2}{q_{e1}} [A]_{11}^{-1} \right) \tag{2.28}$$

with

$$[A] = [q] + p\,[U] - j[k] \tag{2.29}$$

$$[A] = \begin{bmatrix} \frac{1}{q_{e1}} & \cdots & 0 & \cdots & 0 \\ \vdots & \ddots & \vdots & \vdots & \vdots \\ 0 & \cdots & 0 & \cdots & 0 \\ \vdots & \vdots & \vdots & \ddots & \vdots \\ 0 & \cdots & 0 & \cdots & \frac{1}{q_{en}} \end{bmatrix} + p \begin{bmatrix} 1 & \cdots & 0 & 0 \\ \vdots & \ddots & \vdots & \vdots \\ 0 & \cdots & 1 & 0 \\ 0 & \cdots & 0 & 1 \end{bmatrix} - j \begin{bmatrix} k_{11} & \cdots & k_{1(n-1)} & k_{1n} \\ \vdots & \ddots & \vdots & \vdots \\ k_{(n-1)1} & \cdots & k_{(n-1)(n-1)} & k_{(n-1)n} \\ k_{n1} & \cdots & k_{n(n-1)} & k_{nn} \end{bmatrix} \tag{2.30}$$

where $[U]$ is the $n \times n$ unit or identity matrix, p is the complex lowpass frequency variable, $[q]$ is an $n \times n$ matrix with all entries zero, except for $q_{11} = 1/q_{e1}$ and $q_{nn} = 1/q_{en}$, and $[k]$ is the so-called general coupling matrix, which is an $n \times n$ reciprocal matrix (that is, $k_{ij} = k_{ji}$) and is allowed to have nonzero diagonal entries k_{ii} for an asynchronously tuned filter [10].

2.3.4 General theory of coupling

A general technique for designing coupled resonator filters is based on coupling coefficients of inter-coupled resonators and the external Q_e factors of the input and output resonators. The external quality factor Q_e is characterized the external coupling between a microwave resonator and the external circuit, which is shown as Q_{ea} and Q_{eb} in figure 2.11 [10].

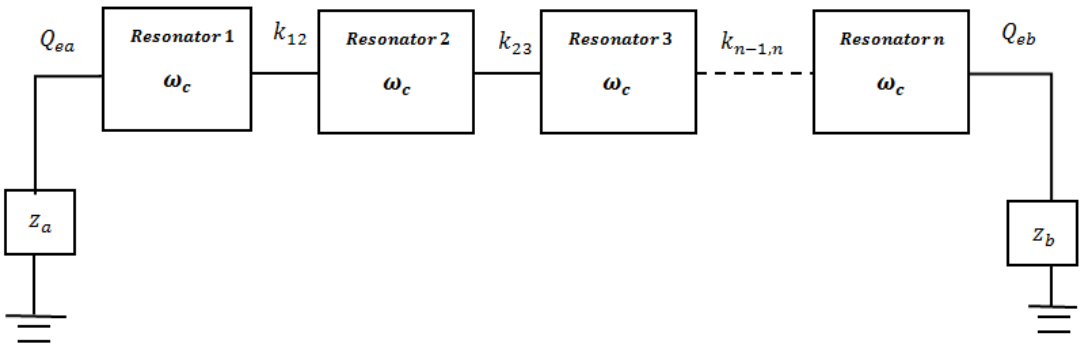

Figure 2.11: Block Diagram of Microwave Filter structure

2.3.4.1 Coupling coefficient

The coupling K_{ij} coefficient of two coupled microwave resonators can be defined on the basis of the ratio of coupled energy to stored energy. It can be defined mathematically [10]

$$K_{12} = \frac{\iiint \varepsilon \underline{E}_1 \bullet \underline{E}_2 dv}{\sqrt{\iiint \varepsilon |\underline{E}_1|^2 dv \times \iiint \varepsilon |\underline{E}_2|^2 dv}} + \frac{\iiint \mu \underline{H}_1 \bullet \underline{H}_2 dv}{\sqrt{\iiint \mu |\underline{H}_1|^2 dv \times \iiint \mu |\underline{H}_2|^2 dv}} \qquad (2.31)$$

where E and H represent the electric and magnetic field vectors, respectively; The interaction of the coupled resonator is mathematically described by the dot operation of their space vector fields, which allows the coupling to have either

positive or negative sign. A positive sign would imply that the coupling enhances the stored energy of uncoupled resonators, whereas a negative sign would indicate a reduction. Therefore, the electric and magnetic coupling could either have same effect if they have the same sign, or have the opposite effect if their signs are opposite [10].

The magnitude of the coupling coefficient defines the separation *d* of the two resonance peaks (as illustrated in figure 2.12). Normally the stronger coupling the wider separation *d* of the two resonance peaks $|S_{21}|$ and deeper the trough in the middle [10].

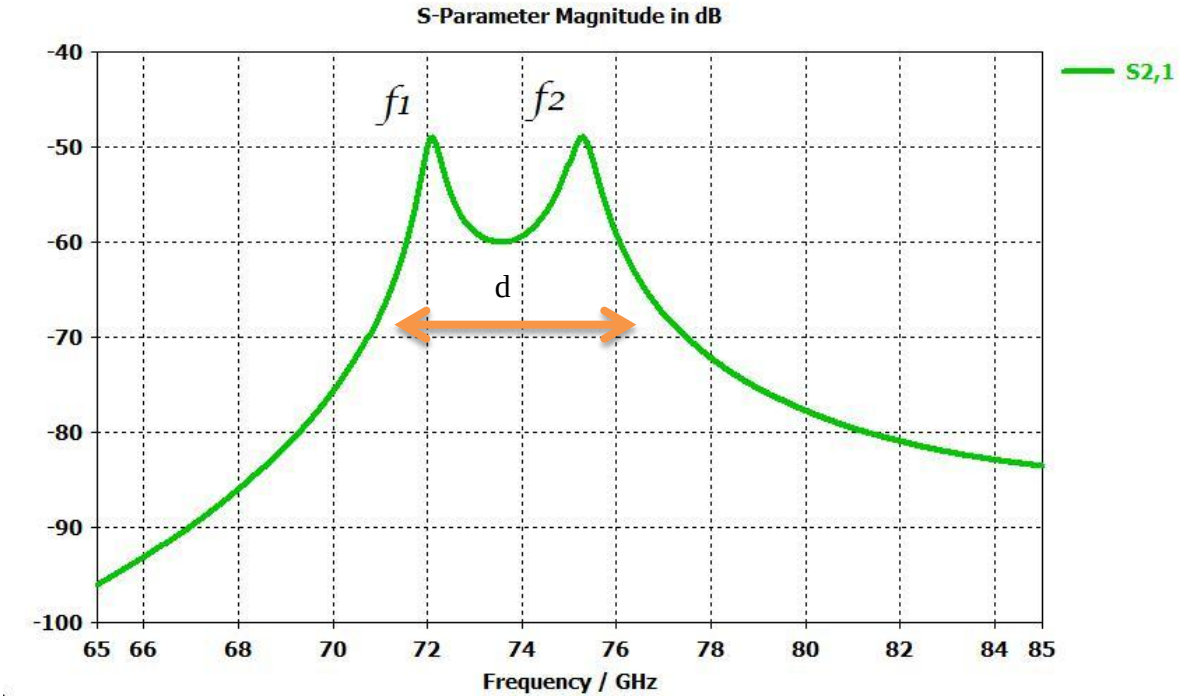

Figure 2.12: Resonant response of coupled resonator structure

The coupling coefficient can be defined in terms of f_1 and f_2

$$K = \pm \frac{f_2^{\,2} - f_1^{\,2}}{f_2^{\,2} + f_1^{\,2}} \qquad (2.32)$$

f_1 Is the lower resonance frequency and f_2 is the higher resonance frequency.

2.4 Quality factors of microwave filter

The quality factor Q is useful measure of sharpness and energy loss of resonator circuit. It can be defined as [10]:

$$Q = \omega \frac{\text{average energy stored}}{\text{average energy loss/second}}$$

As can been from this definition, low loss implies a higher quality factor, Q .

External quality factor Q_e can be defined in terms of resonance frequency f_0 and bandwidth Δf of the resonator circuit, which is stated below [16]

$$Q_e = \frac{f_0}{\Delta f} \tag{2.33}$$

$$\Delta f = f_2 - f_1$$

A high Q factor results in a steep roll-off and narrow bandwidth of the resonator as shown in figure 2.13 [16].

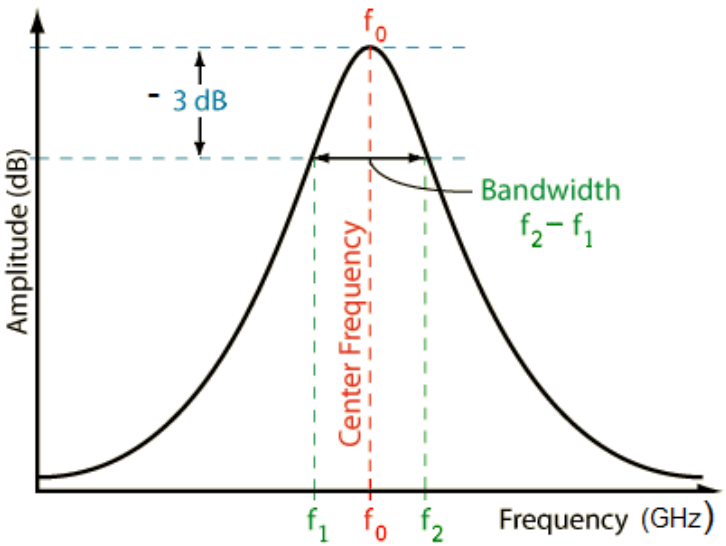

Figure 2.13: Graph of quality factor [16]

2.5 Filter design procedure

2.5.1 Chebyshev response

The response of a chebyshev filter has an equal ripple in the passband and a maximally flat stopband as shown in figure 2.14. The transfer function of the chebyshev response is described by the amplitude square of the S_{21} as follows [10]:

$$\left|S_{21}(j\Omega)\right|^2 = \frac{1}{1+\varepsilon^2 T_n^{\,2}(\Omega)} \tag{2.34}$$

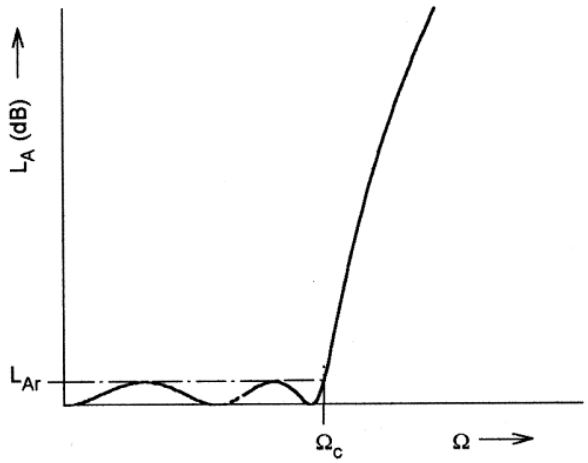

Figure 2.14: Chebyshev lowpass filter response.

Where ε is the ripple constant and given by:

$$\varepsilon = \sqrt{10^{\frac{L_{Ar}}{10}} - 1} \tag{2.35}$$

where L_{Ar} is the passband ripple in dB.

$T_n(\Omega)$ Is first kind chebyshev function of order n, defined by:

$$T_n(\Omega) = \begin{cases} \cos(n\cos^{-1}\Omega) & |\Omega| \le 1 \\ \cosh(n\cosh^{-1}\Omega) & |\Omega| \ge 1 \end{cases} \tag{2.36}$$

The chebyshev filter has the following general rational transfer function [10]:

$$S_{21}(P) = \frac{\prod_{i=1}^{n}\left[\eta^2 + \sin^2(i\pi/n)\right]^{1/2}}{\prod_{i=1}^{n}\left[p + p_i\right)]} \tag{2.37}$$

With

$$p_i = j\cos\left[\sin^{-1} j\eta + \frac{(2i-1)\pi}{2n}\right] \tag{2.38a}$$

$$\eta = \sinh\left(\frac{1}{h}\sinh^{-1}\frac{1}{\varepsilon}\right) \tag{2.38b}$$

All the transmission zeros of the transfer function are located at infinity. Therefore, chebyshev filters are known as all pole filters. The poles of the chebyshev filter are located on an ellipse in the left half plane with major axis of size $\sqrt{1+\eta^2}$ on the $j\Omega$-axis and minor axis of size η on the σ-axis [10]. For an 5^{th} order chebyshev filter, the pole distribution is shown in figure 2.15.

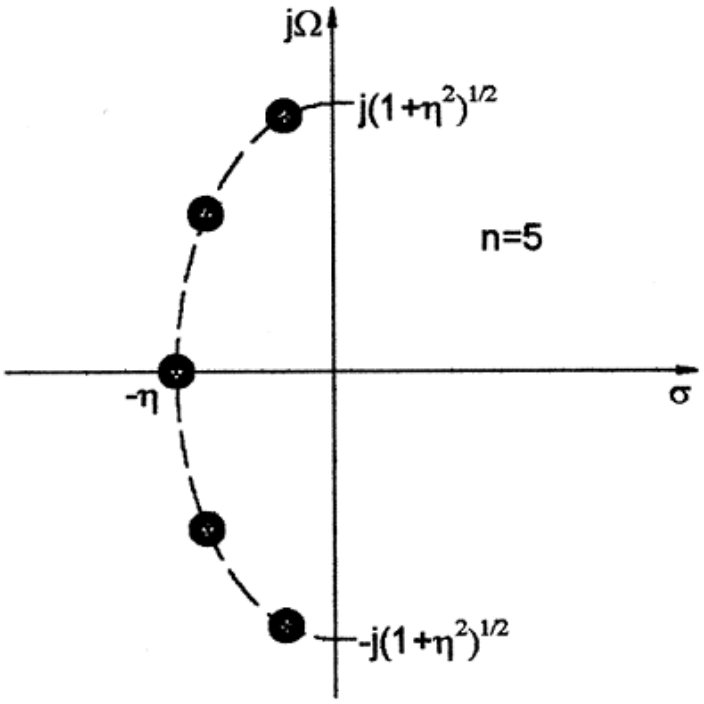

Figure 2.15: Pole distribution for chebyshev response.

Lowpass prototype filters generally have the element values normalized to make the source resistance equal to one (g_0=1), and the angular cutoff frequency Ω_c =1 (rad/sec). Generally, n-pole lowpass prototype for Butterworth, Chebyshev and Gaussian responses have two possible forms that give the same response. The forms are dual from each other and are shown in figure 2.16.

g_i For *i=1 ... n* represents series inductor or shunt capacitor, where n is the order of the filter and represents the number of reactive elements in the prototype structure. g_0 is known as the source resistance or inductance, whereas g_n +1 is defined as the load resistance or the load conductance [10].

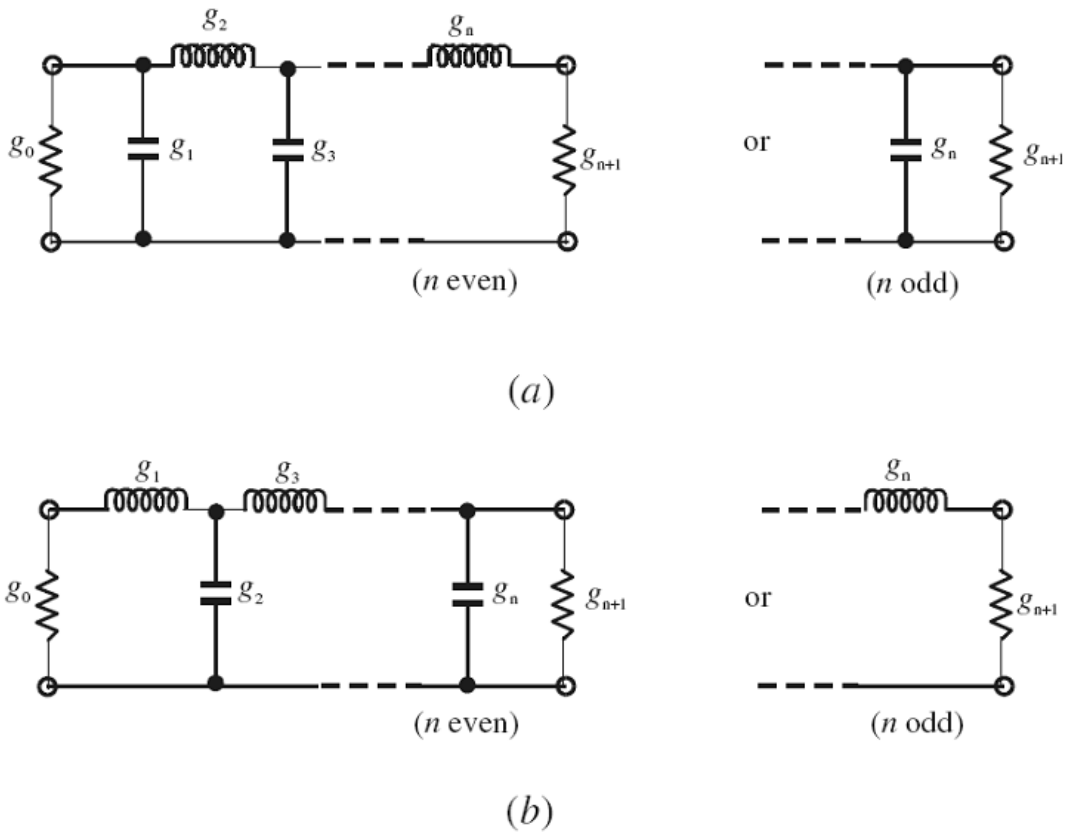

Figure 2.16: N-pole lowpass prototype filters with (a) ladder structure and (b) its dual.

2.5.2 Chebyshev lowpass prototype filters

The element values for chebyshev lowpass prototype networks shown in Figure 2.16 can be computed for a given passband ripple L_{Ar} dB and angular cutoff frequency of Ω_c =1 (rad/sec) using the following equations [10]:

$$g_0 = 1 \tag{2.39}$$

$$g_1 = \frac{2}{\gamma}\sin\left(\frac{\pi}{2N}\right) \tag{2.40}$$

$$g_i = \frac{1}{g_{i-1}} \frac{4\, sin\left[\frac{(2i-1)\pi}{2N}\right].sin\left[\frac{(2i-3)\pi}{2N}\right]}{\gamma^2 + sin^2\left[\frac{(i-1)\pi}{N}\right]} \quad = 1,2,3,\ldots..N \tag{2.41}$$

$$g_{N+1} = \begin{cases} 1 & N-odd \\ \coth^2\left(\frac{\beta}{4}\right) & N-even \end{cases} \tag{2.42}$$

Where

$$\beta = \ln\left[\coth\left(\frac{L_{Ar}}{17.37}\right)\right] \tag{2.43}$$

$$\gamma = \sinh\left(\frac{\beta}{2N}\right) \tag{2.44}$$

The element values for chebyshev lowpass prototype network for passband ripple L_{Ar} =0.04321dB are given in Table 2.1 for filter order of n=1 to 9, g_0 =1, and Ω_c =1 and others passband ripple tables for L_{Ar} =0.1dB , L_{Ar} =0.01dB can be found in [10]

Table 2.1: Element values for Chebyshev lowpass prototype for L_{Ar} =0.04321 dB.

n	g_1	g_2	g_3	g_4	g_5	g_6	g_7	g_8	g_9	g_{10}
1	0.2	1.0								
2	0.6648	0.5445	1.221							
3	0.8516	1.1032	0.8516	1.0						
4	0.9314	1.2920	1.5775	0.7628	1.2210					
5	0.9714	1.3721	1.8014	1.3721	0.9714	1.0				
6	0.9940	1.4131	1.8933	1.5506	1.7253	0.8141	1.2210			
7	1.008	1.4368	1.9398	1.6220	1.9398	1.4368	1.008	1.0		
8	1.0171	1.4518	1.9667	1.6574	2.0237	1.6107	1.7726	0.8330	1.2210	
9	1.0235	1.4619	1.9837	1.6778	2.0649	1.6778	1.9837	1.4619	1.0235	1.0

The order of the filter is determined according to the required specifications; such as the minimum stopband attenuation L_{As} dB at $\Omega = \Omega_s$ for Ω_s >1 and passband ripple L_{Ar} dB. The order of Chebyshev lowpass prototype response is calculated by [10]:

$$n \geq \frac{\cosh^{-1}\sqrt{\frac{10^{0.1L_{As}}-1}{10^{0.1L_{Ar}}-1}}}{\cosh^{-1}\Omega_s} \tag{2.45}$$

2.5.3 Bandpass transformation

To transform lowpass prototype to bandpass response with passband edge angular Frequencies of ω_1 and ω_2, the following transformation formula is used [10]:

$$\Omega = \frac{\Omega_c}{\text{FBW}}\left(\frac{\omega}{\omega_0} - \frac{\omega_0}{\omega}\right) \tag{2.46}$$

With

$$FBW = \frac{\omega_2 - \omega_1}{\omega_0} \quad \text{And} \quad \omega_0 = \sqrt{\omega_1\omega_2} \tag{2.47}$$

Where FBW is the fractional bandwidth and ω_0 is the center angular frequency. For inductive element in the prototype network, the reactance is [10]:

$$\Omega_g \rightarrow \omega\frac{\Omega_c g}{FBW\ \omega_0} - \frac{1}{\omega}\frac{\Omega_c\omega_0 g}{FBW} = \omega L - \frac{1}{\omega C} \tag{2.48}$$

So, the inductive element g in the lowpass prototype network is transformed to a series LC resonator in the Bandpass filter. The elements of the series resonator taking in consideration the impedance scaling are [10]:

$$L_s = \left(\frac{\Omega_c}{FBW\ \omega_0}\right)\gamma_0 g \qquad C_s = \left(\frac{FBW}{\omega_0\Omega_c}\right)\frac{1}{\gamma_0 g} \tag{2.49}$$

Similarly, for capacitive element g in the lowpass prototype network, the admittance is:

$$\Omega_g \rightarrow \omega \frac{\Omega_c g}{FBW\ \omega_0} - \frac{1}{\omega} \frac{\Omega_c \omega_0 g}{FBW} = \omega C - \frac{1}{\omega L} \tag{2.50}$$

So, the capacitive element g in the lowpass prototype network is transformed to a parallel LC resonator in the Bandpass filter. The elements of the parallel resonator taking in consideration the impedance scaling are:

$$L_p = \left(\frac{FBW}{\omega_0 \Omega_c} \right) \frac{\gamma_0}{g} \qquad C_p = \left(\frac{\Omega_c}{FBW\ \omega_0} \right) \frac{g}{\gamma_0} \tag{2.51}$$

Note that the center angular frequency is $\omega_0 = \frac{1}{\sqrt{LC}}$, and hence for series resonator $\omega_0 L_s = \frac{1}{\omega_0 C_s}$, and for parallel resonator $\omega_0 L_p = \frac{1}{\omega_0 C_p}$ [10].

$$\gamma_0 = \begin{cases} Z_0 / g_0 & for\ g_0 \text{ being the resistance} \\ g_0 / Y_0 & for\ g_0 \text{ being the conductance} \end{cases}$$

The lowpass prototype to bandpass element transformation is shown in figure 2.17. [10]

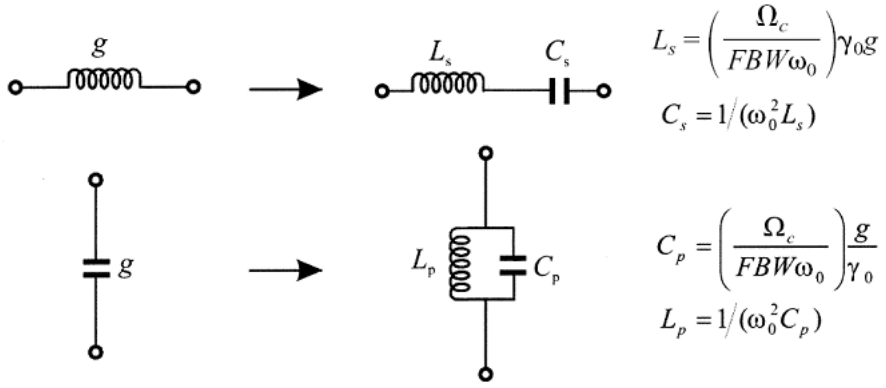

Figure 2.17: Basic element transformation from lowpass prototype to bandpass.

The transformation of the lowpass prototype of the circuit shown in figure 2.16 to bandpass is shown in figure 2.18. [10]

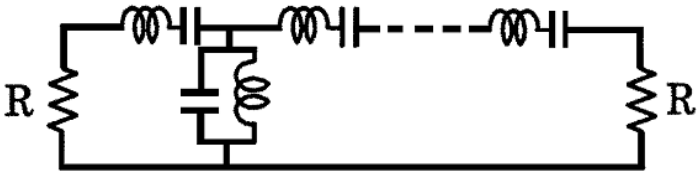

Figure 2.18: Lumped element Bandpass filter.

The J and K inverters are used to convert the previous circuit to an equivalent form that is more suitable for implementation. The use of J inverters makes the circuit with only parallel resonators as shown in figure 2.19 (a), whereas the use of k inverters makes the circuit with only series resonators as shown in figure 2.19 (b) [18]. The J and K inverters are called impedance/admittance inverters, and there are various forms that operate as admittance invertors [10].

The J inverters in in figure 2.19 (a) can be replaced by π-type capacitors and the resulting circuit will contain shunt resonators connected by series capacitors as shown in Figure 2.20 (a) , and the capacitors represent capacitive coupling coefficients between adjacent resonators [10].

Similarly, the K inverters can be replaced by inductors and the resulting circuit will contain series resonators connected by parallel inductors as shown in Figure 2.20 (b) , and the inductors represent inductive coupling coefficients between adjacent resonators. [17] The lumped LC resonators shown in figure 2.20 can be replaced by distributed circuits such as microwave resonators, but this is convenient only for narrow band filters because the reactance or susceptance of the microwave resonators are approximately equal to those of lumped elements only near resonance, which is a small frequency range [10].

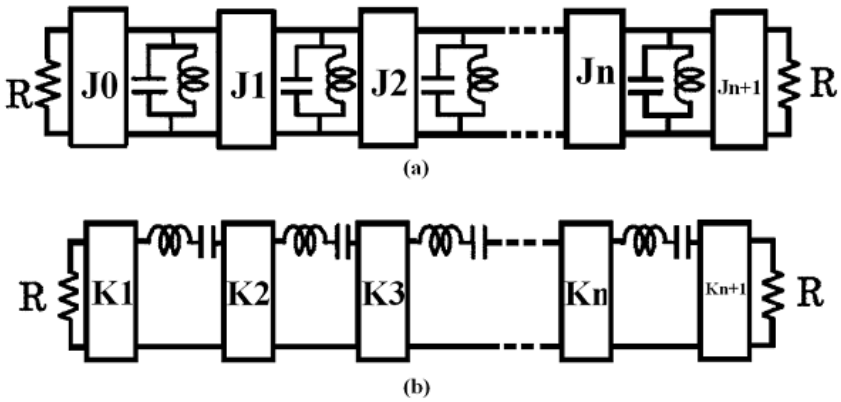

Figure 2.19: Bandpass filter using (a) J-inverters. (b) K-inverters.

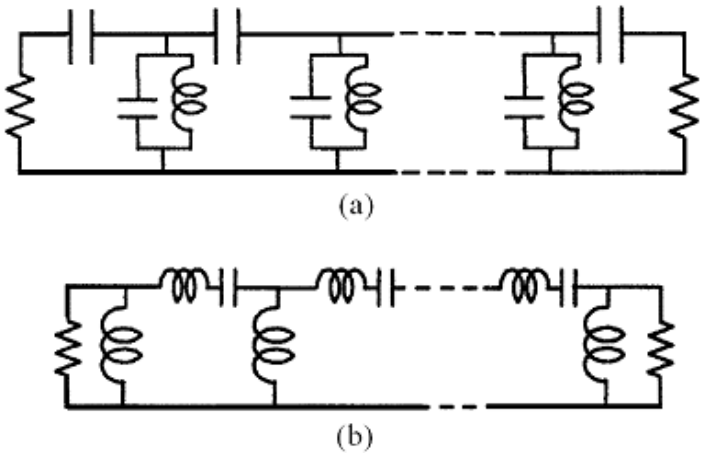

Figure 2.20: Bandpass filter circuits (a) capacitive coupling between resonators (b) inductive Coupling between resonators.

2.5.4 Prototype *k* and *q* values

Define k and q as prototype values, where k represents coupling between two resonators, and q represents the external coupling. The q prototype values can be derived from prototype g vales as follows [19]:

$$q_1 = g_0 g_1 \tag{2.52}$$

$$q_n = \begin{cases} g_n g_{n+1} & for\ n \quad odd \\ g_n / g_{n+1} & for\ n \quad even \end{cases} \tag{2.53}$$

Where q_1 and q_n are related to the input and output coupling respectively. The prototype value is derived from prototype g values as follows:

$$K_{ij} = k_{ij} \frac{BW}{f_0} \tag{2.54}$$

$$Q_1 = q_1 \frac{f_0}{BW} \qquad Q_n = q_n \frac{f_0}{BW} \tag{2.55}$$

Where f_0 is the resonant frequency of the bandpass filter and BW is the absolute bandwidth. Q_e is known as the external quality factor, and the external coupling coefficient is equal to

$$K_e = 1/Q_e \tag{2.56}$$

$$Q_{ea} = \frac{g_0 g_1}{FBW} \tag{2.57}$$

$$Q_{eb} = \frac{g_n g_{n+1}}{FBW} \tag{2.58}$$

And the coupling between resonators is

$$Kc_k = \frac{FBW}{\sqrt{g_k g_{k+1}}} \tag{2.59}$$

$$FBW = \frac{BW}{f_0} \tag{2.60}$$

2.6 Summary

In this chapter coupled resonator networks with two ports have been presented. It has presented the derivation of the coupling matrix of electric and magnetic coupled resonator circuits. The different types of microwave filters despite physical structure have been shown and transformation method of low pass prototype filter to bandpass filter has been discussed. In the next chapter diplexers synthesis will be discussed.

References

[1] R. Levy and S. Cohn, "A history of microwave filter research, design, and development," *IEEE Transaction Microwave Theory Tech., vol. 32, Sept. 1984, pp. 1055-1067.*

[2] R. Levy, R. Snyder, and G. Matthaei, "Design of microwave filters," *IEEE Transaction Microwave. Theory Tech., vol. 50, March 2002, pp. 783-793.*

[3] I. Hunter, L. Billonet, B. Jarry, and P. Guillon, "Microwave filter -applications and technology", *IEEE Transaction Microwave. Theory Tech., vol. 50, March 2002, pp. 794-805.*

[4] B. Rawat and R. Miller,"Design of a Tapered Coaxial Resonator Filter for Mobile Communications", IEEE *Transaction on Vehicular Tech. vol. 41, no. 1, Feb. 1992, pp. 1-5.*

[5] N. Esfahani, P. Rezaee, K. Schünemann, R. Knöchel, M. Tayarani, "Miniaturized Coaxial Cylindrical Cavity Filters Based on Sub-Wavelength Metamaterial Loaded Resonator", IEEE transaction microwave theory tech. 12-16 Sept. 2011, pp. 1086 - 1089.

[6] A. Atia and A. Williams, "Narrow-bandpass waveguide filter," IEEE Trans. Microwave Theory Tech., vol. 20, Apr. 1972, pp. 258.265.

[7] L. Accatino, G. Bertin, and M. Mongiardo, "Elliptical cavity resonators for dual-mode narrow-band filters", IEEE Transaction Microwave. Theory Tech., vol. 45, Dec. 1997 pp. 2393.2401.

[8] C. Wang, H. Yao, K. Zaki, and R. Mansour, "Mixed modes cylindrical planar dielectric resonator filters with rectangular enclosure,", IEEE Transaction Microwave Theory Tech., vol. 43, Dec. 1995, pp. 2817.2823.

[9] H. Yao, C. Wang, and K. Zaki, "Quarter wavelength ceramic combline fitters,", IEEE Transaction Microwave Theory Tech., vol. 44, Dec. 1996, pp. 2673.2679.

[10] J. Hong and M. Lancaster, "Microstrip filters for RF/Microwave applications". New York, NY: John Wiley, 2001.

[11] J. Hong and M. Lancaster, "Couplings of microstrip square open-loop resonators for cross-coupled planar microwave filters," IEEE Transaction Microwave. Theory Tech., vol. 44, Dec. 1996, pp. 2099.2109.

[12] J. Hong and M. Lancaster, "Theory and experiment of novel microstrip slow-wave open-loop resonator filters," IEEE Transaction Microwave. Theory Tech., vol. 45, Dec. 1997, pp. 2658.2665.

[13] J. Hong and M. Lancaster, "Cross-coupled microstrip hairpin resonator filters," *IEEE Transaction Microwave Theory Tech., vol. 46, Jan. 1998, pp. 118.122.*

[14] J. Hong, M. Lancaster, D. Jedamzik and R. Greed, "On the development of superconducting microstrip filters for mobile communications applications," *IEEE Transaction Microwave Theory Tech., vol. 47, Sept. 1999., pp. 1656.1663*

[15] P. Blondy, A. Brown, D. Cros, and G. Rebeiz, "Low loss micro-machined filters for millimeter-wave telecommunication systems", *IEEE MTT-S Int. Microwave Symp. Dig. , June 1998, pp. 1181-1184.*

[16] David M. Pozar, Microwave Engineering, 3rd edition, John Wiley & Sons, 2005.

[17] Y. Li, B. Pan, C. Lugo, M. Tentzeris, and J. Papapolymerou,″ Design and Characterization of a W-Band Micromachined Cavity Filter Including a Novel Integrated Transition From CPW Feeding Lines ", *IEEE transaction microwave theory and tech., VOL. 55, NO. 12, December 2007 USA , pp. 2902-2910*

[18] I. Awai, "Meaning of Resonator's Coupling Coefficient in Bandpass Filter Design" , *J-EAST Electronics and Communications in Japan, Part 2, Vol. 89, No. 6, 2006.*

[19] R. Rhea, "HF Filter Design and Computer Simulation", *Noble Publishing Corporation, USA, 1994.*

Chapter 3

Overview of Microwave Diplexers

3.1 Introduction

In this research, a diplexer design for E-band is proposed. This component will be used as a front-end in the microwave transceiver of a point-to-point in mobile backhaul application that offers Gigabit wireless connectivity over a distance of a mile or more. It is specified to work at the frequency channel bands [CH1: 71-76 GHz and CH2: 81-86 GHz]. The diplexer will be designed using, two methods:

1. Use external waveguide *H-plane T*-junction.
2. Use waveguide *H-plane* manifold structures.

These methods will be explained in depth in the next sections.

3.2 Waveguide T-junction

Waveguide junctions are used when power in a waveguide needs to be split or some extracted. There are a number of different types of waveguide junction that can be use, each type having different properties; the different types of waveguide junction affect the energy contained within the waveguide in different ways [1].

3.2.1 Waveguide junction types

There are different types of waveguide junction. The major types are listed below [1]:

1. H-Plane T-Junction: This type of waveguide junction gains its name because top of the "*T*" in the *T*-junction is parallel to the plane of the magnetic field, *H* lines in the waveguide see figure 3.1.

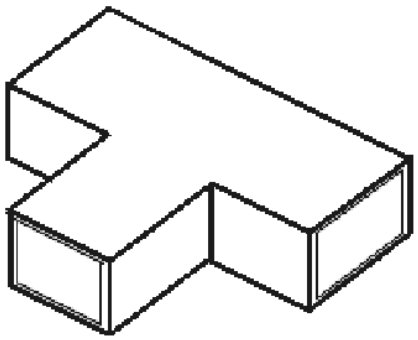

Figure 3.1: (a) Waveguide *H*-type junction

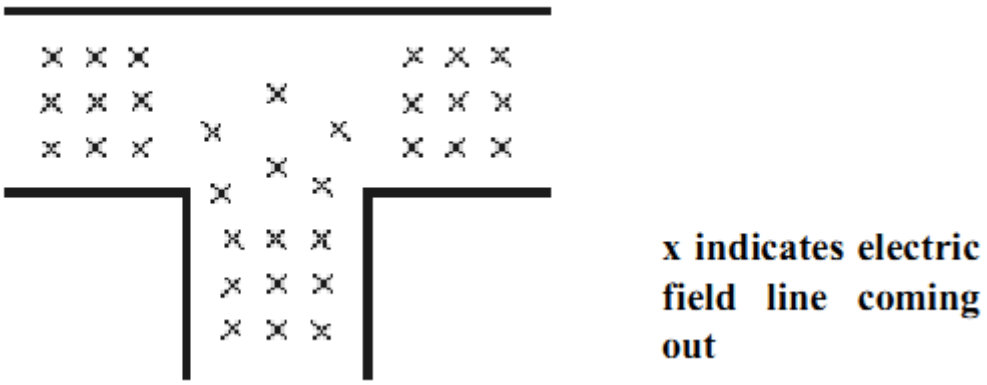

(b) Waveguide *H-type* junction electric fields

2. E-Plane T-Junction: This form of waveguide junction gains its name as an *E*-type T junction because the top of the "*T*" extends from the main waveguide in the same plane as the electric field in the waveguide see figure 3.2.

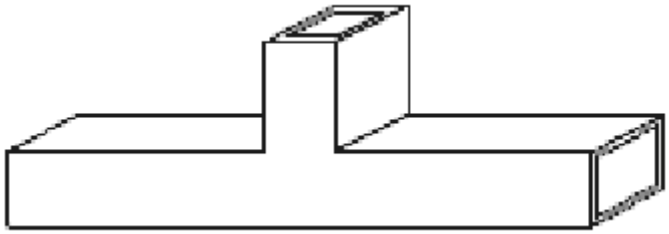

Figure 3.2: (a) Waveguide *E*-type junction

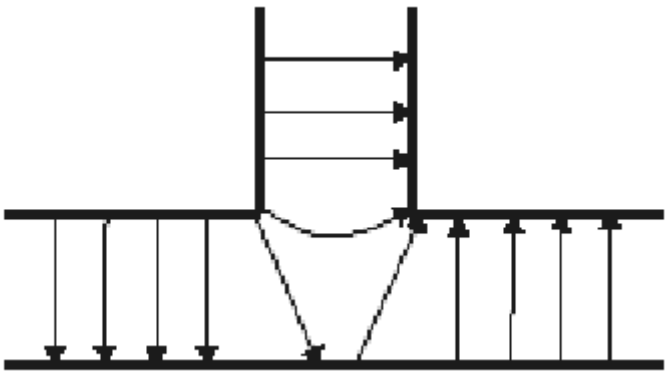

(b) Waveguide *E*-type junction *E* fields

Waveguide *T*-junctions are important components in many microwave applications, *T*-junctions are often used in diplexer configurations, and it was always felt that the *T*-junction required certain dimensional parameters to achieve an acceptable match within the relevant frequency ranges. Therefore, The optimized *T*-junctions are used in the design of a wide bandwidth, low loss, high power diplexer [2].

3.3 Traditional Diplexer

Diplexers are typically employed to connect the R_X and T_X filters of a transceiver to a single antenna through a suitable three-port junction [3]. This is conventionally achieved by using a two of bandpass filters , and divider. The channel filters pass frequencies within a specified range, and reject frequencies outside the specified range, and the divider splits the signal going into the filters, or combines the signals coming from the filters [4]. The most commonly used distribution configurations are *E*-plane or *H*-plane 2-furcated power dividers [5, 6], circulators [7], manifold structures [8-11], Y- junction [12] and T -junction [13].

Figure 3.3 shows the configuration of two-channel diplexer with a 1:2 divider diplexer network whereas figure 3.4 shows a circulator configuration, where each channel consists of a bandpass filter and a channel-dropping circulator [7].

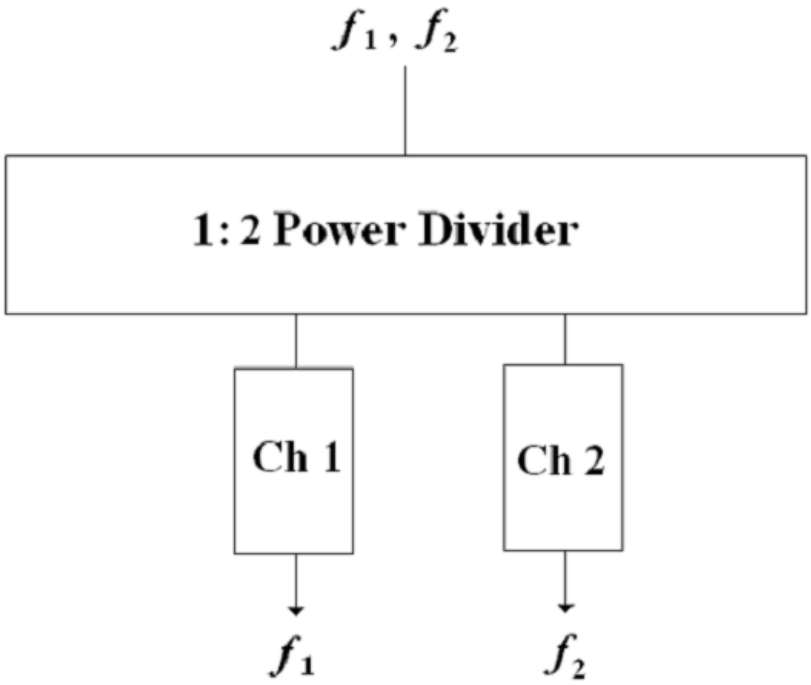

Figure 3.3: Configuration of Diplexer with a 1:2 divider network.

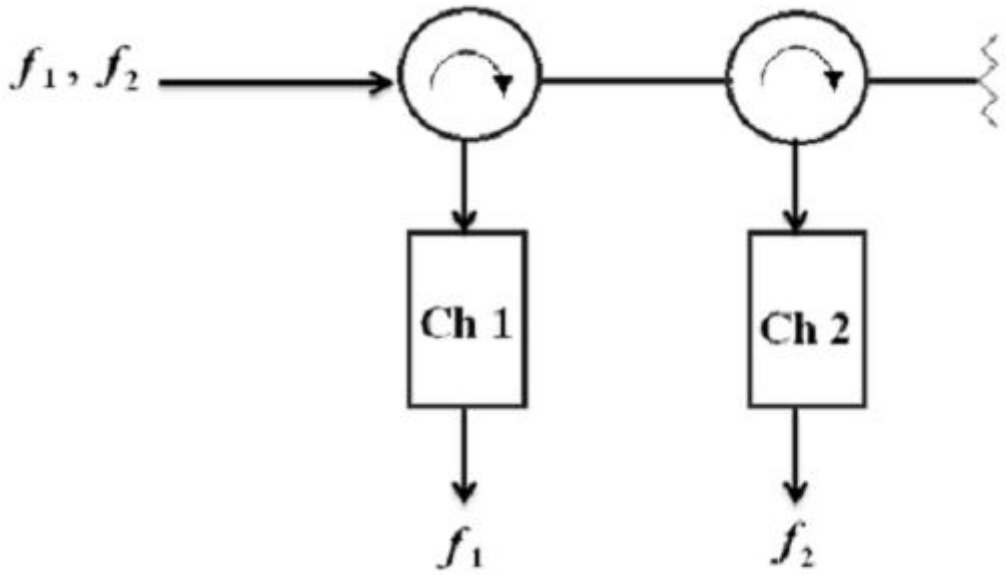

Figure 3.4: Diplexer using circulator element.

In manifold configurations, channel filters are connected by transmission lines: Microstrip, coaxial, waveguide, etc. and *T*-junctions . The configuration of the *T*-junction diplexer shown in figure 3.5 , and manifold diplexer is shown in figure 3.6 [8] and it consists of a two of waveguide filters connected to a short- circuited length of waveguide (the manifold).

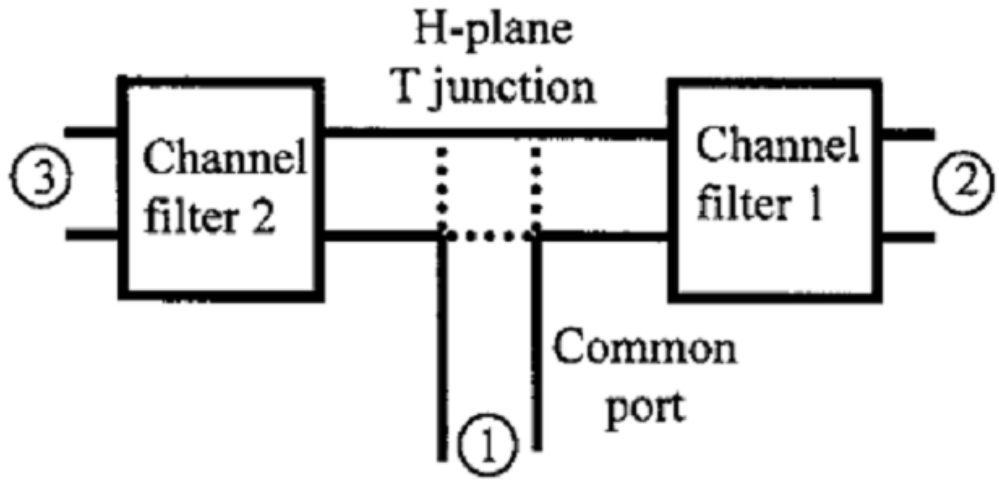

Figure 3.5: Block Diagram of *H*-plane diplexer

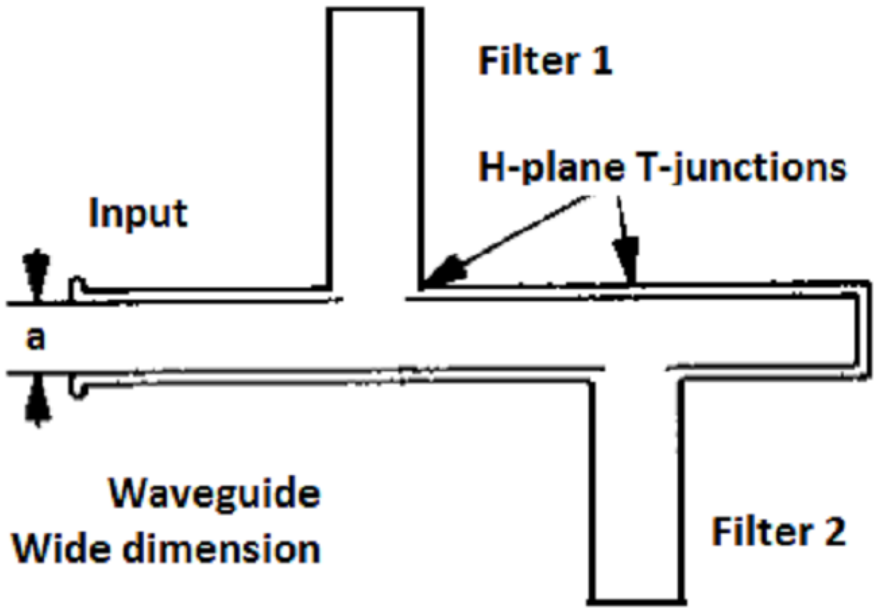

Figure 3.6: waveguide manifold implementation

In [12], resonant Y-junction for the design of compact rectangular waveguide diplexers is presented. The junction contains an elliptic ridge which serves as common dual-mode resonator for both channel filters as shown in Figure 3.7. The junction itself constitutes therefore the first resonators of the filters, thus allowing for considerable size reduction with respect to the conventional diplexer implementation.

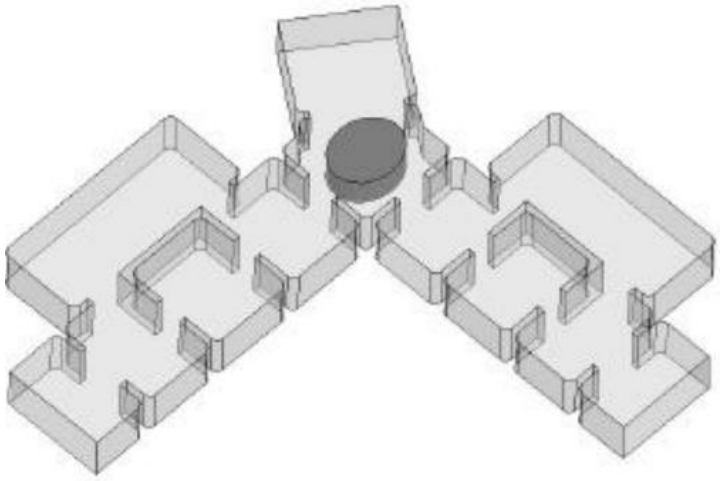

Figure 3.7: Structure of the Y-junction diplexer.

3.3.1 Configuration of a conventional Diplexer

This section presents equivalent circuit and design equations of a conventional diplexer, The equivalent circuit of a diplexer consisting of two bandpass filters with a rectangular H-Plane waveguide *T*-junction is shown in figure 3.8 [13], where the transformer ratio *n* and the susceptance b_0 can be calculated using formulas in [14].

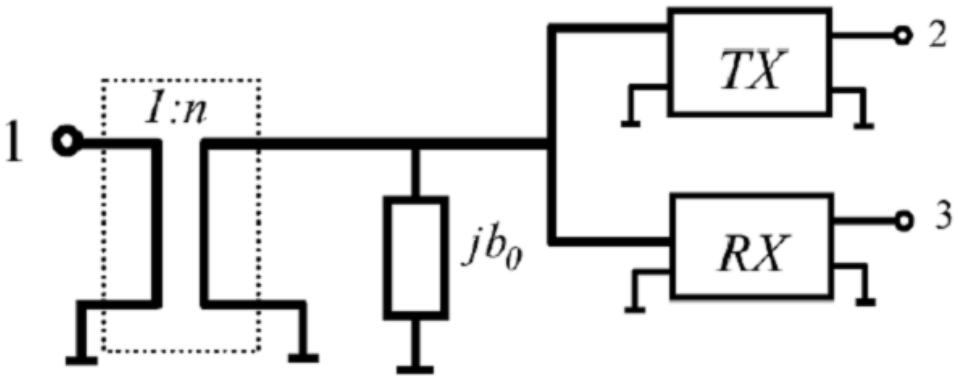

Figure 3.8: Architecture of diplexer with H-plane waveguide T-junction.

The diplexer in figure 3.8 has input admittance at port 1 as follows [14],

$$y_{in} = n^2(jb_0 + y_{in}^{TX} + y_{in}^{RX}) \tag{3.1}$$

Where y_{in}^{TX} is the admittance at input port of the TX filter with the other port terminated with the reference load, and similarly, y_{in}^{RX} is the admittance at the input port of the R_X filter with the other port matched. These admittances are expressed in terms of S_{11} parameters of the individual T_X and R_X filters as follows,

$$y_{in}^{TX} = \frac{1 - s_{11}^{TX}}{1 + s_{11}^{TX}} \tag{3.2}$$

$$y_{in}^{RX} = \frac{1 - s_{11}^{RX}}{1 + s_{11}^{RX}} \tag{3.3}$$

The S_{11} parameter of the diplexer is expressed in terms of the input admittance y_{in} as follows,

$$S_{11} = \frac{1 - y_{in}}{1 + y_{in}} \tag{3.4}$$

The transmission parameters s_{21} and s_{31} of the diplexer are expressed as follows [12],

$$s_{21} = \frac{s_{21}^{TX}\,(1 + y_{in}^{TX})}{\frac{1}{n} + jnb_0 + n.y_{in}^{TX} + n.y_{in}^{RX}} \tag{3.5}$$

$$s_{31} = \frac{s_{21}^{RX}\,(1 + y_{in}^{RX})}{\frac{1}{n} + jnb_0 + n.y_{in}^{TX} + n.y_{in}^{RX}} \tag{3.6}$$

3.4 Literature review on E-Band Diplexers

Many structures of diplexers have been proposed in literature. In [15], a 60 GHz diplexer filter for Gigabit wireless applications is presented. The diplexer filter is based on 10- pole bandpass blocks combined by a purposefully designed waveguide junction.

A very compact outline is achieved by stacking pairs of resonators, which are fabricated as cavities inside a central part of the filter body. Three plastic molded parts are fabricated in perfect fit and assembled by a glue- and solder-less press-fitting process as shown in figure 3.9.

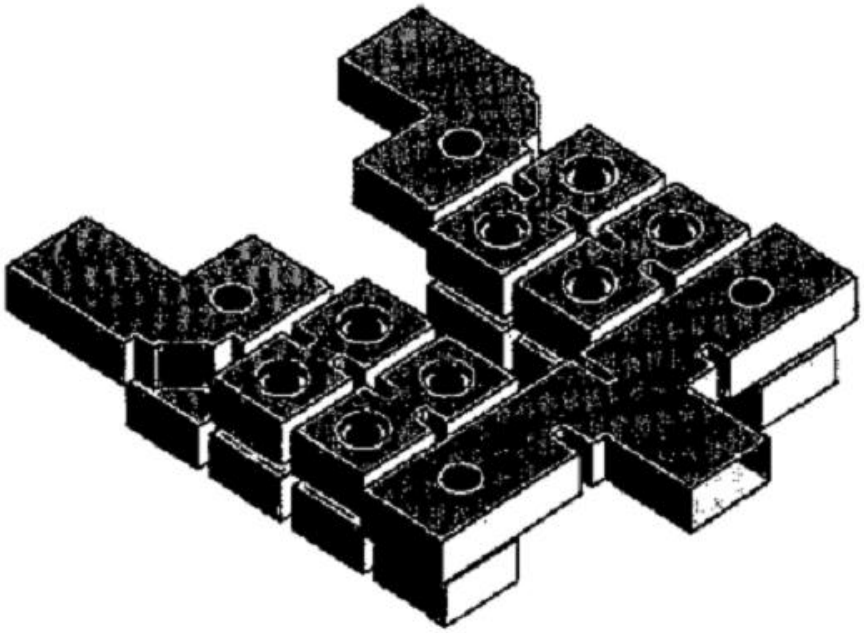

Figure 3.9: 60 GHz Diplexer 3D Design.

3.5 Diplexers with a common resonator junction

Diplexers with a common resonator junction have a common port coupled to T_X and R_X filter by a common resonator (an extra resonator besides those of the T_X and R_X filters) as illustrated in figure 3.10 [16].

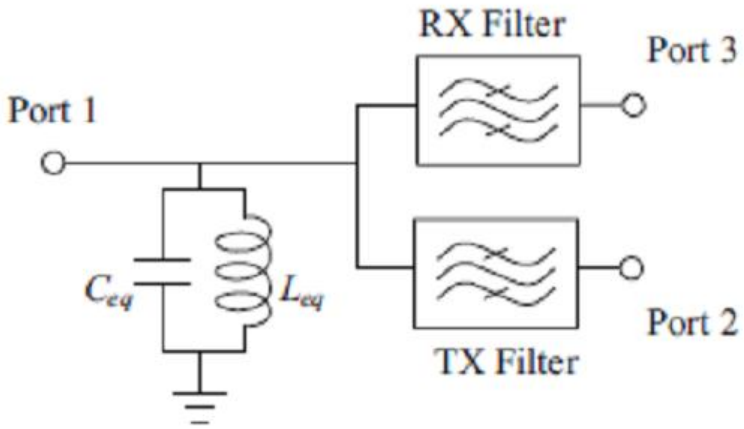

Figure 3.10: Diplexer resonator as common junction.

3.6 Summary

In this chapter an overview of microwave diplexers has been presented. Different types of microwave diplexers configurations such as H-plane T-junction, manifold and star junction diplexers have been shown and the analysis of H-plane waveguide T-junction diplexer has been presented. In the next chapter, an E-band waveguide diplexer for gigabit wireless connectivity will be designed with two methods by utilizing CST2012.

References

[1] [available on] : *http://www.radio-electronics.com/info/antennas/waveguide/waveguide-junctions-e-h-type-magic.php*

[2] J. Bornemann and M. Mokhtaari ,"The Bifurcated E-Plane T-Junction and Its Application to Waveguide Diplexer Design ", *Department of Electrical and Computer Engineering, University of Victoria, Victoria, BC, V8W 3P6, Canada*

[3] R. Cameron, C. Kudsia, and R. Mansour, Microwave filters for communication systems. Wiley, 2007.

[4] I. Carpintero, M. Cruz, A. Lamperez, and M. Palma, ”Generalized multiplexing network,” *U.S. Patent 0114082 A1, Jun. 1, 2006.*

[5] J. Cruz, J. Garai, J. Rebollar, and S. Sobrino, "Compact full ku-band triplexer with improved E-plane power divider," *Progress In Electromagnetics Research, Vol. 86, pp. 39-51, 2008.*

[6] J. Dittloff, J. Bornemann, and F. Arndt, "Computer aided design of optimum E- or H-plane N-furcated waveguide power dividers," *in Proc. European Microwave Conference, Sept. 1987, pp. 181-186.*

[7] C. E. Saavedra, “Diplexer Using a Circulator and Inter-changeable Filters,” *Proceeding of the 7th International Caribbean Conference on Devices, Circuits and Systems, Mexico, 28-30 April 2008, pp. 1-5.*

[8] M. Guglielmi, "Optimum CAD Procedure For Manifold Diplexers, ", *IEEE MTT-S International,1993, vol.2 ,pp.1081 - 1084.*

[9] D. Rosowsky and D. Wolk, “A 450-W Output Multiplexer for Direct Broadcasting Satellites,” *IEEE Transactions on Microwave Theory and Techniques, vol. 30, no. 9, Sept. 1982, pp. 1317-1323.*

[10] M.Uhm, J. Lee, J. Park, and J. Kim,“ An Efficient Optimization Design of a Manifold Multiplexer Using an Accurate Equivalent Circuit Model of Coupling Irises of Channel Filters,” *IEEE MTT-S Int. Microwave Symp., Long Beach, CA, 2005, pp. 1263-1266.*

[11] J. Rhodes and R. Levy, “Design of general manifold multiplexers,” *IEEE Transactions on Microwave Theory and Techniques, vol. 27, no. 2, pp. 111-123, 1979.*

[12] S. Bastioli, L. Marcaccioli and R. SorrentiNo, “An Original Resonant Y-junction for Compact Waveguide Diplexers,” *IEEE MTT-S International Microwave Symposium Digest, Boston, 7-12 June 2009, pp. 1233-1236.*

[13] Y.Rong, H. Yao and A. Zaki,”Millimeter-Wave Ka-Band Plane Diplexers and Multiplexers,” *IEEE Transactions on microwave Theory and Techniques, Vol. 47, Dec. 1999, pp. 2325-2330.*

[14] G. Macchiarella and S. Tamiazzo, “Novel approach to the synthesis of microwave diplexers,” *IEEE Transactions on Microwave Theory and Techniques, vol. 54, no. 12,*

pp. 4281-4290, 2006.

[15] M. Wanger, D. Stanelli , P. Nuechter , U. Goebel, " Compact 60GHz Diplexer in Meteallized plastic technology for Gigabit Wireless Links" ,*34th European microwave conference in Amsterdam, PP. 1009-1012, 2004.*

[16] R. Wang, and J. Xu, "Synthesis and Design of Microwave Diplexers with a Common Resonator Junction ", *Microwave and Millimeter Wave Technology (ICMMT), Vol. 2012, pp.1 – 4.*

Chapter 4

Design of Diplexer for E-band Systems

4.1 Introduction

The microwave filter is necessary and vital component in a huge variety of electronic systems, including mobile radio, satellite communications and radar. This chapter exhibits design and realization of bandpass Chebyshev filter for E-band [71-76 GHz] downlink, and [81-86 GHz] uplink. Two diplexers have been designed, the first is a T-junction diplexer, and the second is a manifold diplexer. The implementation of these devices has been done using rectangular waveguide cavity resonators that are suitable for low-cost mass fabrication. Also, they have advantages in microwave frequencies due to their high unloaded quality factors and their ability to handle large amounts of power.

The theory of waveguides and rectangular waveguide cavities relevant to the design process of waveguide cavity components is first discussed here. Then the extraction of coupling coefficients and external quality factors from physical structure will be shown. Different coupling structures involving inductive/capacitive irises will be illustrated. Design and simulation results of the proposed diplexers will be presented throughout this chapter.

4.2 Waveguide

Waveguides, like transmission lines, are structures used to guide electromagnetic waves from point to point. However, the fundamental characteristics of waveguide and transmission line waves (modes) are quite different. The differences in these modes result from the basic differences in geometry for a transmission line and a waveguide [1].

Waveguides can be generally classified as either metal waveguides as shown in Figure 4.1 or dielectric waveguides as shown in figure 4.2. Metal waveguides normally take the form of an enclosed conducting metal pipe. The waves propagating inside the metal waveguide may be characterized by reflections from the conducting walls. The dielectric waveguide consists of dielectrics only and employs reflections from dielectric interfaces to propagate the electromagnetic wave along the waveguide [1].

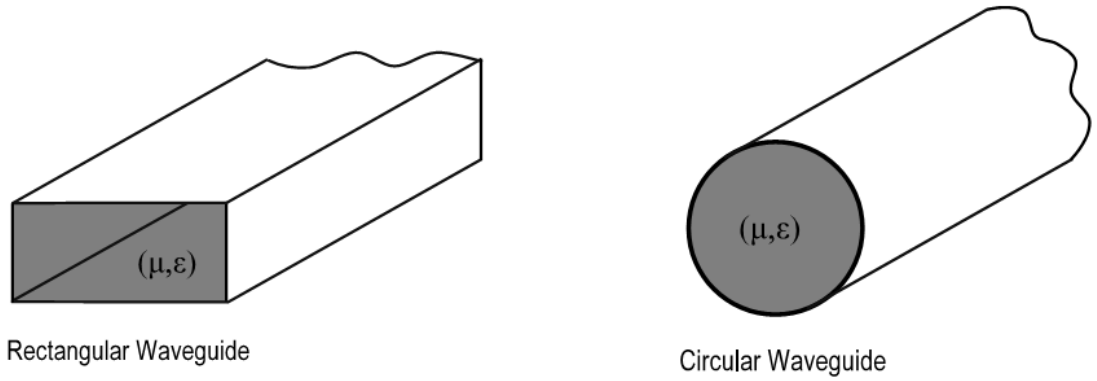

Figure 4.1: Metal waveguide

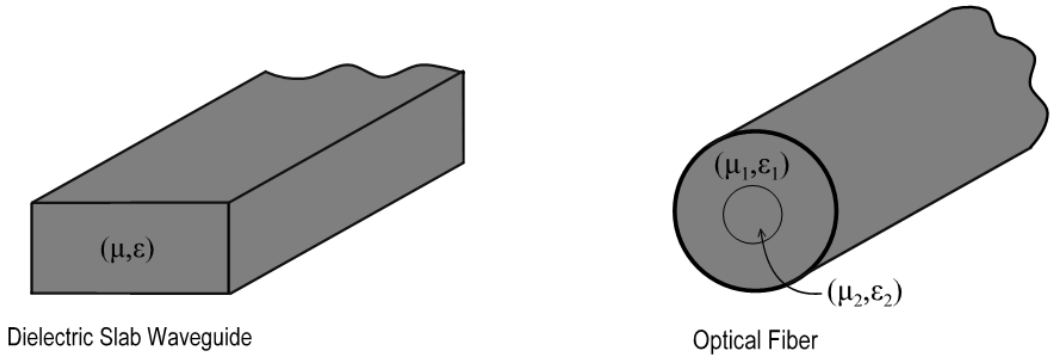

Figure 4.2: Dielectric waveguide

4.3 Rectangular Waveguide Cavity Resonator

Rectangular waveguides were one of the earliest types of transmission lines used to transport microwave signals and are still used today for many applications. A large variety of components such as filters, couplers, detectors, isolators, attenuators, and slotted lines are commercially available for various standard waveguide bands from (1 GHz to over 220 GHz) [1].

A rectangular cavity may be considered as a section of a rectangular waveguide terminated at both sides with conducting plates. Figure 4.3 shows a rectangular cavity of width a, height b, and length d, for $b < a < d$ [1].

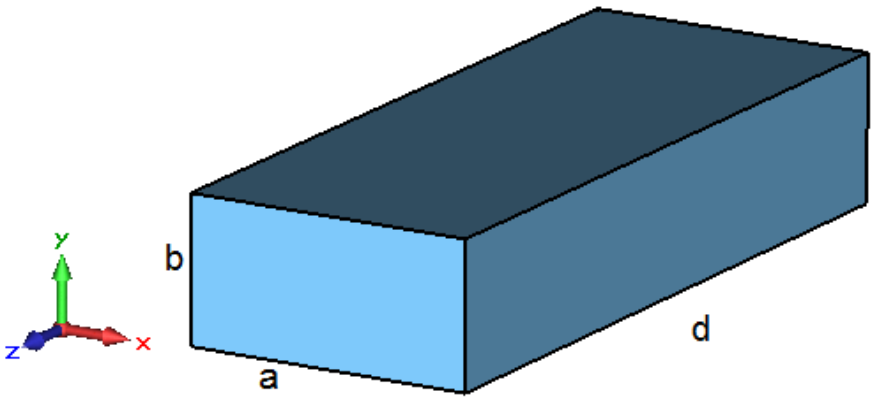

Figure 4.3: Rectangular Waveguide Cavity

For a rectangular waveguide, the transverse electric fields (E_x, E_y) of the TE_{mn} or TM_{mn} mode can be written as [1],

$$\overline{E_t}(x,y,z) = \vec{e}(x,y)[A^+ e^{-j\beta_{mn}z} + A^- e^{j\beta_{mn}z}] \tag{4.1}$$

where $\vec{e}(x,y)$ represents the transverse variations in the x and y directions, A^+, A^- are the arbitrary amplitudes of the travelling waves in the +z and –z directions. The propagation constant β_{mn} is given by

$$\beta_{mn} = \sqrt{k^2 - \left(\frac{m\pi}{a}\right)^2 - \left(\frac{n\pi}{b}\right)^2} \tag{4.2}$$

Where $k = 2\pi f_0\sqrt{\mu\varepsilon}$, and μ and ε are the permeability and permittivity of the material filling the waveguide, f_0 the operating frequency.

The boundary conditions of the waveguide cavity at z=(0,d) require that $\overline{E}(x,y,z) = 0$. Applying the condition $\overline{E}_t = 0$ at z=0 to equation (4.1) yields

$A^+ = -A^-$, and applying the condition $\overline{E}_t = 0$ at z=d, yields $\beta_{mn} d = l\pi$, where l=1, 2, 3…, this means that the cavity length must be an integer multiple of a half-guide wavelength at the resonant frequency. The cut-off wavenumber of the rectangular cavity can be defined as:

$$K_{mnl} = \sqrt{\left(\frac{m\pi}{a}\right)^2 + \left(\frac{n\pi}{b}\right)^2 + \left(\frac{l\pi}{d}\right)^2} \tag{4.3}$$

where the *indices* m, n, l correspond to the number of half wavelength variations in the x, y, z directions, respectively. The TE_{mnl} or the TM_{mnl} modes will have a resonant frequency,

$$f_{mnl} = \frac{ck_{mnl}}{2\pi\sqrt{\mu_r\varepsilon_r}} = \frac{c}{2\pi\sqrt{\mu_r\varepsilon_r}}\sqrt{\left(\frac{m\pi}{a}\right)^2 + \left(\frac{n\pi}{b}\right)^2 + \left(\frac{l\pi}{d}\right)^2} \tag{4.4}$$

Where c is the velocity of light $3\times10^8 m/s$, If b < a < d, the mode with the lowest resonant frequency, known as the dominant mode, will be TE_{101} mode. The field configuration of the dominant TE_{101} mode is shown in figure 4.4, where the dashed lines represent the magnetic field, and the solid lines and the circles represent the electric field [2].

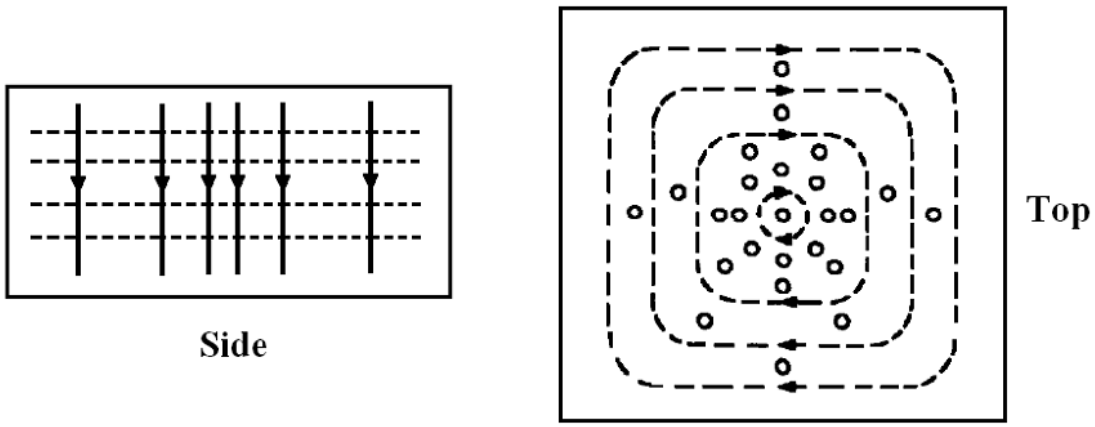

Figure 4.4: Field configuration of dominant TE_{101} mode

4.4 Unloaded Quality Factor

The unloaded quality factor $\boldsymbol{Q_u}$ is a figure of merit for a resonator. It describes the quality of the resonator in terms of losses and energy storage. For example, a high Q resonator implies low energy loss and good energy storage, whereas a low Q cavity implies higher losses [3]. A general definition for $\boldsymbol{Q_u}$ that applies to any type of resonator is,

$$\boldsymbol{Q_u = \omega \frac{Time-average\ energy\ stored\ in\ the\ resonator}{Average\ power\ lost\ in\ the\ resonator}} \tag{4.5}$$

The losses in a resonator can generally be associated with the conductor, dielectric material, and radiation. The total $\boldsymbol{Q_u}$ may be defined by adding these losses together as follows,

$$\frac{1}{Q_u} = \frac{1}{Q_c} + \frac{1}{Q_d} + \frac{1}{Q_r} \tag{4.6}$$

Where $\mathbf{Q_c}$, $\mathbf{Q_d}$ and $\mathbf{Q_r}$ are the quality factors associated with losses from conductor and dielectric making up the cavity and radiation from the cavity respectively. The loaded quality factor $\boldsymbol{Q_l}$ may be defined in terms of the unloaded quality factor $\boldsymbol{Q_u}$ and the external quality factor $\boldsymbol{Q_e}$ as follows [1],

$$\frac{1}{Q_L} = \frac{1}{Q_u} + \frac{1}{Q_e} \tag{4.7}$$

where $\boldsymbol{Q_e}$ is the quality factor associated with effective losses through the external coupling circuit, and it is defined as the ratio of the energy stored in the resonator to the energy coupled to the external circuit. The extraction of the external quality factor from the physical structure will be described in the next section.

Considering an air-filled waveguide cavity resonator, for the TE_{101} mode, the unloaded quality factor due to the losses in the conducting walls is given by [1],

$$Q_c = \frac{(k_{101}ad)^3 b\eta}{2\pi^2 R_s (2a^3b + 2bd^3 + a^3d + ad^3)} \tag{4.8}$$

Where $\boldsymbol{\eta = \sqrt{\mu/\varepsilon}}$ is the wave impedance, and $\boldsymbol{R_s}$ is the surface resistance of the conductive walls (with conductivity of σ), and it is calculated by [1]:

$$R_s = \sqrt{\frac{\omega\mu}{2\sigma}} \tag{4.9}$$

In coupled-resonator circuits with a filtering response, resonators with finite unloaded quality factors result in passband insertion loss. As the $\boldsymbol{Q_u}$ values of the resonators decrease, not only the passband insertion loss of the filtering response increases, but also the selectivity becomes worse. Hence, it is crucial for the designer to choose resonators with high $\boldsymbol{Q_u}$ values so that insertion loss specification is met. Generally, the insertion loss is proportional to the number of resonators, and inversely proportional to the fractional bandwidth (*FBW*) of the bandpass filter. The increase in (dB) in insertion loss (ΔIL) at the center frequency of the filtering response is given by [1],

$$\Delta IL = 4.343 \sum_{i=1}^{n} \frac{\Omega_c}{FBW \cdot Q_{ui}} g_i \quad dB \tag{4.10}$$

where Ω_c is the low pass cut-off frequency, and $\boldsymbol{g_i}$ represents the lowpass prototype element value of resonator *i*, as in equation (2.41).

4.5 Coupling in physical terms

After determining the normalized coupling matrix [*k*] for a coupled resonator topology, the actual coupling matrix [*K*] of a coupled resonator device with given specification can be calculated by prototype de-normalization of the matrix [*k*] at a desired bandwidth and a center frequency f_0, as follows,

$$K_{i,j} = k_{i,j}.FBW \tag{4.11}$$

Where *FBW* is the fractional bandwidth, the actual external quality factor $\boldsymbol{Q_e}$ is related to the normalized quality factor $\boldsymbol{q_e}$ by,

$$Q_e = \frac{q_e}{FBW} \tag{4.12}$$

The next step is to construct a structure of coupled resonators and implement the required coupling coefficients of the matrix [*K*] physically. The extraction of the coupling coefficient $\boldsymbol{K_{ij}}$ of two coupled resonators and the external quality factor $\boldsymbol{Q_e}$ from the physical structure is presented in the next subsections.

4.5.1 Extraction of coupling coefficient from physical structure

In general, every two coupled resonators may have the same or different resonant frequency, where the coupling coefficient between the resonators defined as the ratio of coupled energy to stored energy [4]. In coupled resonator circuits, the coupling between them can be electric or magnetic or mixed coupling. Here, the coupling coefficient for a selected resonator pair can be obtained from the physical structure using electromagnetic (EM) simulation. To extract the coupling coefficient of two asynchronously coupled resonators, a general formula that applies to any type of resonators is used [5],

$$K = \pm\frac{1}{2}\left(\frac{\omega_{02}}{\omega_{01}} + \frac{\omega_{01}}{\omega_{02}}\right) \times \sqrt{\left(\frac{\omega_2^2 - \omega_1^2}{\omega_2^2 + \omega_1^2}\right)^2 - \left(\frac{\omega_{02}^2 - \omega_{01}^2}{\omega_{02}^2 + \omega_{01}^2}\right)^2} \tag{4.13}$$

where ω_{01} and ω_{02} are the resonant frequencies of the two coupled resonators, ω_1 and ω_2 are the lower and higher frequencies in the magnitude of S_{21} response of the two coupled resonator structure with the ports are very weakly coupled to the resonators. The characteristic parameters ω_{01}, ω_{02}, ω_1 and ω_2 can be determined using full-wave EM simulations as computer simulation technology (CST 2012). Figure 4.5 shows an example of a structure of two inductively coupled waveguide cavities that are weakly coupled to the ports, and figure 4.6 depicts the simulated $|S_{21}|$ response showing the frequency peaks ω_1 and ω_2.

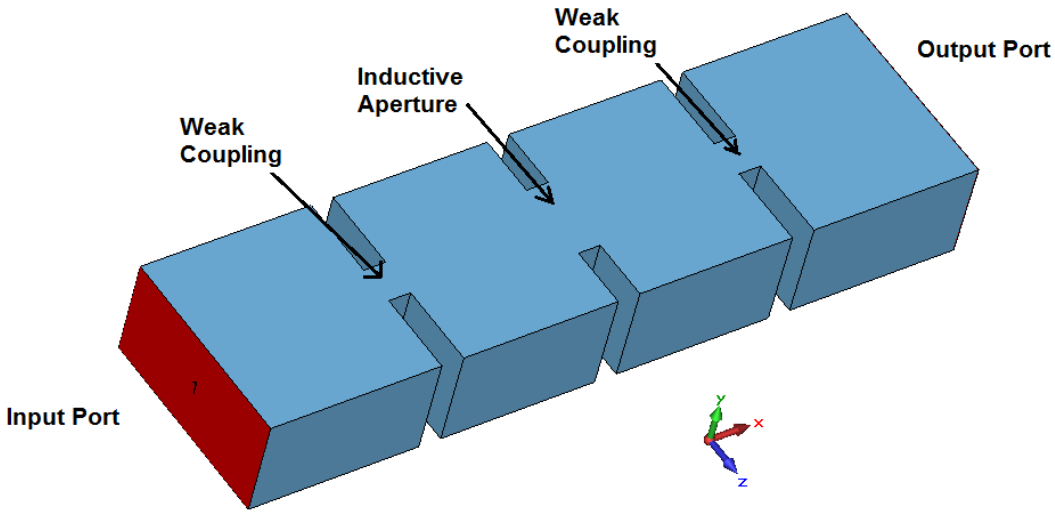

Figure 4.5: Two inductively coupled waveguide cavity resonators

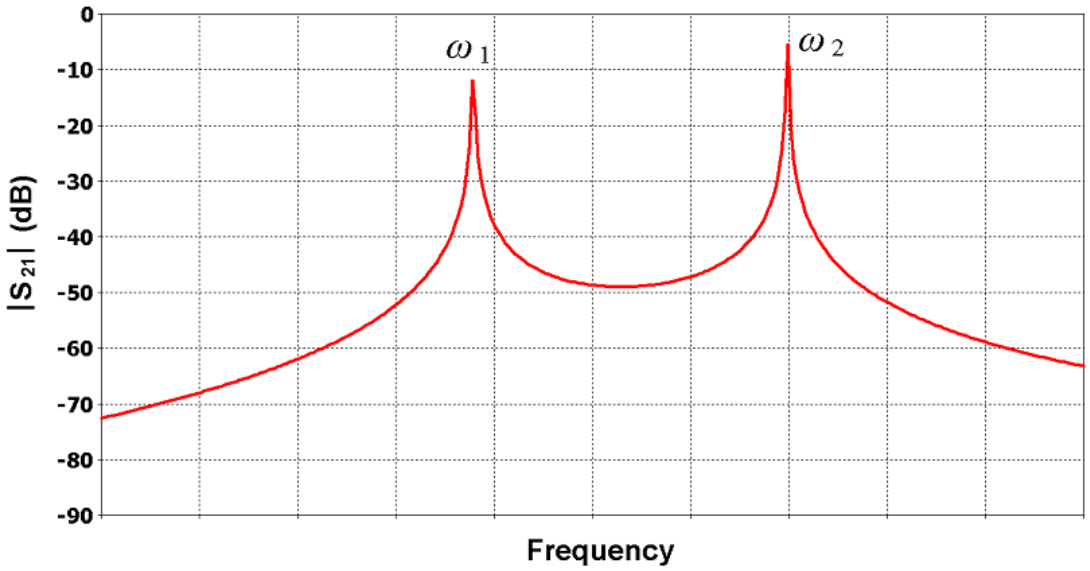

Figure 4.6: $|S_{21}|$ of two coupled resonators showing two frequency peaks [6]

The formula in equation (4.13) is applicable for synchronously coupled resonators, and in this case it is simplified to [4],

$$K = \pm\frac{\omega_2^2 - \omega_1^2}{\omega_2^2 + \omega_1^2} = \pm\frac{f_2^{\,2} - f_1^{\,2}}{f_2^{\,2} + f_1^{\,2}} \tag{4.14}$$

The coupling coefficient usually corresponds to a magnetic coupling or an electric coupling. These two types of coupling exhibit opposite signs for the coupling coefficient [4].

4.5.2 Extraction of external quality factor from physical structure

The external quality factor of a single resonator can be found by simulating $|S_{21}|$ response with one port weakly coupled. Figure 4.7 shows an example of a waveguide cavity that is externally coupled to the input port via inductive iris, and weakly coupled to the output port. The external quality factor $\boldsymbol{Q_e}$ can then be calculated from the simulated $|S_{21}|$ response using the following formula [5],

$$Q_e = \frac{\omega_0}{\Delta\omega_{\pm 3dB}} \tag{4.15}$$

Where $\boldsymbol{\omega_0}$ the resonant frequency of the loaded resonator and $\boldsymbol{\Delta\omega_{\pm 3dB}}$ is the 3dB bandwidth, as shown in figure 4.8

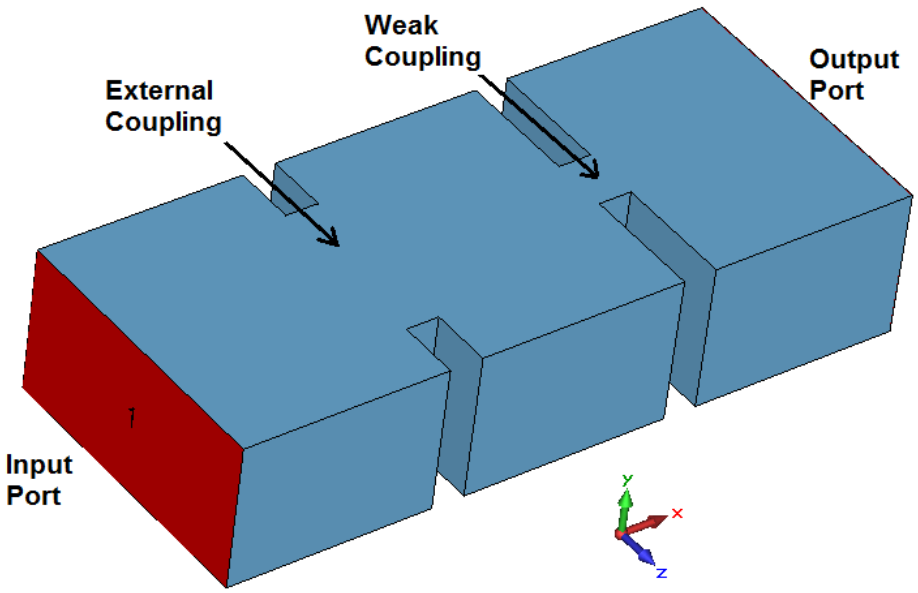

Figure 4.7: Externally coupled waveguide cavity resonator

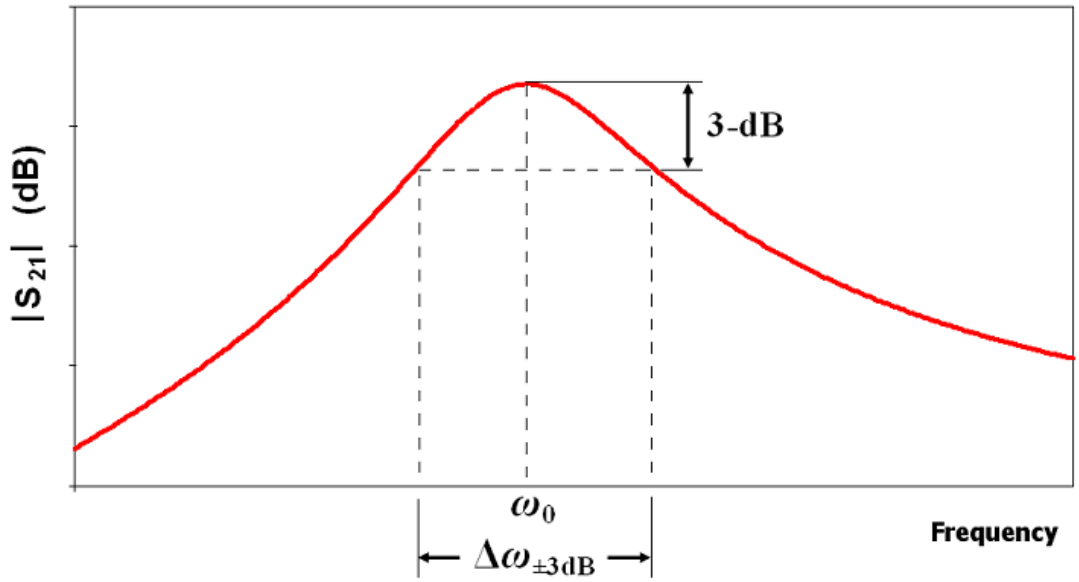

Figure 4.8: Response of |S21| for loaded resonator [6]

4.5.3 Inductive and capacitive irises

Coupled resonators filter and diplexer have been implemented using waveguide cavity resonators. The initial dimensions of the coupling irises can be determined for the required coupling coefficients by following the procedure explained in section 4.5.

Figure 4.9 shows different coupling structures for two waveguide cavities coupled together using capacitive or inductive irises. Half wavelength cavities that resonate at the fundamental TE_{101} mode are commonly used in rectangular waveguide filters [5].

4.6 Filter for downlink channel

A 5^{th} order waveguide cavity resonator bandpass filter has been designed with chebyshev response. The waveguide filter has been designed according to the iris coupled resonators as shown in section 4.3. The filter is designed at E- band [71GHz-76GHz] downlink channel of mobile backhauling with the center frequency of 73.5 GHz, bandwidth 5 GHz and the reflection loss of 20dB at the passband. The input and output external quality factors and the coupling coefficients are computed for fractional bandwidth FBW=6.8% as discussed in section 2.5. The computed values are: $K_{12}=K_{45}=0.0589$, $K_{23}=K_{34}=0.0432$, and $\boldsymbol{Q_e}$ =14.279.

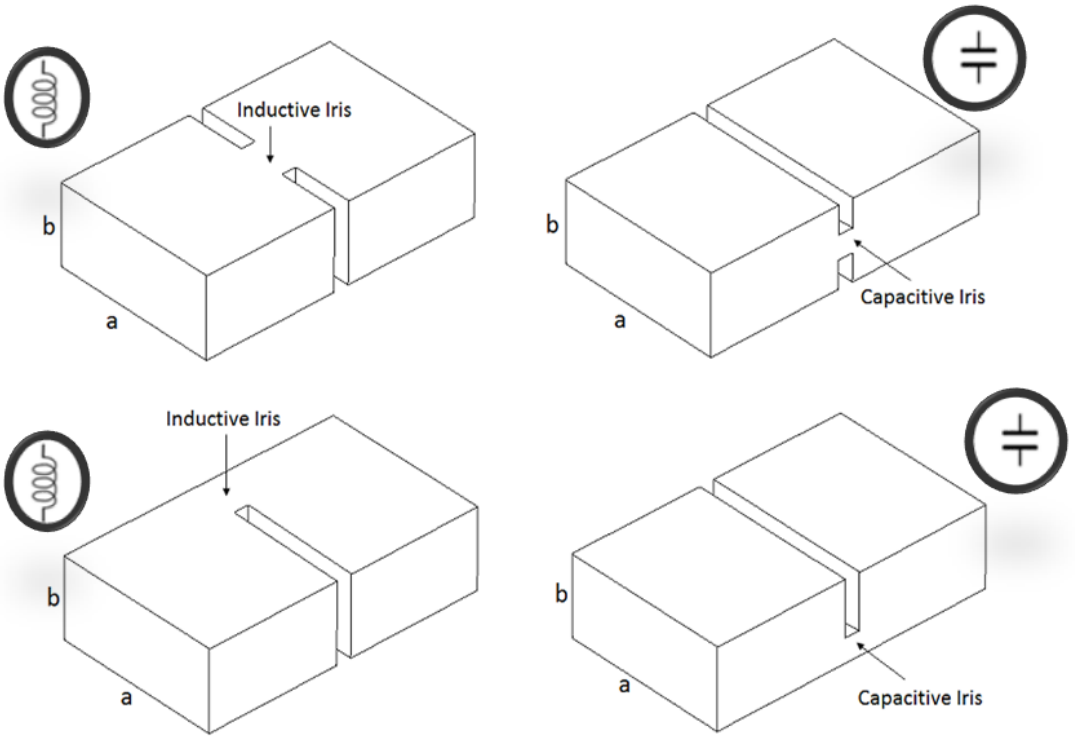

Figure 4.9: Different coupling structures for inductive and capacitive irises [6]

In CST2012 microwave studio (MWS) [7] based on finite integral technique (FIT) has been used to find the initial dimensions of the waveguide cavities and the inductive coupling irises of filter. Each pair of coupled resonators has been simulated separately to find the dimensions of the length of resonators and coupling iris corresponding to the required coupling coefficient by following the procedure in section 2.5.4 and section 4.5.1. The dimensions of coupling irises corresponding to external quality factors have been found from CST simulation by following the procedure in section 2.5.4 and section 4.5.2. The structure of the bandpass filter is initially designed with the obtained initial values as shown in Figure 4.10, and the CST simulation response of the initial structure of the filter is obtained in figure 4.11. After this , from the initial response, the bandpass filter has been optimized by CST frequency domain solver to satisfy the required specifications we need. The lengths of the cavity resonators and the widths of the coupling irises have been optimized to arrive to the final simulated response given in Figure 4.12. The initial and final dimensions of the waveguide cavities are shown in table 4.1. The coupling matrix for downlink filter is as follows:

$$k = \begin{bmatrix} 0 & 0.0589 & 0 & 0 & 0 \\ 0.0589 & 0 & 0.0432 & 0 & 0 \\ 0 & 0.0432 & 0 & 0.0432 & 0 \\ 0 & 0 & 0.0432 & 0 & 0.0589 \\ 0 & 0 & 0 & 0.0589 & 0 \end{bmatrix} \quad \text{For} \quad k_e = \frac{1}{Q_e} = 0.07$$

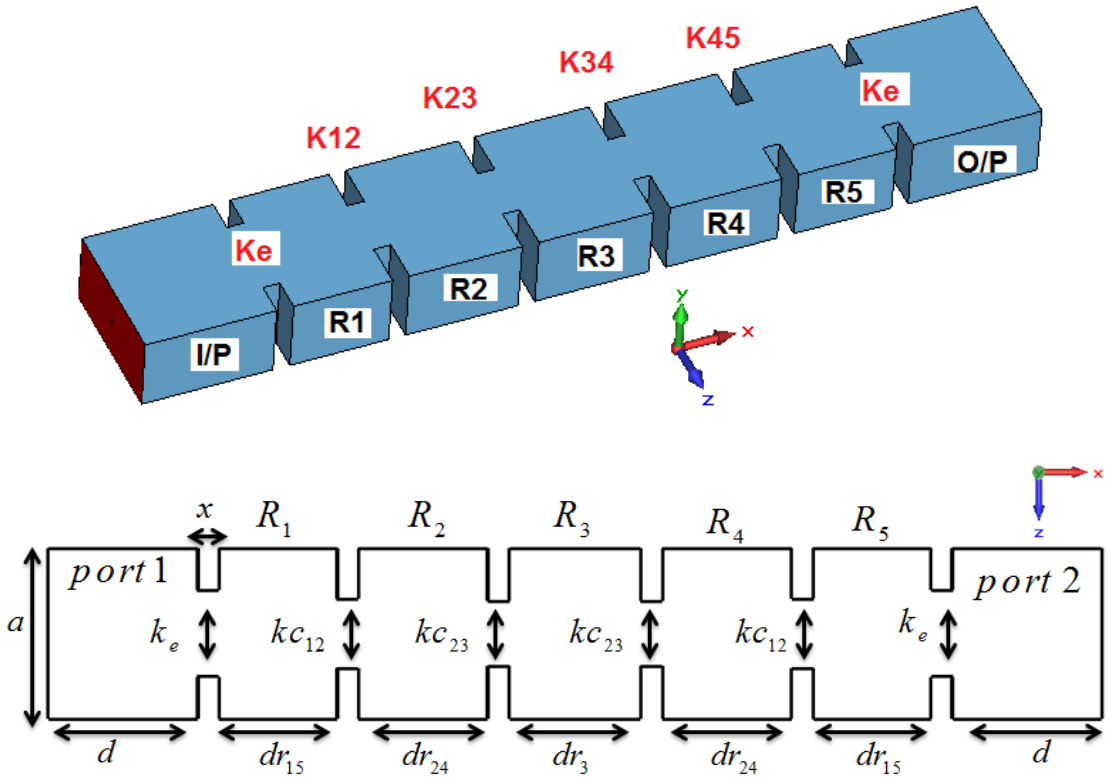

Figure 4.10: Bandpass downlink filter structure with inductive irises

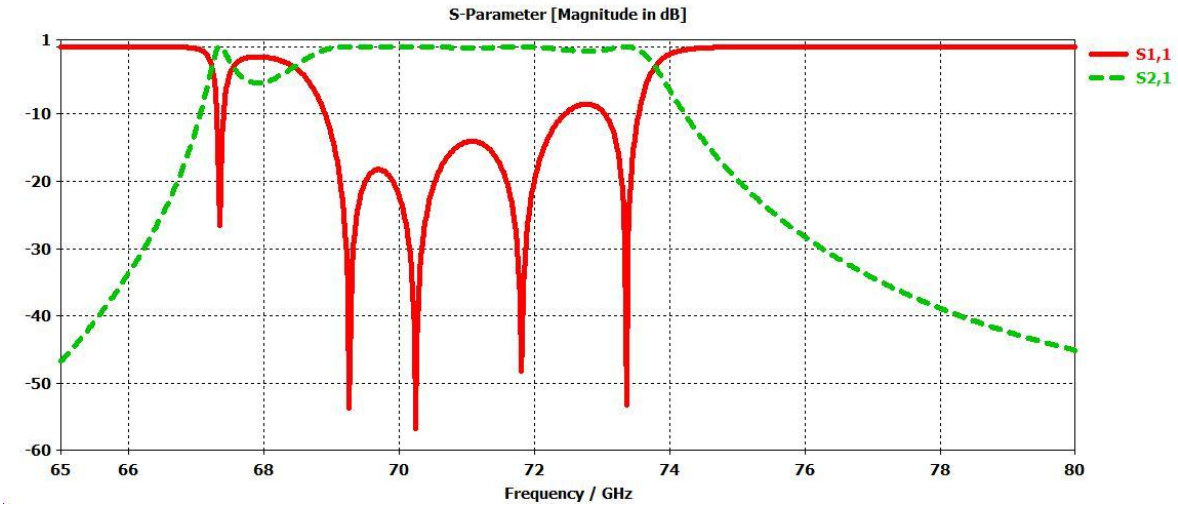

Figure 4.11: Initial response for downlink filter

Table 4.1: Dimensions for filter downlink channel

Parameter	Initial (mm)	Final V (mm)	Description "WR-12"
a	3.0988	3.0988	Width
b	1.5494	1.5494	Height
d	2.712	2.712	Length of port
dr_{15}	2.2	2.0476	Length of R1 & R5
dr_{24}	2.44	2.339	Length of R2&R4
dr_3	2.48	2.3792	Length of R3
Kc_{12}	1.34	1.28	Length of iris between (R1&R2)
Kc_{23}	1.2244	1.19	Length of iris between (R2&R3)
x	0.35	0.35	Distances between resonators
K_e	1.8	1.756	External coupling between ports and near resonator

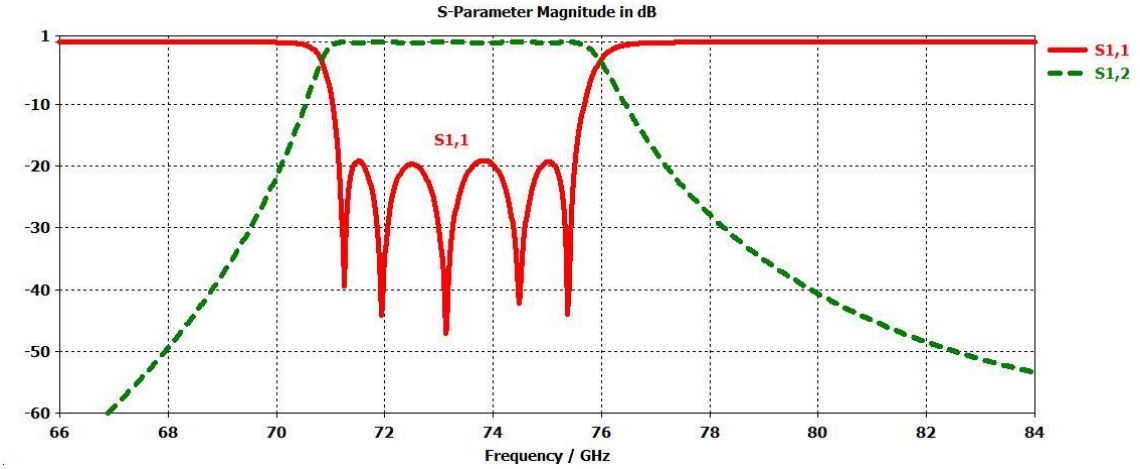

Figure 4.12: Final filter response downlink channel

4.7 Filter for uplink channel

In a similar way to the previous section, , a filter is designed at E- band [81GHz-86GHz] for uplink channel of mobile backhauling with the center frequency of 83.5 GHz, bandwidth 5 GHz and the reflection loss of 20dB at the passband. The input and output external quality factors and the coupling coefficients are computed for fractional bandwidth FBW=5.98% as follows: $K_{12}=K_{45}=0.0518$, $K_{23}=K_{34}=0.03808$, and $\boldsymbol{Q_e}$ =16.222.

The 3D CST structure of uplink filter is shown in figure 4.13, and the response of the initial structure of filter is obtained in figure 4.14. The lengths of the cavity resonators and the widths of the coupling irises have been optimized to arrive to the final simulated response given in figure 4.15. The initial and final dimensions of the waveguide cavities are shown in table 4.2. The coupling matrix of the uplink filter is given below.

$$k = \begin{bmatrix} 0 & 0.0518 & 0 & 0 & 0 \\ 0.0518 & 0 & 0.03808 & 0 & 0 \\ 0 & 0.03808 & 0 & 0.03808 & 0 \\ 0 & 0 & 0.03808 & 0 & 0.0518 \\ 0 & 0 & 0 & 0.0518 & 0 \end{bmatrix} \quad \text{For } k_e = \frac{1}{Q_e} = \frac{1}{16.222} = 0.0616$$

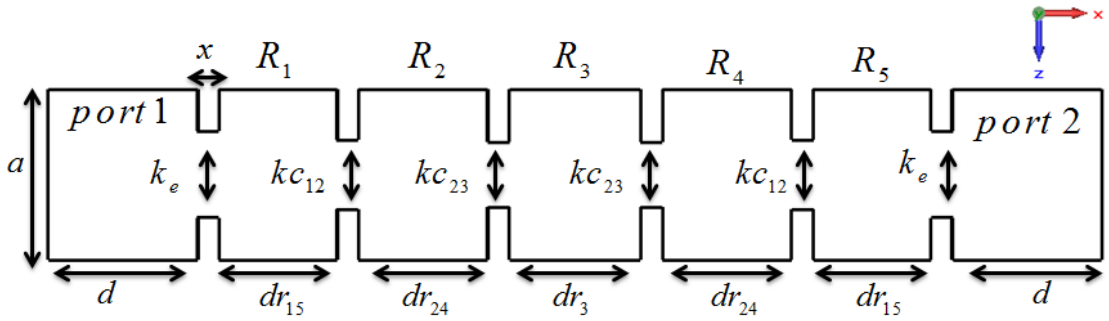

Figure 4.13: Bandpass uplink filter structure with inductive irises

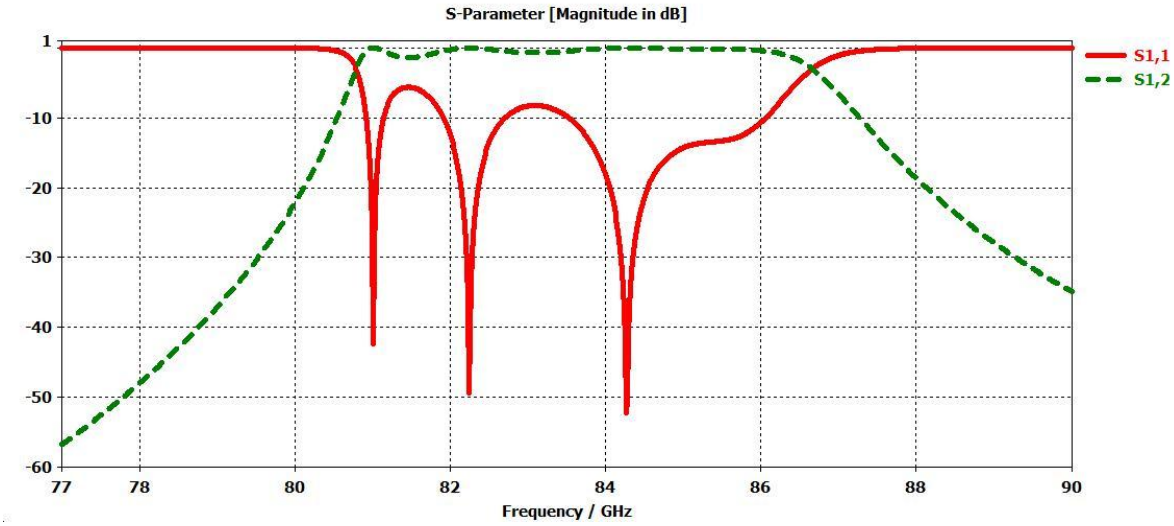

Figure 4.14: Initial response for uplink filter

Table 4.2: Dimensions for filter uplink channel

Parameter	Initial (mm)	Final (mm)	Description "WR-12"
a	3.0988	3.0988	Width
b	1.5494	1.5494	Height
d	2.2046	2.2046	Length of port
dr_{15}	1.8	1.6522	Length of R1 & R5
dr_{24}	2.02	1.9	Length of R2&R4
dr_3	2.05	1.93	Length of R3
Kc_{12}	1.14	1.1296	Length of iris between (R1&R2)
Kc_{23}	1.052	1.047	Length of iris between (R2&R3)
x	0.35	0.35	Distances between resonators
K_e	1.58	1.8	External coupling between ports and near resonator

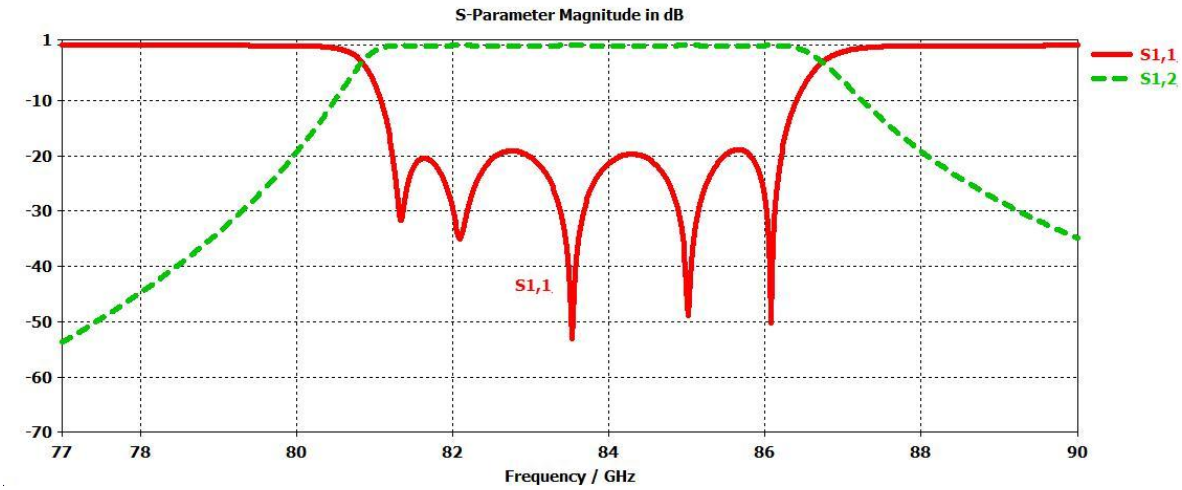

Figure 4.15: Final filter response uplink channel

4.8 E-band Diplexer design

Microwave diplexers are typically employed to connect the *RX* and *TX* filters of a transceiver to a single antenna through a suitable three port junction. The increasing development over the last years of mobile communication systems has stimulated the need for compact high selectivity diplexers to be used in both combiners for base stations and millimeter wave point-to-point radio links.

An *E-band* [71GHz – 86GHz] , 10-resonator diplexer has been designed and implemented using waveguide cavity resonators. The diplexer has a 5 GHz bandwidth of each channel, a center frequency of 73.5 GHz for channel 1 and 83.5 GHz for channel 2, and a desired return loss at the passband of each channel of 20 dB and desired isolation of 60 dB.

4.8.1 *H-plane* waveguide T-junction

It is desirable to have the T-junction with one of its ports well matched over a reasonable wide frequency band for high power system. The purpose of the T-junction is to divide power equally without any reflection. To do so, we usually add an iris or a post in the junction area so that this iris or post behaves as an inductor and makes each port of the tee-junction matched, by changing its shape and the location, it can divide power equally without reflection [8].

The two filters have been connected together with ridge waveguide T-Junction that is shown in figure 4.16 and its response is shown in figure 4.17. The ridge has been used to achieve matching by controlling the ridge width and length *x*, *y* respectively.

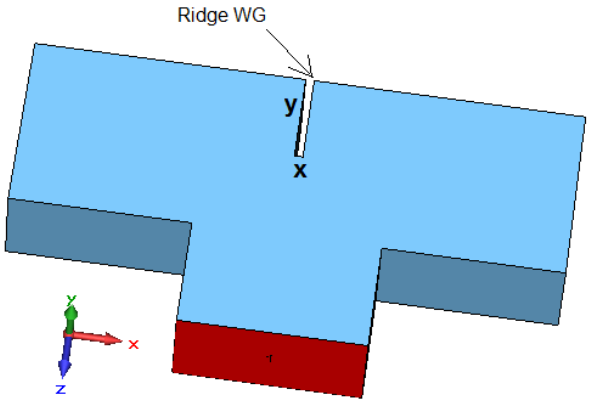

Figure 4.16: Ridge waveguide T-junction

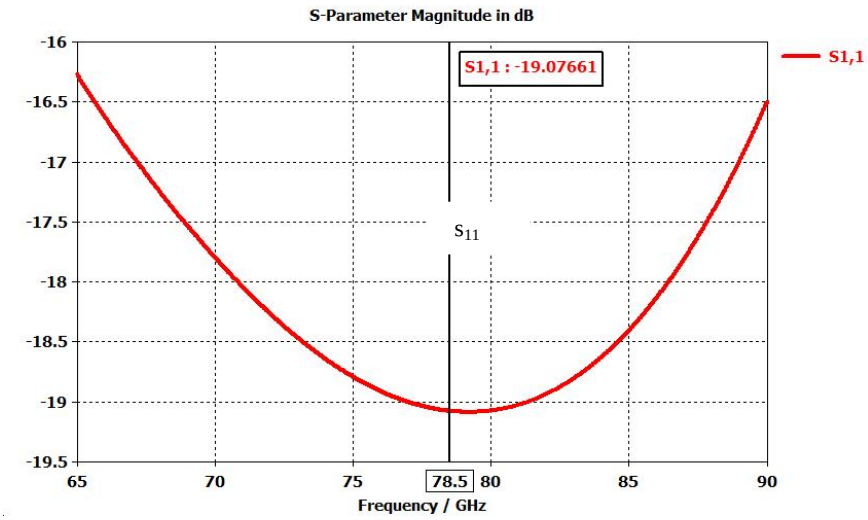

Figure 4.17: s_{11} response of ridge waveguide T-junction

4.8.2 Diplexer design with T-junction

After achieving matching in the T-junction, the diplexer has been designed with two channels and connected by T-junction. The diplexer structure is shown in figure 4.18, 4.19 respectively and the initial response is shown in figure 4.21.

The most common method for the design of microwave diplexers is based on optimization [9], [10]. The entire configuration, i.e. filters, is determined by minimizing a proper objective function that often depends on tens of variables.

Finally the whole diplexer is optimized by CST frequency solver to obtain the desired specifications shown in table 4.3. The final response of the T-junction diplexer is shown in figure 4.22. Moreover the parameters for initial and final designs are presented in table 4.4.

Table 4.3: Specification of the E-band diplexer

Band	Frequency Range [GHz]	Specification	
Low Guard Band	0-69.5	Rejection	20 dB Minimum
Channel 1	71 – 76	Insertion Loss	0.5 dB Maximum
		Reflection Loss	14 dB Minimum
		Isolation	60 dB Minimum
Mid Guard Band	77.5 – 79.5	Rejection	20 dB Minimum
Channel 2	81 – 86	Insertion Loss	0.5 dB Maximum
		Reflection Loss	14 dB Minimum
		Isolation	60 dB Minimum
High Guard Band	87.5 – 96.7	Rejection	20 dB Minimum

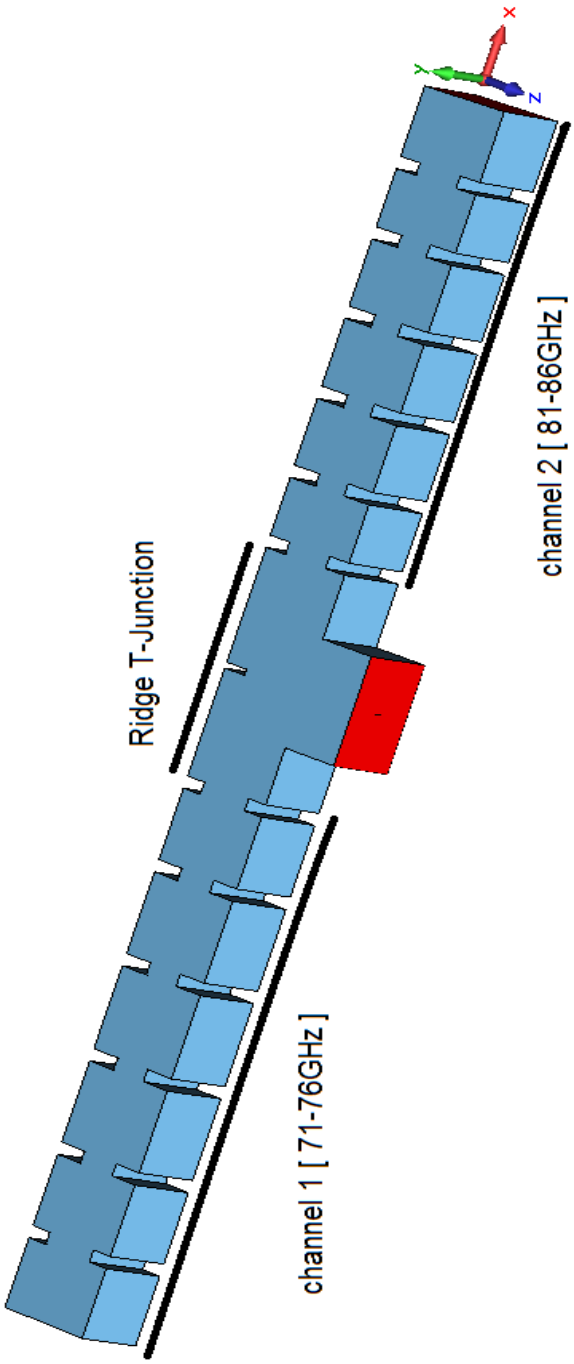

Figure 4.18: 3D CST E-band *H-plane* T-Junction diplexer

Figure 4.18: (a) 3D CST E-band diplexer

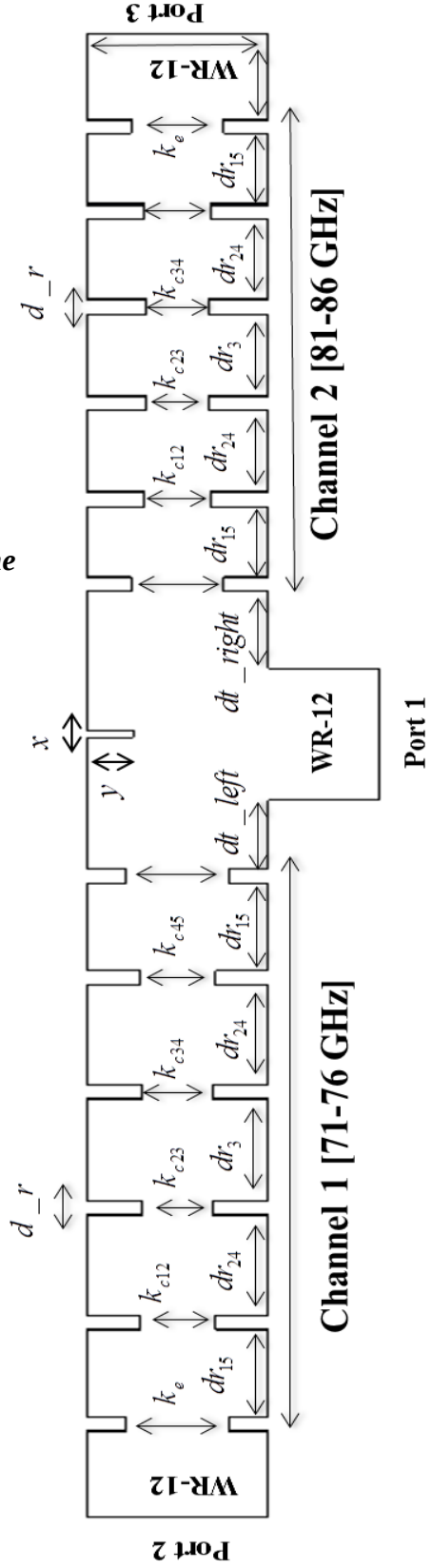

Figure 4.19: layout *H-plane* T-junction E-band diplexer

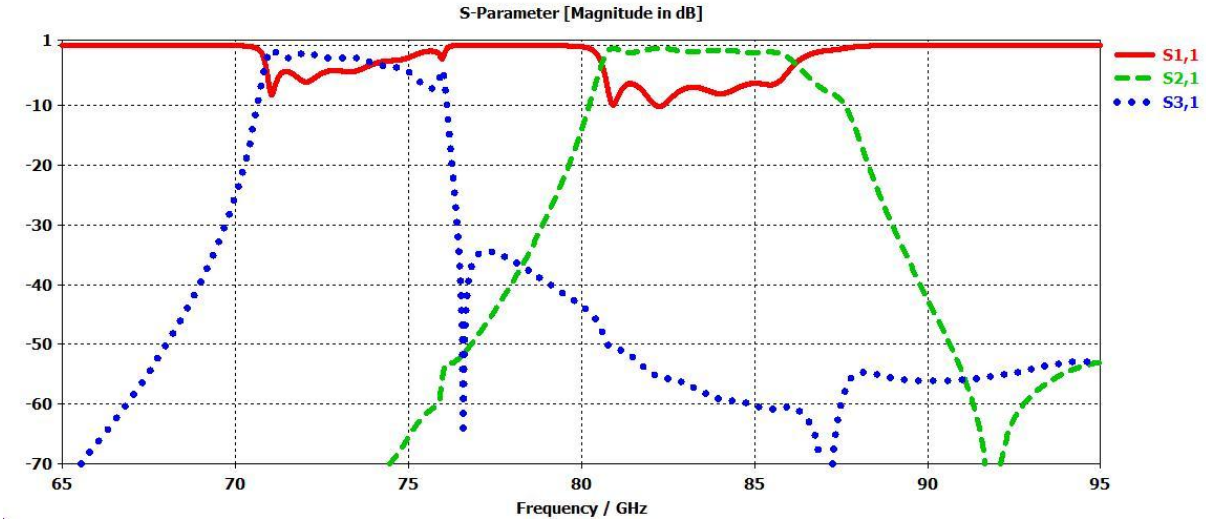

Figure 4.20: Initial response for T-Junction E-band diplexer

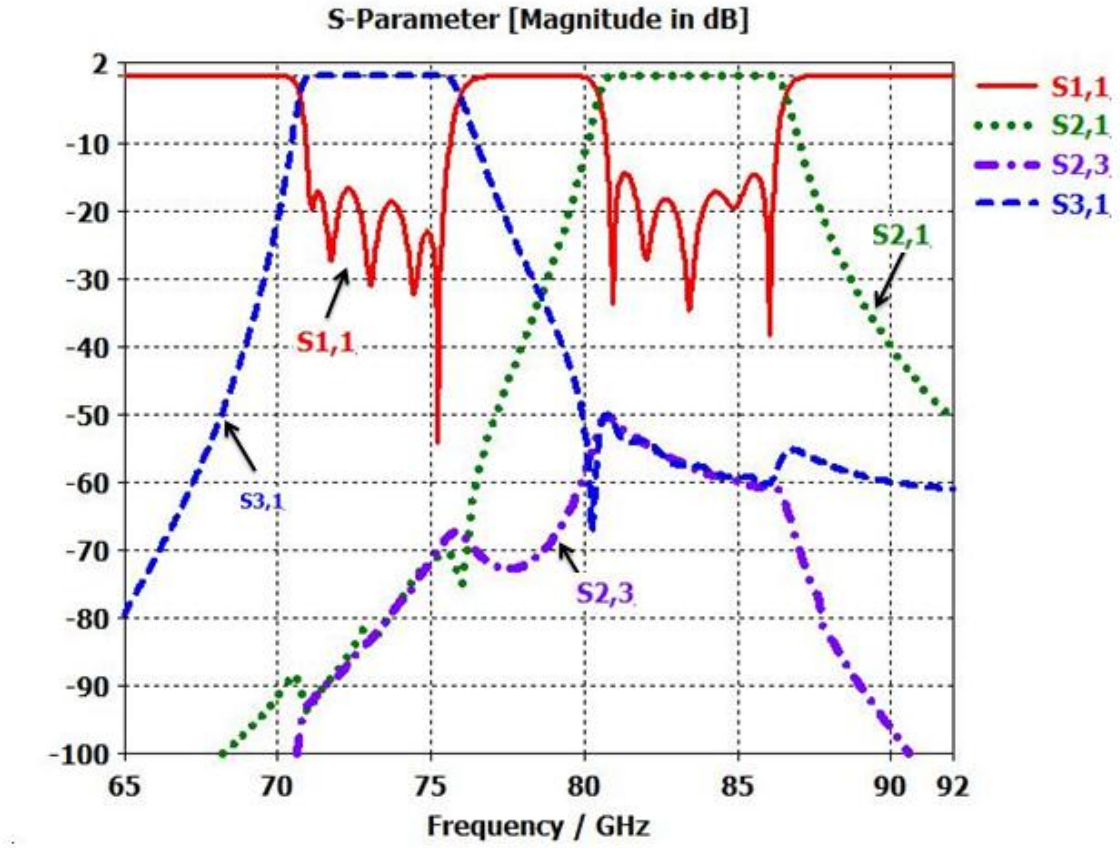

Figure 4.21: Final response for E- band *H-plane* T-junction diplexer

Table 4.4: Initial and final dimensions of the E-band T-junction diplexer

Parameter	Initial (mm)	Final (mm)	Description "WR-12"
a	3.0988	3.0988	Width
b	1.5494	1.5494	Height
d	4	4	Length of port
dr15_f70	2.0475	2.0475	Length of R1 & R5 filter 70GHz
dr24_f70	2.34	2.34	Length of R2&R4 filter 70GHz
dr3 _f70	2.379	2.379	Length of R3 filter 70GHz
Kc12_f70	1.28115	1.28115	Length of iris between (R1&R2) filter 70GHz
Kc23_f70	1.193595	1.193595	Length of iris between (R2&R3) filter 70GHz
d_r	0.35	0.35	Distances between adjacent resonators
Ke_f80	1.58	1.596	External coupling between ports and near resonator
Ke_f70	1.755	1.77	External coupling between ports and near resonator
dr15_f80	1.6525	1.6525	Length of R1 & R5 filter 80GHz
dr24_f80	1.901	1.901	Length of R2&R4 filter 80GHz
dr3_f80	1.935	1.935	Length of R3 filter 80GHz
Kc12_f80	1.131	1.131	Length of iris between (R1&R2) filter 80GHz
Kc23_f80	1.046	1.046	Length of iris between (R2&R3) filter 80GHz
d_port_f70	2	2	Length port 70GHz
d_port_f80	2	2	Length port 80GHz
d_right	2.8	1.73	Length of right arm of T-junction
d_left	1.7	1.62	Length of left arm of T-junction
X	0.16	0.17	Width of ridge T-junction
Y	1.363	1.5	Length of ridge T-junction

4.9 Manifold Diplexer

Waveguide manifold diplexers have been widely used in wireless applications that require high power capability and low insertion loss in the passband of each channel. The manifold is simulated as a cascade of H-plane T-junctions, with the perpendicular ports not facing the same side of the manifold (Fig. 4.23(b)). The purpose of the T-junction is to divide power and phase equally without any reflection as discussed in section 4.8.1. So we used ridge of H-plane T-junction in manifold diplexer for two tee power divider. CST simulator is used to simulate the single H-plane T-junction, which the distance between elements is larger than a quarter of the guide wavelength, $\boldsymbol{\lambda_g/4}$ [11].

The typical manifold diplexer consists of a two waveguide filters connected to a short circuited length of waveguide or open circuit as shown in figure 4.22. Here will be used short circuit. The overall design for manifold diplexer is shown in figure 4.23, 4.24 respectively. The frequency solver optimization used to get desired response as shown in figure 4.25 and all dimensions shown in table 4.5.

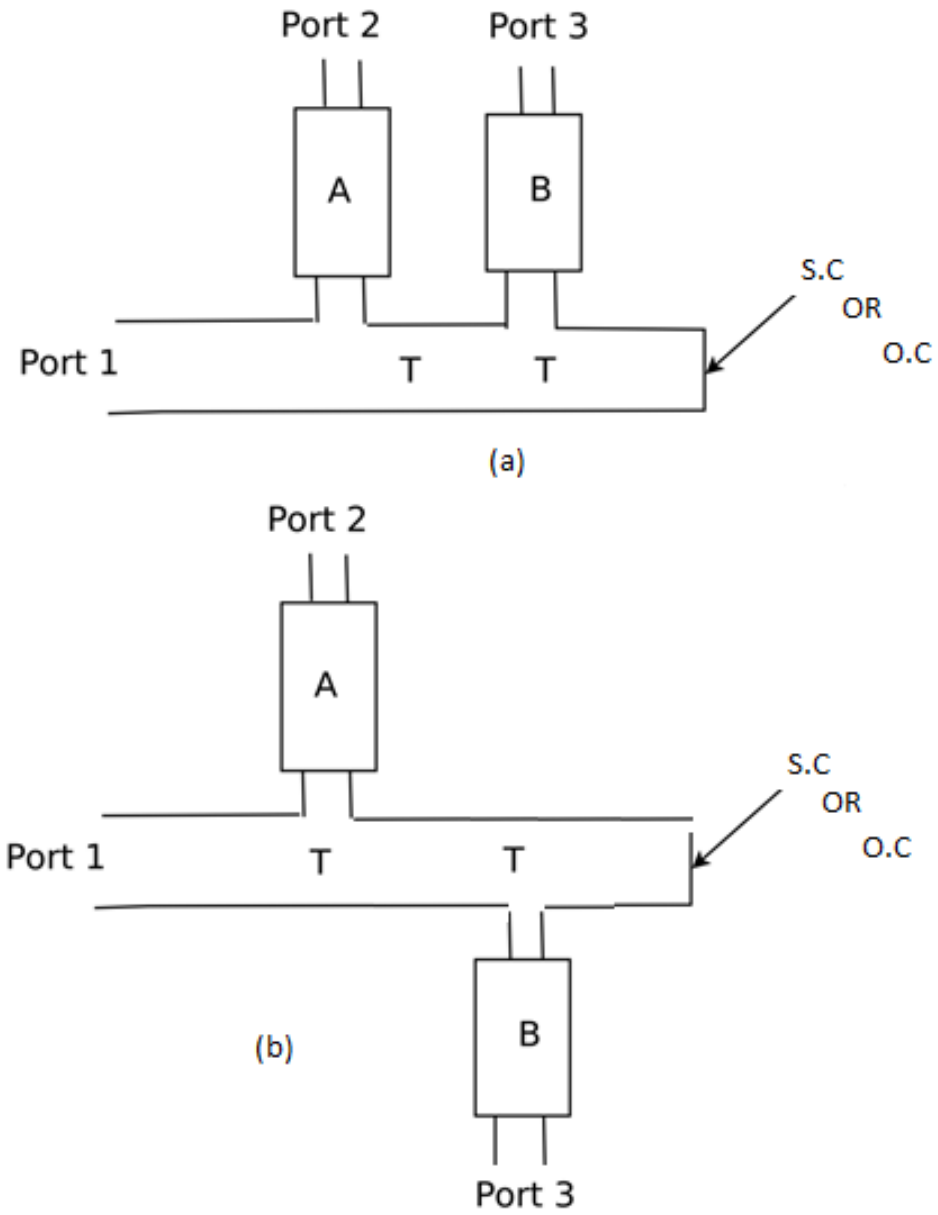

Figure 4.22: Equivalent network representation of the H - manifold diplexer

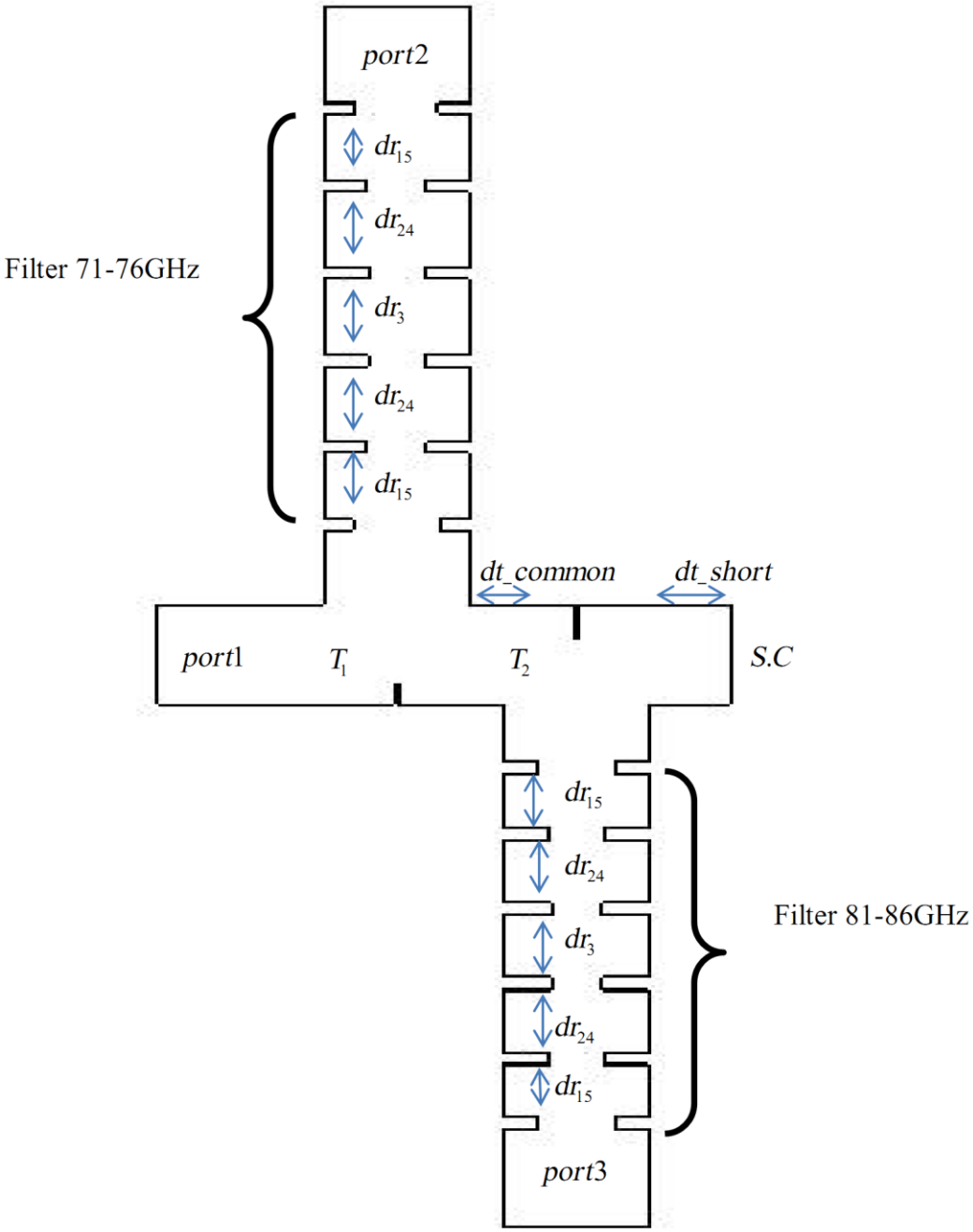

Figure 4.23: Equivalent layout representation of the H - manifold diplexer

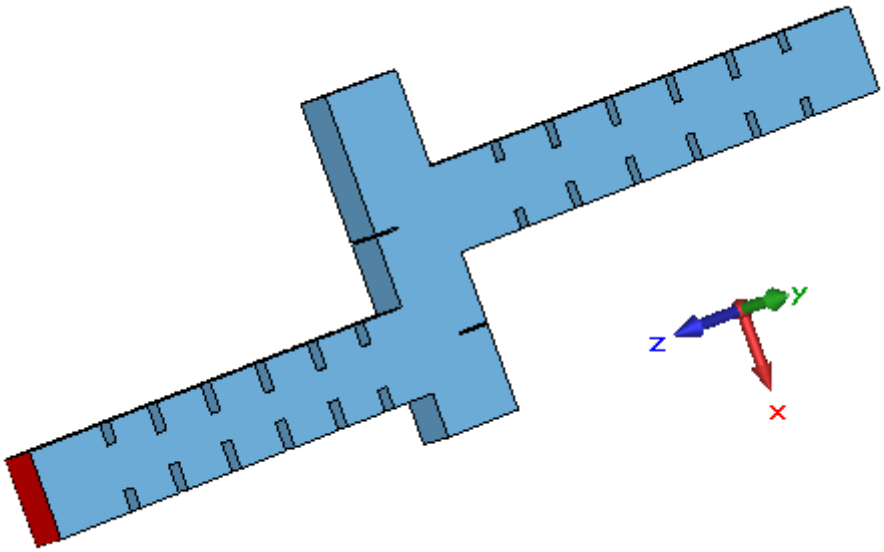

Figure 4.24: 3D CST of manifold diplexer

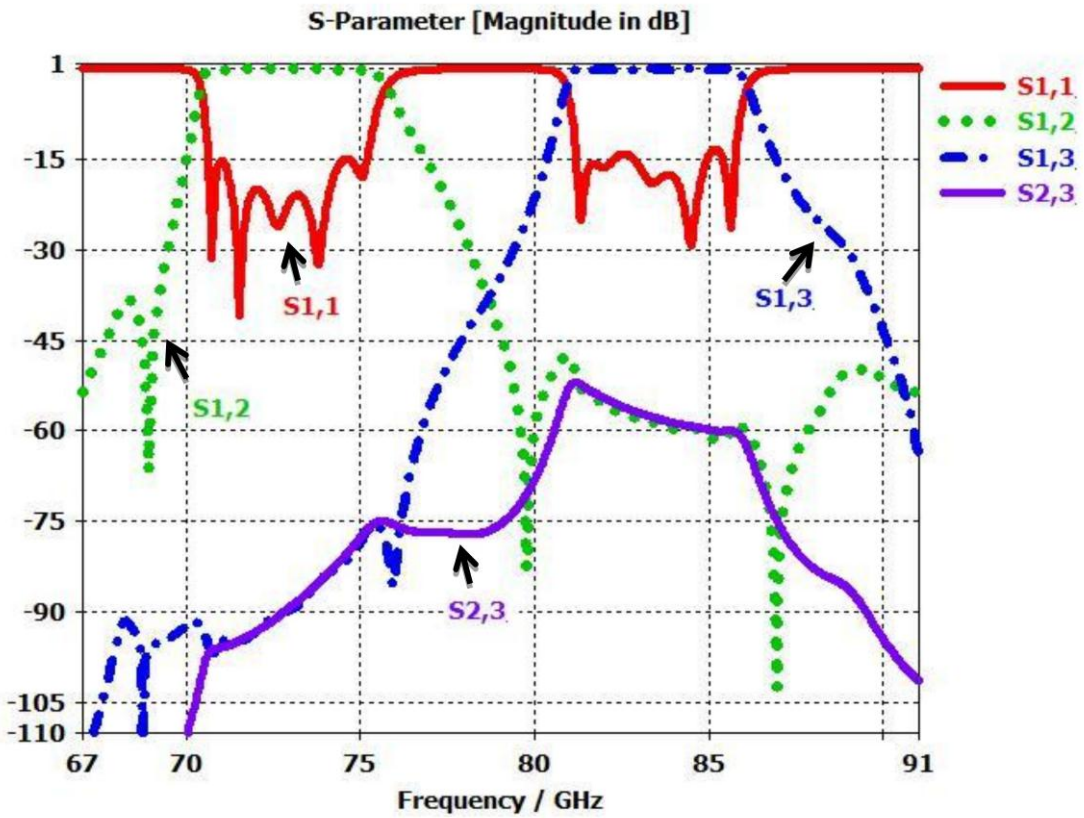

Figure 4.25: Final response of H - manifold diplexer

Table 4.5: All initial and final dimensions of the E-band manifold diplexer

Parameter	Initial (mm)	Final (mm)	Description "WR-12"
a	3.0988	3.0988	Width
b	1.5494	1.5494	Height
d	4	4	Length of port
dr15_f70	2.0475	2.0475	Length of R1 & R5 filter 70GHz
dr24_f70	2.34	2.34	Length of R2&R4 filter 70GHz
dr3 _f70	2.379	2.379	Length of R3 filter 70GHz
Kc12_f70	1.28115	1.28115	Length of iris between (R1&R2) filter 70GHz
Kc23_f70	1.193595	1.193595	Length of iris between (R2&R3) filter 70GHz
d_r	0.35	0.35	Distances between adjacent resonators
Ke_f80	1.58	1.596	External coupling between ports and near resonator
Ke_f70	1.755	1.77	External coupling between ports and near resonator
dr15_f80	1.6525	1.6525	Length of R1 & R5 filter 80GHz
dr24_f80	1.901	1.901	Length of R2&R4 filter 80GHz
dr3_f80	1.935	1.935	Length of R3 filter 80GHz
Kc12_f80	1.131	1.131	Length of iris between (R1&R2) filter 80GHz
Kc23_f80	1.046	1.046	Length of iris between (R2&R3) filter 80GHz
dt_port_f70	2	2	Length port 70GHz
dt_port_f80	2	2	Length port 80GHz
dt_short	2.8	1.7269	Length of right arm of T-junction
d_left	1.7	1.62	Length of left arm of T-junction
X1	0.07	0.1	Width of ridge T1-junction
Y1	1.3	0.1019	Length of ridge T1-junction
X2	0.07	0.08	Width of ridge T2-junction
Y2	0.9	1.05169	Length of ridge in T2-junction
Ke_f80_in	1.58	1.58637	External coupling between ports and near resonator
Ke_f70_in	1.755	1.819	External coupling between ports and near resonator
dt_common	2.121	1.6	Distance between two t junction

4.10 Comparison Between two Diplexers

Figure 4.26 shows that the comparison between the two different design methods of waveguide diplexer for E-band technology. The evaluation of the obtained results show that the common waveguide H-plane T-junction gives the best results for return loss -16.6 dB at downlink channel and -14.5 dB at uplink channel with insertion loss -0.03dB. The manifold diplexer takes the second grade of this comparison which has -14.8 dB return loss at downlink channel and -13.8 dB at uplink channel with -0.14 dB insertion loss. The isolation S_{23} between two uplink and downlink channels for both diplexers is as follows: - 65 to - 95 dB for T-junction diplexer and -75 to -95 dB for manifold diplexer. Moreover the T-junction has sharper transitions than manifold diplexer.

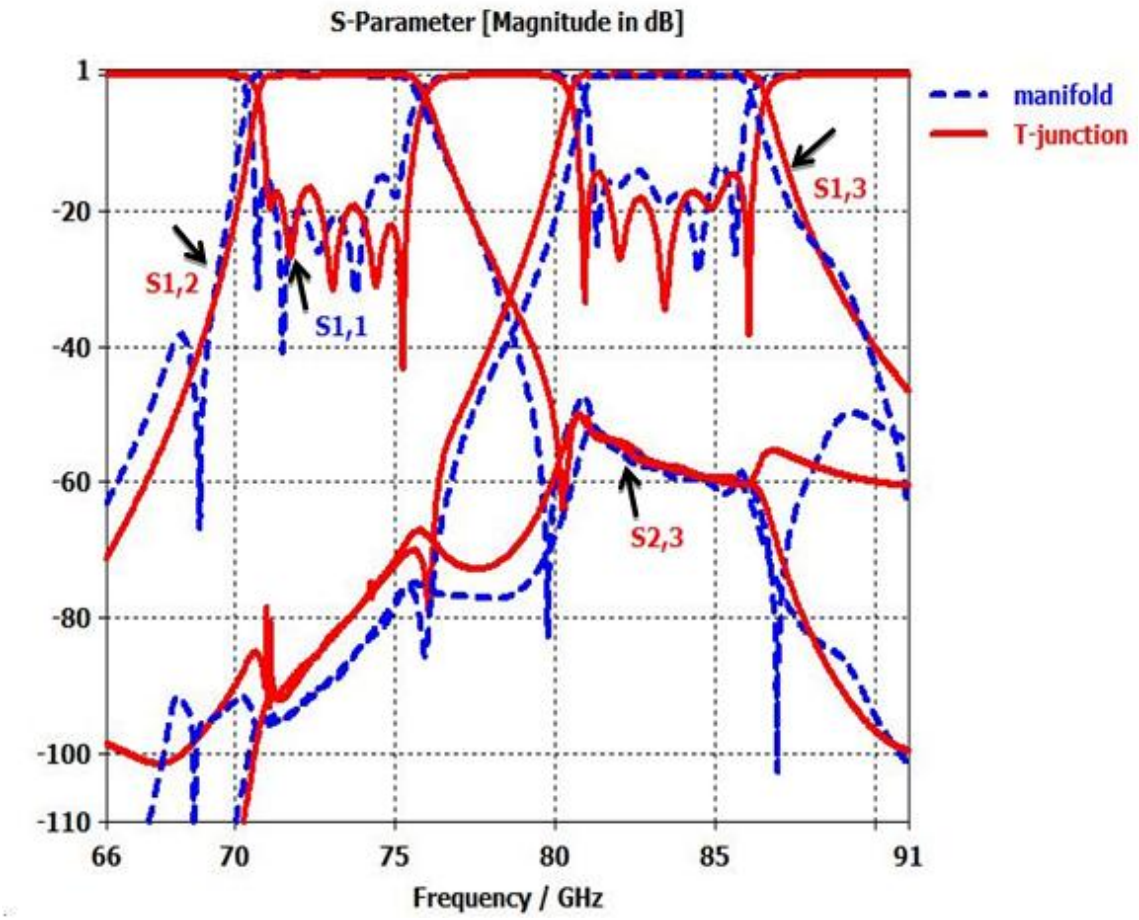

Figure 4.26: Comparison of manifold and *T-junction* diplexers

4.11 Comparisons with Commercial Diplexer

At the end of work, we will compare our diplexers designed be using CST2012 Microwave Studio was based on Finite Integration Technique (FIT) and some commercial E-band diplexers made by the companies MESL Microwave and K&L. The comparison is shown in table 4.6. See appendix A for datasheet of diplexers.

Table 4.6: Comparison with MESL and K&L companies

Brand	MESL , K&L Diplexer	Thesis Diplexer
Pass Band Frequencies	71-76 GHz &81-86 GHz	71-76 GHz &81-86 GHz
Return Loss	14 dB minimum	15 dB minimum
Isolation	60 dB minimum	65 dB for "T- junction" , and 75 dB for "manifold" minimum

4.12 Summary

In this chapter the design procedure of two diplexers for E-band system has been presented. The first diplexer contains a T-junction and the second contains a manifold. The relationship between the coupling coefficients and the physical structure of coupled resonators in order to find the physical dimensions of the diplexer has been shown. Then, the whole structures of the designed diplexers and their responses resulting from computer simulation technology (CST2012) have been shown. Finally a comparison between the two designs has been made and another comparison with commercial diplexers has also been made.

References

[1] Microwave engineering , David Pozar, third edition , chapter 3 pp106-135

[2] I. Bahl and P. Bhartia, Microwave Solid State Circuit Design. *2nd edition, Wiley, 2003*

[3] J. Hong and M. Lancaster, Microstrip Filters for RF/Microwave Applications, *John Wiley & Sons, Inc. NY, 2001.*

[4] J. Hong, "Couplings of asynchronously tuned coupled microwave resonators," *IEEE Proceedings Microwaves, Antennas and Propagation, vol.147, no.5, pp.354-358, Oct. 2000, Birmingham Univ., UK.*

[5] J. Hong and M. Lancaster, Microstrip Filters for RF/Microwave Applications, *John Wiley & Sons, Inc. NY, 2011.*

[6] T. Skaik, "Synthesis of Coupled Resonator Circuits with Multiple Outputs using Coupling Matrix Optimization ", *PhD thesis, the University of Birmingham, March 2011.*

[7] CST Microwave Studio. Darmstadt, Germany, 2012 [available on]: *http://www.cst.com/*

[8] J. lee ," A New type of the matching structure of a H-plane T-junction for a high power system", *IEEE, Antennas and Propagation Society International Symposium (APSURSI), 2010, Seoul, South Korea*

[9] J. Uher, J. Bornemann, U. Rosenberg, "Waveguide Components for Antenna Feed Systems", *Artech House,INC, 1993*

[10] M. Guglielmi,' Simple CAD procedure for microwave filters and multiplexer', *IEEE Transaction on MTT, vo1.42, no 7, July 1994, pp. 1347-1352, Europe Space Res. & Technol. Centre, Noordwijk, Netherlands*

[11] *G.* Goussetis, A. Shelkovnikov, and D. Budimir, "Ridged Waveguide Manifold Multiplexers with Improved Performance", *Microwave Conference 33rd European, 2003, pp. 207-209, Munich*, Germany.

Chapter 5

Conclusions and future work

5.1 Conclusions

In this thesis, two waveguide diplexers were synthesized and designed to meet an *E-band* system, specifically [channel 1: 71-76 GHz downlink and channel 2: 81-86 GHz uplink] which has permitted worldwide for ultra-high capacity point-to-point wireless communications system for gigabits connectivity.

The diplexers' design is based on two bandpass waveguide filters connected by an H-plane T-junction for the first diplexer, and by a manifold (waveguide sections and T-junctions) for the second diplexer.

At first, each bandpass filter is designed individually, to have fractional bandwidth (*FBW*) 6.8% at channel 71-76 GHz and 5.988% at channel 81-86 GHz . 5^{th} pole chebyshev filter with a passband ripple of 0.0432 dB is chosen for design. The waveguide filter consists of five coupled rectangular waveguide resonators coupled together using inductive apertures.

CST 2012 software was used for simulation and design of diplexer, with using parameter sweep and optimization methods to obtain the desired results. The evaluation of the obtained results ,show that a common *H-plane T-junction* gives the best results for return loss of -15.2 dB and insertion loss of -0.03dB. The manifold diplexer takes the second grade of this comparison which has -14.5 dB return loss and -0.14 dB insertion loss. Moreover, the T-junction has sharper transitions than manifold diplexer.

Traditional H-plane T-junction and manifold junction are used to form diplexer. A ridge has been added in the junctions to mitigate for the poor matching at the inputs of the waveguide filters. The addition of the ridges has improved the return loss for both the T-junction and manifold diplexers.

5.2 Future work

The work on waveguide diplexer can be further developed for resonating junction between two band pass filters. This junction is an extra cavity coupled directly with the channel filters without employing any external junction as the H-plane T-Junction and manifold. I expect for this method the diplexer will be miniaturized and the response will be sharp.

It is intended to get the diplexers fabricated and tested to validate the design method. The fabrication will be done in a place where fabrication and measurement equipment are available.

Appendix A

A.1 Constants

$\varepsilon_0 = 1.85 \times 10^{-12} F / m$

$\mu_0 = 4\pi \times 10^{-7} H / m$

A.2 K&L E-band diplexer

Table A.1: specification of diplexer channel

◆ Compliance Matrix:

Characteristics	Specifications
CH1: 71-76 GHz Insertion Loss: Return Loss: Tx/Rx Isolation:	 0.7 dB max (0.5 dB typical) 14 dB min 60 dB
CH2: 81-86 GHz Insertion Loss: Return Loss: Tx/Rx Isolation:	 0.7 dB max (0.5 dB typical) 14 dB min 60 dB

Figure A.1: E-band waveguide diplexer

A.2.1 Outline Drawing

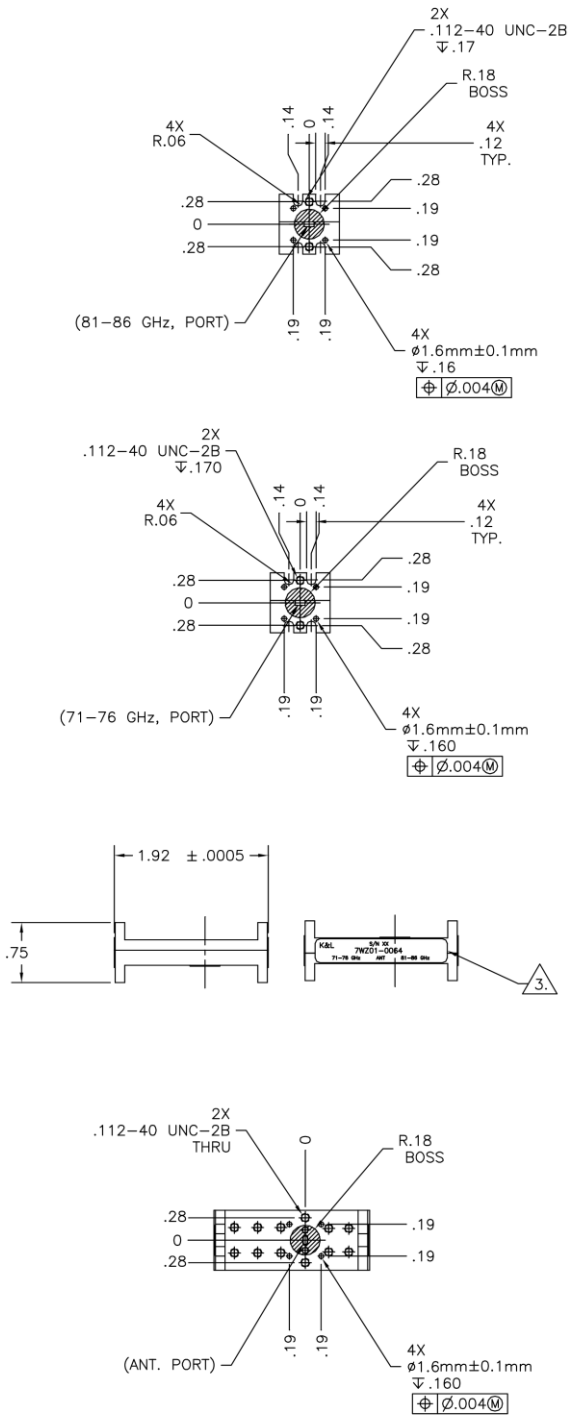

Figure A.2: E-band diplexer dimensions

A.3 MESL Microwave E-band diplexer

Table A.2: MESL diplexer specification

MESL E-Band Diplexer Specification	
Pass Band Frequencies:	71-76GHz & 81-86GHz
Return Loss:	14dB minimum
Insertion Loss:	0.7dB maximum
High/Low Channel Attenuation:	60dB minimum

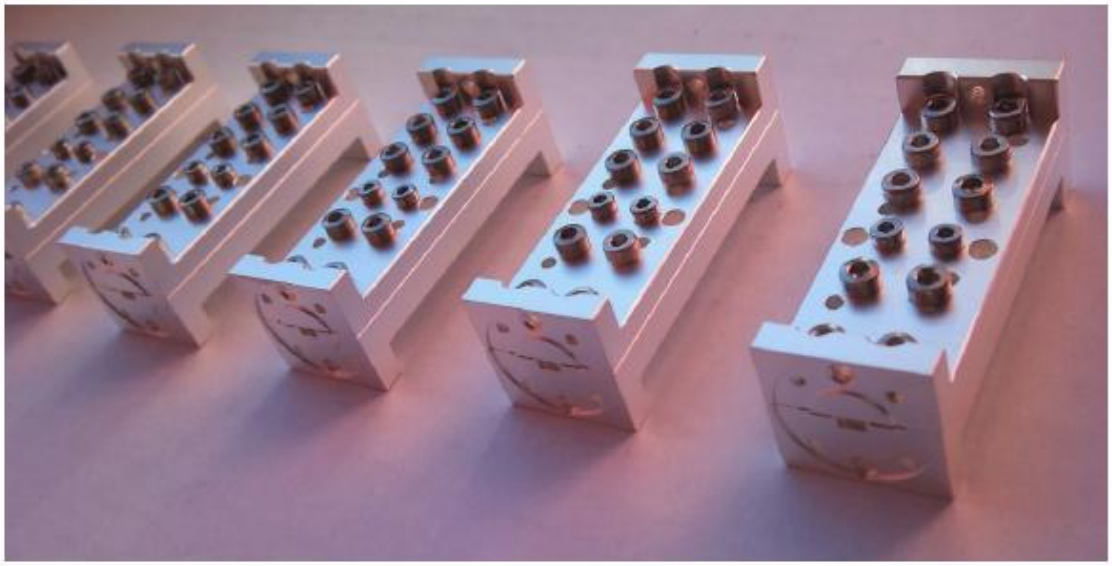

Figure A.3: MESL E-band diplexer